

NONLINEAR BEHAVIOUR AND STRESS CONCENTRATIONS IN NATURAL
FIBER COMPOSITES UNDER TRANSVERSE LOADING

A THESIS SUBMITTED TO
THE GRADUATE SCHOOL OF NATURAL AND APPLIED SCIENCES
OF
MIDDLE EAST TECHNICAL UNIVERSITY

BY

ONUR ÇAKMAKÇI

IN PARTIAL FULFILLMENT OF THE REQUIREMENTS
FOR
THE DEGREE OF MASTER OF SCIENCE
IN
MECHANICAL ENGINEERING

FEBRUARY 2019

Approval of the thesis:

**NONLINEAR BEHAVIOUR AND STRESS CONCENTRATIONS IN
NATURAL FIBER COMPOSITES UNDER TRANSVERSE LOADING**

submitted by **ONUR ÇAKMAKÇI** in partial fulfillment of the requirements for the degree of **Master of Science in Mechanical Engineering Department, Middle East Technical University** by,

Prof. Dr. Halil Kalıpçılar
Dean, Graduate School of **Natural and Applied Sciences**

Prof. Dr. M.A. Sahir Arıkan
Head of Department, **Mechanical Engineering**

Prof. Dr. F. Suat Kadiođlu
Supervisor, **Mechanical Engineering, METU**

Assoc. Prof. Dr. Barıř Sabuncuođlu
Co-Supervisor, **Mechanical Eng., Hacettepe Uni.**

Examining Committee Members:

Assoc. Prof. Dr. Ergin Tönük
Mechanical Engineering, METU

Prof. Dr. F. Suat Kadiođlu
Mechanical Engineering, METU

Assoc. Prof. Dr. Barıř Sabuncuođlu
Mechanical Engineering, Hacettepe University

Assoc. Prof. Dr. Hüsnu Dal
Mechanical Engineering, METU

Prof. Dr. Bora Yıldırım
Mechanical Engineering, Hacettepe University

Date: 12.02.2019

I hereby declare that all information in this document has been obtained and presented in accordance with academic rules and ethical conduct. I also declare that, as required by these rules and conduct, I have fully cited and referenced all material and results that are not original to this work.

Name, Surname: Onur akmakçı

Signature:

ABSTRACT

NONLINEAR BEHAVIOUR AND STRESS CONCENTRATIONS IN NATURAL FIBER COMPOSITES UNDER TRANSVERSE LOADING

Çakmakçı, Onur
Master of Science, Mechanical Engineering
Supervisor: Prof. Dr. F. Suat Kadiođlu
Co-Supervisor: Assoc. Prof. Dr. Barıř Sabuncuođlu

February 2019, 143 pages

Natural fiber reinforced polymer composite materials attracted attention of the researchers recently. Some of them, especially flax fiber composites, do have quite favorable mechanical properties compared to synthetic fibers like E-glass. In this study, micromechanical model of flax fiber reinforced composite under transverse loading is investigated and compared with conventional synthetic fibers. The study includes variety of strains and response of the material under large deformations. Finite element models employing representative volume elements like single fiber, hexagon and random are utilized. Fiber volume fractions of 40% and 60% are applied for the multiple fiber packaging types. According to the results, increasing fiber volume ratio affected the magnitude of the stress concentrations proportionally. Stress concentrations spread more uniformly with increasing strain inputs. The presence of neighboring fibers affected the stress concentrations of each other. Results of the comparison case studies revealed that stiffness contrast between fiber and the matrix significantly contributes to the high stress concentrations. The most uniform transverse stress concentration state observed was the flax fiber's for all comparison cases with conventional fibers.

Keywords: NFPCs, Flax Fiber Composites, Stress Concentrations, Micromechanics,
Transverse Loading

ÖZ

ENİNE YÜKLEME ALTINDAKİ DOĞAL ELYAFLI KOMPOZİTLERDE GERİLME YOĞUNLAŞMALARI VE DOĞRUSAL OLMAYAN DAVRANIŞLARIN İNCELENMESİ

Çakmakçı, Onur
Yüksek Lisans, Makina Mühendisliği
Tez Danışmanı: Prof. Dr. F. Suat Kadioğlu
Ortak Tez Danışmanı: Doç. Dr. Barış Sabuncuoğlu

Şubat 2019, 143 sayfa

Doğal elyaf katkılı kompozit malzemeler son yıllarda araştırmacıların fazlasıyla ilgisini çekmektedir. Bu malzemelerden bazıları, özellikle keten elyafı, E-Cam gibi sentetik elyaflara kıyasla oldukça iyi mekanik özellikler sergilemektedir. Bu tez çalışmasında, mikromekanik olarak modellenmiş bir keten elyaf katkılı kompozitin enine yükleme altındaki davranışları incelenmiştir ve söz konusu malzeme alışlagelmiş sentetik elyaflarla kıyaslanmıştır. Çalışma birden çok gerinim girdisini ve malzemenin yüksek deformasyon altındaki tepkisini içermektedir. Tek, altıgen ve rastgele elyaf dağılımlı temsili hacim elemanlara sahip sonlu elemanlar modelleri kullanılmıştır. Analizler çoklu elyaf modelleri için %40 ve % 60 hacimsel elyaf oranlarında gerçekleştirilmiştir. Elde edilen sonuçlara göre, artan hacimsel elyaf oranı gerilme yoğunlaşma büyüklüklerini doğru orantılı olarak etkilemektedir. Yüksek gerinim girdilerinde gerilme yoğunluklarının daha düzgün dağıldığı gözlemlenmiştir. Elyaf ve reçine arasındaki katılık farkının kıyaslama analiz çalışması sonuçlarına göre yüksek gerilme yoğunlaşmalarında oldukça etkili olduğu anlaşılmıştır. Tüm kıyaslama analizlerinde enine yükleme koşulunda en düzenli gerilme yoğunlaşmalarının keten elyaf katkılı kompozitlerde görüldüğü tespit edilmiştir.

Anahtar Kelimeler: Dođal Elyafly Kompozitler, Keten Elyafy, Gerilme Yođunlařmaları, Mikromekanik, Enine Yükleme

to my mother, father and brother

ACKNOWLEDGMENTS

Firstly, I would like to express my gratitude and regards to my supervisors Prof. Dr. F. Suat Kadiođlu and Assoc. Dr. Bariř Sabuncuođlu for their guidance and support. Their continuous assistance and positive attitude encouraged me greatly to finish my study.

I also would like to thank my parents, Meliha akmakı, Halis akmakı and my brother Enes akmakı for their loving support.

I would like to thank my colleagues in Turkish Aerospace. Many thanks to my dear friend Abdulkadir eki for his technical and morale supports. Finally many special thanks to my chiefs Bariř Erođlu and zge Gmen, for their patience, sympathetic and kind attitudes during my study.

TABLE OF CONTENTS

ABSTRACT	v
ÖZ	vii
ACKNOWLEDGMENTS	x
TABLE OF CONTENTS	xi
LIST OF TABLES	xiv
LIST OF FIGURES	xv
LIST OF ABBREVIATIONS	xxiii
CHAPTERS	
1. INTRODUCTION	1
1.1. Aims and Objectives of the Study	1
1.2. Research Methodology	3
1.3. Outline of the Study	4
2. LITERATURE REVIEW	7
2.1. Introduction to Natural Fiber Reinforced Polymer Composites	7
2.1.1. Constituents of NFPCs.....	8
2.1.1.1. Fiber	8
2.1.1.2. Matrix.....	12
2.1.2. Mechanical Properties of NFPCs.....	14
2.1.3. Selection of Natural Fiber and Matrix Assembly	20
2.2. Flax Fiber and Its Composites.....	21
2.2.1. Flax Fiber: an introduction	21
2.2.1.1. Flax Fiber Composition and Morphology.....	22

2.2.1.2. Flax Fiber Mechanical Properties	23
2.2.2. Flax Fiber Composites Mechanical Properties.....	28
2.3. Finite Element and Micromechanical Modeling of Flax Fiber Composites ..	31
2.3.1. Prediction of Elastic Properties	32
2.3.2. Development of Finite Element Models	41
2.3.3. Constitutive Models	47
3. OBJECTIVE OF THE THESIS	55
4. MATERIAL MODELING OF THE FLAX FIBER COMPOSITE.....	61
4.1. Flax Fiber Material Model	61
4.1.1. Flax Modeling Using Linear Elastic Approach.....	61
4.1.2. Flax Modeling Using Hyperelastic Approach.....	64
4.2. Epoxy Matrix Material Modeling	70
4.3. Material Models Used in Thesis	71
5. FEM DESCRIPTION OF THE FLAX FIBER COMPOSITE	73
5.1. Single Fiber RVE of Flax-Epoxy Composite	73
5.2. Hexagon RVE of Flax-Epoxy Composite.....	76
5.3. Random RVE of Flax-Epoxy Composite.....	78
5.4. Evaluation Method of Stress Outputs	84
6. ANALYSIS RESULTS	87
6.1. Single Fiber RVE Results	88
6.1.1. Young's Modulus Duality Case Study.....	88
6.1.2. Comparison Case Study with Orthotropic and Hyperelastic Flax Fiber ..	91
6.1.3. Stress Concentrations for Varying Strains	93
6.1.4. Comparison Case Study with Glass and Carbon Fiber	98

6.1.5. Element Type Comparison	101
6.2. Hexagon RVE Results	104
6.2.1. Stress Concentrations for Varying Strains ($vf = 0.4$).....	104
6.2.2. Stress Concentrations for Varying Strains ($vf = 0.6$).....	107
6.2.3. Stress Concentrations for Different Fiber Volume Fraction Ratios	110
6.2.4. Comparison Case Study with Glass and Carbon Fiber ($vf = 0.4$).....	112
6.2.5. Comparison Case Study with Glass and Carbon Fiber ($vf = 0.6$).....	114
6.3. Random RVE Results.....	116
6.3.1. Stress Concentrations for $vf = 0.4$	117
6.3.2. Stress Concentrations for $vf = 0.6$	120
6.3.3. Comparison Case Study with Glass and Carbon Fiber for $vf = 0.4$	123
6.3.4. Comparison Case Study with Glass and Carbon Fiber for $vf = 0.6$	124
7. GENERAL CONCLUSIONS.....	129
7.1. Summary	129
7.2. Key Findings and Outcomes	130
7.3. Future Work	131
REFERENCES.....	133
APPENDIX A.....	141

LIST OF TABLES

TABLES

Table 2.1. Natural fiber production rate (Reprinted from [10] with permission from Elsevier).....	9
Table 2.2. Mechanical Properties of several plant fibers [10, 12-19].....	10
Table 2.3. Chemical Composition of some common natural fibers [10].....	11
Table 2.4. Structural Parameters of Several Natural Fibers [11, 18, 24-29]	12
Table 2.5. Natural and Biodegradable Matrices [32].	13
Table 2.6. Optimum fiber volume ratios for different NFPCs [5, 24, 30, 41, 44-51] 19	
Table 2.7. Some Properties of flax and synthetic fibers [11, 17, 30]	20
Table 2.8. Tensile properties of elementary fibers [62].....	26
Table 3.1. Literature review summary	58
Table 4.1. Flax fiber orthotropic constants, compiled from literature.....	64
Table 4.2. Ogden Strain Energy Function Parameters Calculated by ABAQUS® ...	69
Table 4.3. Reduced Polynomial Strain Energy Function Parameters Calculated by ABAQUS®.....	69
Table 4.4. Epoxy matrix elastic properties	70
Table 4.5. Elastic properties of synthetic fibers	72
Table 5.1. Single RVE boundary conditions	75
Table 5.2. Boundary conditions for hexagon RVE.....	78
Table 6.1. Flax Fiber RVE analyses solution times.....	87
Table 6.2. CPU time for Single Fiber RVE with C3D8 and C3D8R elements	101

LIST OF FIGURES

FIGURES

Figure 1.1. Research Methodology of the thesis.....	4
Figure 2.1. Industrial use of NFPC examples [3, 4].....	7
Figure 2.2. Classification of Natural Fibers [9]	8
Figure 2.3. (a) Technical and elementary fiber; (b) SEM image of an elementary fiber. Copyright (2003) Wiley. Used with permission from [21].....	10
Figure 2.4. Schematical representation of plant cell structure. (Reprinted from [36] with permission from Elsevier)	15
Figure 2.5. Bast fiber extraction & production stages [38].....	16
Figure 2.6. Tensile strength of NFPCs with or without treatment [5, 39, 40] (Reprinted from [5] with permission from Elsevier)	17
Figure 2.7. (a) Flax field with flowers; (b) Retting of a flax field [53].	21
Figure 2.8. (a) Schematic representation of flax fibre [25]; (b) Flax fiber bundle (Reprinted from [54] with permission from Elsevier)	22
Figure 2.9. (a) Internal structure of elementary flax fiber (Reprinted from [55] with permission from Elsevier); (b) Representation of crystalline and amorphous cellulose. Copyright (1963) Wiley. Used with permission from [57].....	23
Figure 2.10. Stress-Strain curve of an elementary flax fiber (Reprinted from [61] with permission from Elsevier)	25
Figure 2.11. Stress-strain curve of E-Glass and elementary flax fibers (Dashed line: E-Glass; Straight Line: Hermes Flax; Dotted Lines: linear part of the curve where Young's modulus is measured) (Reprinted from [62] with permission from Elsevier)	25
Figure 2.12. Tensile test results on elementary flax fiber. Dotted line represents stress- strain curve, full line is tangent modulus. [60].....	26

Figure 2.13. Tensile stress vs strain curve of flax fiber bundle/PP composite with chemical treated (hollow shape) and untreated (solid shapes) fibers. (Reprinted from [63] with permission from Elsevier)..... 27

Figure 2.14. Textile architecture forms used in flax fiber composites, (a) woven, (b) braided, (c) knitted, (d) non-crimp fabric [20] 29

Figure 2.15. Stress-strain curves of various flax/epoxy composites with different forms [20] 30

Figure 2.16. Stress-strain curve for various MFAs in flax-polyester composite (Copyright (2012) Wiley. Used with permission from [65])..... 31

Figure 2.17. Stress-strain curves for laminates (a) $[0^\circ]_8$, (b) $[0^\circ,90^\circ]_2S$, (c) $[0^\circ,90^\circ,+45^\circ,-45^\circ]_S$, (d) $[-45^\circ,+45^\circ]_2S$ [66] 35

Figure 2.18. Variation of Young’s Modulus with changing volume fraction ratio (hollow circles: experimental values; dashed line: equation results) (Reprinted from [67] with permission from Elsevier)..... 36

Figure 2.19. Evolution of stiffness with volume fraction ratio (Reprinted by permission from Springer Nature: [69]) 37

Figure 2.20. (a) Tensile modulus vs fiber length curve, (b) Tensile strength vs fiber length curve hollow and solid points represent flax/PP and flax/MAPP respectively. (Reprinted by permission from Springer Nature: [64]) 38

Figure 2.21. (a) Stiffness and (b) Strength vs fibre volume fraction plots; hollow points: axial experimental results; full points: transverse experimental results; dotted lines uncorrected rule of mixture data; full lines: corrected rule of mixture and anisotropy included data. (Reprinted from [70] with permission from Elsevier)..... 40

Figure 2.22. (a) X-Ray imaging and (b) FE Model of quasi-UD flax/epoxy composite [71]..... 42

Figure 2.23. Representative unit cell in uniaxial tension. (Reprinted from [72] with permission from Elsevier)..... 43

Figure 2.24. Stress-strain diagrams with volume fraction ratio of 0.2 for (a) Flax/PP and (b) Flax/PPM. Reprinted from [72] with permission from Elsevier)..... 44

Figure 2.25. (a) Staggered geometry of post processed FEM, (b) Discretized fibers, (c) Idealized schematic lamella representation (Reprinted from [73] with permission from Elsevier).....	44
Figure 2.26. Bundle strength vs Gauge length plot. (Reprinted from [73] with permission from Elsevier).....	45
Figure 2.27. (a) Microstructures with different orientations; (b) Discretization of flax fibers with tetrahedron elements (Reprinted from [74] with permission from Elsevier)	46
Figure 2.28. (a) Stress-Strain curve with simulation and experimental values; (b) Variation of tensile modulus with respect to aspect ratio (Reprinted from [74] with permission from Elsevier).....	46
Figure 2.29. (a) FE modeling of elementary flax fiber; (b) micro fibril arrangement [75].....	47
Figure 2.30. Stress-Strain diagrams for loading angles (a) 0°, 15°; (b) 30°, 45°, 75° (Reprinted from [76] with permission from Elsevier)	49
Figure 2.31. Stress-strain plot with experimental data and simulation (Reprinted from [78] with permission from Elsevier)	50
Figure 2.32. Author's philosophy of modeling NFPCs. (Reprinted from [79] with permission from Elsevier).....	51
Figure 2.33. Comparison of experimental results and theoretical model of Flax/PLA composite for (a) small and (b) high strain rates (Reprinted from [79] with permission from Elsevier).....	52
Figure 3.1. Max. principal stress distribution in the matrix with (a) circular and (b) hexagonal fiber cross sections [80].....	56
Figure 4.1. (a) Plane of symmetry, (b) planes of symmetry of orthotropic materials	62
Figure 4.2. (a) Flax fiber stress-strain curve (Reprinted from [61] with permission from Elsevier) ; (b) representative linear and hyperelastic stress-strain curve [86] ..	65
Figure 4.3. Test data input to ABAQUS®.....	66
Figure 4.4. Scaled Stress-Strain curve used for the transverse load application.....	67

Figure 4.5. Output of (a) Ogden; (b) Reduced polynomial strain energy functions..	68
Figure 4.6. Stress-strain plot of evaluated hyperelastic potential functions and the literature test data.....	70
Figure 4.7. Epoxy matrix total stress-strain: (a) the entire curve; (b) zoomed view up to 0.02 strain [87].....	71
Figure 5.1. Single fiber RVE dimensions	74
Figure 5.2. Single RVE mesh structure	75
Figure 5.3. Boundary conditions shown on the RVE	76
Figure 5.4. Hexagon RVE: a) Dimensions, b) isometric view with 0.4 and 0.6 fiber volume fractions with the same fiber diameter.....	77
Figure 5.5. Mesh structure of hexagon RVE	77
Figure 5.6. Boundary conditions shown in hexagon RVE	78
Figure 5.7. Boundary conditions for random RVE.....	79
Figure 5.8. Representation PBC and Random RVE.....	82
Figure 5.9. Random RVEs with fiber volume fraction of (a) 0.6 and (b) 0.4	83
Figure 5.10. Mesh structures of random RVEs with fiber volume ratios of (a) 0.6 and (b) 0.4.....	84
Figure 5.11. Calculated stress components for the thesis: (a) radial stress; (b) shear stress; (c) horizontal stress concentration measurement direction along RVE; (d) Path around the fiber from which stress concentration is measured.....	85
Figure 6.1. Mesh sensitivity analysis results	88
Figure 6.2. Single Fiber RVE Radial stress concentrations of along flax-matrix interface with dual transverse moduli for 0.2% strain input.....	89
Figure 6.3. Single Fiber RVE Shear stress concentration along fiber matrix interface with dual transverse moduli 0.2% strain input.	90
Figure 6.4. Single Fiber RVE horizontal stress concentration along the path between fiber and the model edge with dual transverse moduli 0.2% strain input.....	90
Figure 6.5. Single Fiber RVE Radial stress concentrations along flax-matrix interface for orthotropic (blue) and hyperelastic (red) modeling approaches for 0.2% strain input	91

Figure 6.6. Single Fiber RVE shear stress concentrations along flax-matrix interface for orthotropic (blue) and hyperelastic (red) modeling approaches for 0.2% strain input.	92
Figure 6.7. Single Fiber RVE horizontal stress concentration along the path between fiber and the model edge for orthotropic (blue) and hyperelastic (red) modeling approaches for 0.2% strain input.....	92
Figure 6.8. Distribution of maximum principle stress for the input strains values of (a) 0.2 %; (b) 2%	94
Figure 6.9. Single Fiber RVE radial stress concentrations along flax-matrix interface for various transverse strain inputs starting from 0.1% to 5%.....	95
Figure 6.10. Single RVE shear stress concentrations along flax-matrix interface for various transverse strain inputs starting from 0.1% to 5%.....	96
Figure 6.11. Single Fiber RVE horizontal stress concentration along the path between fiber and the model edge for various transverse strain inputs starting from 0.1% to 5%.	97
Figure 6.12. Single Fiber RVE radial stress concentrations along flax-matrix interface for flax (blue), carbon (red) and glass (green) fibers for 0.2% strain input.	99
Figure 6.13. Single Fiber RVE shear stress concentrations along flax-matrix interface for flax (blue), carbon (red) and glass (green) fibers for 0.2% strain input.	99
Figure 6.14. Single Fiber RVE horizontal stress concentration along the path between fiber and the model edge for flax (blue), carbon (red) and glass (green) fibers for 0.2% strain input.....	100
Figure 6.15. Radial stress concentration distribution for comparison with C3D8 and C3D8R type elements	101
Figure 6.16. Shear stress concentration distribution for comparison with C3D8 and C3D8R type elements	102
Figure 6.17. Horizontal stress concentration distribution for comparison with C3D8 and C3D8R type elements.....	102
Figure 6.18. Contour plots for single RVE (a) C3D8, (b) C3D8R element type comparison with 5% transver strain input.....	103

Figure 6.19. Distribution of maximum principle stresses for the input strains values of (a) 0.2 %, (b) 2.5 %.....	104
Figure 6.20. Hexagon RVE radial stress concentrations along flax-matrix interface for varying transverse strain input starting from 0.1 % to 5% with fiber volume fraction of 0.4.....	105
Figure 6.21. Hexagon RVE shear stress concentrations along flax-matrix interface for varying transverse strain input starting from 0.1% to 5% with fiber volume fraction of 0.4	106
Figure 6.22. Distribution of max. principle stresses for the input strains values of (a) 0.2 %, (b) 2.5 %	107
Figure 6.23. Hexagon RVE radial stress concentrations along flax-matrix interface for varying transverse strain input starting from 0.001 to 0.05 with fiber volume fraction of 0.6.....	108
Figure 6.24. Hexagon RVE shear stress concentrations along flax-matrix interface for varying transverse strain input starting from 0.001 to 0.05 with fiber volume fraction of 0.6.....	109
Figure 6.25. Hexagon RVE radial stress concentrations along fiber-matrix interface for fiber volume fraction of 0.4 (blue) and 0.6 (red) with 0.2 % transverse strain input	110
Figure 6.26. Hexagon RVE shear stress concentrations along fiber-matrix interface for fiber volume fraction of 0.4 (blue) and 0.6 (red) with 0.2% transverse strain input.....	111
Figure 6.27. Hexagon RVE horizontal stress concentration along the path between fiber and the model edge for fiber volume fraction of 0.4 (blue) and 0.6 (red) with 0.2% transverse strain input.....	111
Figure 6.28. Hexagon RVE radial stress concentrations along fiber-matrix interface for flax (blue), Carbon (Red) and Glass (green) fibers with fiber volume fraction of 0.4 for 0.2% strain input	112
Figure 6.29. Hexagon RVE shear stress concentrations along fiber-matrix interface for flax (blue), Carbon (Red) and Glass (green) fibers with fiber volume fraction of 0.4 for 0.2% strain input	113

Figure 6.30. Hexagon RVE horizontal stress concentration along the path between fiber and the model edge for flax (blue), Carbon (Red) and Glass (green) fibers with fiber volume fraction of 0.4 for 0.2% strain input.	113
Figure 6.31. Hexagon RVE radial stress concentrations along fiber-matrix interface for flax (blue), Carbon (Red) and Glass (green) fibers with fiber volume fraction of 0.6 for 0.2% strain input.....	114
Figure 6.32. Hexagon RVE shear stress concentrations along fiber-matrix interface for flax (blue), Carbon (Red) and Glass (green) fibers with fiber volume fraction of 0.6 for 0.2% strain input.....	115
Figure 6.33. Hexagon RVE horizontal stress concentration along the path between fiber and the model edge for flax (blue), Carbon (Red) and Glass (green) fibers with fiber volume fraction of 0.6 for 0.2% strain input	115
Figure 6.34. Random RVE distribution of maximum principle stresses in the matrix for flax fibers with fiber volume fraction of 0.4 for 0.2% strain input	117
Figure 6.35. Random RVE distribution of shear stresses in the matrix for flax fibers with fiber volume fraction of 0.4 for 0.2% strain input.	118
Figure 6.36. Random RVE radial stress concentrations along fiber-matrix interface for the fiber having maximum stress concentrations with fiber volume ratio of 0.4 for 0.2% strain input	118
Figure 6.37. Random RVE shear stress concentrations along fiber-matrix interface for the fiber having maximum stress concentrations with fiber volume ratio of 0.4 for 0.2% strain input.	119
Figure 6.38. Random RVE distribution of maximum principle stresses in the matrix for flax fibers with fiber volume fraction of 0.6 for 0.2% strain input.	120
Figure 6.39. Random RVE distribution of shear stresses in the matrix for flax fibers with fiber volume fraction of 0.6 for 0.2% strain input.	121
Figure 6.40. Random RVE radial stress concentrations along fiber-matrix interface for the fiber having maximum stress concentrations with fiber volume ratio of 0.6 for 0.2% strain input.	121

Figure 6.41. Random RVE shear stress concentrations along fiber-matrix interface for the fibers having maximum stress concentrations with fiber volume ratio of 0.6 for 0.2% strain input.....	122
Figure 6.42. Random RVE Radial stress concentrations along the fiber-matrix interface for the fibers having maximum stress concentrations (crosshatched one in section 6.3.1) for fiber volume fraction of 0.4 for 0.2% strain input.....	123
Figure 6.43. Random RVE Shear stress concentrations along the fiber-matrix interface for the fibers having maximum stress concentrations (crosshatched one in section 6.3.1) for fiber volume fraction of 0.4 for 0.2% strain input.....	124
Figure 6.44. Random RVE radial stress concentrations along the fiber-matrix interface for the fibers having maximum stress concentrations (crosshatched one in section 6.3.2) for fiber volume fraction of 0.6 for 0.2% strain input.....	125
Figure 6.45. Random RVE shear stress concentrations along the fiber-matrix interface for the fibers having maximum stress concentrations (crosshatched one in section 6.3.2) for fiber volume fraction of 0.6 for 0.2% strain input.....	126
Figure 8.1. Maximum (a) Principal stress and (b) strain distributions of flax fiber under transverse loading	141
Figure 8.2. Stress Strain curve of maximum strained element	142

LIST OF ABBREVIATIONS

ABBREVIATIONS

BR	Butadiene Rubber
CR	Chloroprene Rubber
DOF	Degree Of Freedom
EPDM	Ethylene Propylene diene rubber
FE	Finite Element
FEA	Finite Element Analysis
FEM	Finite Element Method
IFBT	Impregnated Fiber Bundle Testing
IIR	Butyl Rubber
IROM	Inverse Rule Of Mixtures
MA	Maleic Anhydride
MAPP	Maleic Anhydride-Polypropylene Copolymer
MFA	Micro Fibril Angle
MROM	Modified Rule Of Mixtures
NBR	Nitrile Rubber
NFPC	Natural Fiber reinforced Polymer Composite
NR	Natural Rubber
PBC	Periodic Boundary Conditions
PLA	Poly Lactic Acid
PP	Polypropylene
Pre-preg	Pre-impregnated
PVC	Poly Vinyl Chloride
ROM	Rule Of Mixtures
RTM	Resin Transfer Molding
RVE	Representative Volume Element
SBR	Styrene Butadiene Rubber
SFT	Single Fiber Testing
UD	Unidirectional
VTMO	Vinyl Trimethoxy Silane

CHAPTER 1

INTRODUCTION

Natural fiber reinforced composites have been used in several areas of industry mainly as secondary structural components. Due to new developments during the last decade, better understanding of their mechanical behavior is required. The idea of using natural fiber reinforced composites in primary structural applications, demanded researchers/engineers to explore the material more than ever before. Material behavior of natural fiber reinforced composites under loading conditions depends on various factors like fiber type, resin type, adhesion between fiber-matrix assembly, fiber volume fraction, manufacturing method, harvesting methods, post-processing methods etc. Unlike the synthetic fibers, natural fibers exhibit different responses because of their intrinsic properties. The investigations on this field will allow people to develop and use this eco-friendly material in many fields concerning the adverse effects of synthetic fibers to the environment. To do so, various loading aspects, material modeling and simulation techniques, correlation methods should be investigated. Tailor-made composite materials are quite popular in structural applications in which they are employed on the direction of loading coinciding with the material's stiffest direction. However, considering the other loading directions, material sometimes could unexpectedly yield and fail. In the content of natural fiber composites, studies mostly focus on longitudinal loading conditions. A transverse loading study will give an idea about how these materials response to a different loading cases and how the integrity of the composite is affected at the end.

1.1. Aims and Objectives of the Study

The main aim of this study is to develop a numerical model in order to investigate material behavior with several differences compared to the previously studies

conducted in this field. Computational modeling is performed for the flax fiber composites by using a similarity based finite element approach. The study differs from the previous ones in many aspects. First and the most important is that natural fiber reinforced composite is investigated under transverse loading conditions with high strain setting. Majority of the studies in the literature was performed for longitudinal tensile modes for small strains. The number of studies in transverse loading conditions is quite a few. To be able to fully understand the material, whole behavior should be examined including the transverse response. Considering the structural applications, material strength apart from the main loading directions is vital due to possible combined loading cases. Hence, this study is beneficial considering the understanding of these new materials.

The second aspect is that this study is conducted in micromechanical level with several representative volume element approaches. Conducted studies in literature generally focus on macro level responses of a single finite element model. In the content of this study, natural fiber composite response is investigated both single and multiple fiber assemblies to observe the effect of fibers on stress concentrations on the matrix as well.

Another important benefit of this study is that whole FE models are created parametrically by using scripts, which allows conducting more analyses in minor intervals avoiding using the software's graphical user interface that takes long time for each iteration. Hence, this approach can further enhance the modeling of micro-structural behavior.

The additional objectives of the research are as follows:

1. Understanding the behavior of natural fiber composites under transverse loading conditions;
2. Implementing a method to obtain and quantify the stress concentrations in terms of numerical values;

3. Understanding the parameters of a natural fiber reinforced composite which could influence high stress concentration for prescribed loading;
4. Comparing the natural fibers with conventional synthetic fibers and evaluating the applicability;
5. Investigating the response of the composite under high deformations.

The thesis does not cover the damage, failure and fatigue behavior of natural fiber reinforced composites. Furthermore, the effect environmental conditions like temperature, pressure, humidity are neglected in the content of this study.

1.2. Research Methodology

The study starts with introduction to natural fiber reinforced polymer composites (NFPC). This section focuses on the definition and the concept of the material. Fiber and matrix of NFPCs are introduced. Then the selected natural fiber, flax, and its composites are investigated. An extensive literature survey is conducted since the essence of the study originates from this knowledge. After that, a novel finite element model is created and material models are selected. The description of these models are given in related sections. By using these material and finite element models, simulation studies are carried out with different parameters. At each run, a different aspect of composite is investigated. Stress concentrations occurring in matrices are calculated and plotted via a mathematical software. Next, the results are presented with plots and images. Finally, conclusions are presented. The methodology used in this thesis is summarized in Figure 1.1.

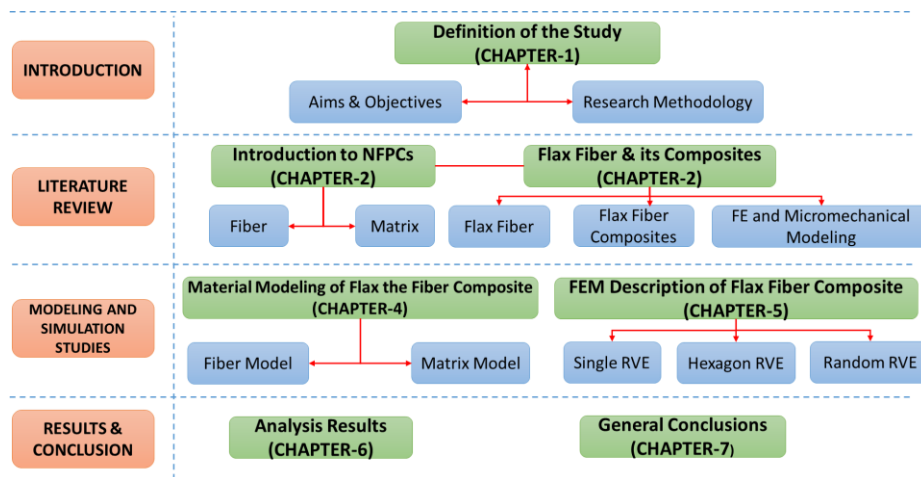


Figure 1.1. Research Methodology of the thesis

1.3. Outline of the Study

This thesis consists of 7 chapters. The summary of each chapter is given below:

CHAPTER 1. Introduction: Information about the content and the format of the thesis is given. Aims, objectives and methodology are mentioned.

CHAPTER 2. Literature Review: A detailed introduction about NFPCs are made. The constituents of NFPCs, i.e. fiber and matrix, and their effects on composite's mechanical properties are explained thoroughly. Mechanical and morphological properties of flax fiber is investigated. Stress-strain behavior is explored thoroughly. Extensive literature survey about the composites made of this fiber is presented.

CHAPTER 3. Objective of the Thesis: Purpose and motivation of the study is explained.

CHAPTER 4. Material Modeling of the Flax Fiber Composite: Material models to be used in FE analyses are given for fiber and the matrix.

CHAPTER 5. FEM Description of the Flax Fiber Composite: 3 different representative volume elements are introduced, namely, single fiber, hexagon and

random. Boundary conditions to apply these RVEs are determined. Details regarding model discretization are explained.

CHAPTER 6. Analysis Results: Created FE model results are presented. Simulations are carried out in Abaqus® finite element solver. Model creation and submission is done by using Python® scripts. Extracted results are post-processed with Matlab® to get stress concentration plots.

CHAPTER 7. General Conclusions: The summary and outcomes of the conducted research are presented. The results are discussed.

APPENDIX A: Analysis regarding flax fiber's elastic state is presented.

CHAPTER 2

LITERATURE REVIEW

2.1. Introduction to Natural Fiber Reinforced Polymer Composites

Natural Fiber Reinforced Polymer Composite (NFPC) is a kind of man-made material consisting of a high strength natural fiber and a polymer resin matrix. NFPC industry is currently a growing market due to this type of material's superior properties like relatively low weight, low cost, non-abrasive nature, biodegradability, and relatively good mechanical properties [1]. Reinforcing fibers are extracted from plants, animals, minerals and subjected to certain chemical processes to be readily used in composite forms. NFPCs are great candidates to be green materials, which at the end will make great contribution to environmental sustainability. Synthetic fiber reinforced composites production processes are cumbersome due to energy requirements and they also have poor recycling properties [2]. NFPC's are commonly used in automobile industry as interior design elements in the present state. Applications of natural fibers are also common in sports industry, house decoration, furniture, musical instruments etc.



Figure 2.1. Industrial use of NFPC examples [3, 4]

2.1.1. Constituents of NFPCs

As in the case of conventional composites, an NFPC is made of a stiff and strong reinforcing fiber and a tough and soft matrix material. In this section, general properties of fibers and matrices are elaborated.

2.1.1.1. Fiber

Natural fibers can be obtained from various sources like plants, animals and geological resources. Plant originated natural fibers contain cellulosic substances, whereas animal based ones contain proteins. Hard and woody nature of plant fibers make them preferable for high performance applications and they are the most common ones whereas the animal based ones are utilized in textile industry.

The performance of the composite is related to strength, orientation, physical properties and interfacial adhesion properties of fibers [1, 5-8].

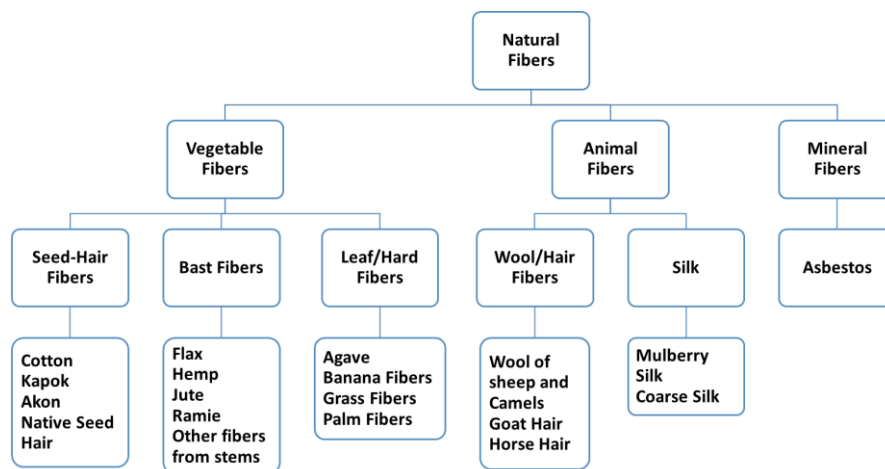


Figure 2.2. Classification of Natural Fibers [9]

Reinforcing plant fibers exist in various forms and shapes: bast fibers (jute, flax, ramie, hemp, kenaf); seed fibers (sisal, pineapple, abaca); grass and reed fibers (rice,

corn, wheat) and core fibers (hemp, kenaf and jute) [10]. World production amount per 10³ ton can be observed in Table 2.1

Table 2.1. *Natural fiber production rate (Reprinted from [10] with permission from Elsevier)*

Fiber Source	World Production (10³ ton)
Cotton Lint	18,450
Jute	2,300
Kenaf	970
Flax	830
Sisal	378
Roselle	250
Hemp	214
Coir	100
Ramie	100
Abaca	70

In general, bast fibers have the highest absolute and specific tensile properties among the other type of plant fibers. Leaf and seed fibers come afterwards. This is mainly due to function of fiber in the plant itself. Bast fibers provide rigidity and stiffness to the plant stems, therefore they should have the highest strength, leaf fibers come across with winds repetitively so they should have toughness, whereas seed fibers do not have any structural responsibility, so they lack those properties unlike the previous ones [11]. A number of mechanical properties of bast, leaf and seed fibers could be seen in Table 2.2

Table 2.2. Mechanical Properties of several plant fibers [10, 12-19]

Fiber	Density (g/cm ³)	Tensile Modulus (GPa)	Specific Tensile Modulus (GPa/gcm ⁻³)	Tensile Strength (MPa)	Specific Tensile Strength (MPa/ gcm ⁻³)	Failure Strain
Bast						
Flax	1.45-1.55	28-100	19-65	343-1035	237-668	2.7-3.2
Hemp	1.45-1.55	32-60	22-39	310-900	214-581	1.3-2.1
Jute	1.35-1.45	25-55	19-38	393-773	291-533	1.4-3.1
Leaf						
Sisal	1.40-1.45	9-28	6-19	347-700	248-483	2.0-2.9
Pineapple	1.44-1.56	6-42	4-27	170-727	118-466	0.8-1.6
Banana	1.30-1.35	8-32	6-24	503-790	387-585	3.0-10.0
Seed						
Cotton	1.50-1.60	5-13	3-8	287-597	191-373	6.0-8.0
Coir	1.10-1.20	4-6	3-5	131-175	119-146	15-30
Oil Palm	0.70-1.55	3-4	2-4	248	160-354	25.0

Not all of the natural fiber types are used for reinforcement purposes. As it is mentioned earlier, bast and some of the leaf fibers are made use of due to their rigid structures whereas most of the seed fibers are used for toughening purposes. In order to elaborate on the mechanical properties of a natural fiber, one should first go into details of basic cell structure. Unit cell of reinforcing natural fibers are composed of two types: technical and elementary. Given in the Figure 2.3, the difference could be noticed. Technical fibers, also defined as fiber bundles, is a group of fiber consisting 10 to 40 fibers whereas elementary fiber is a single one [20].

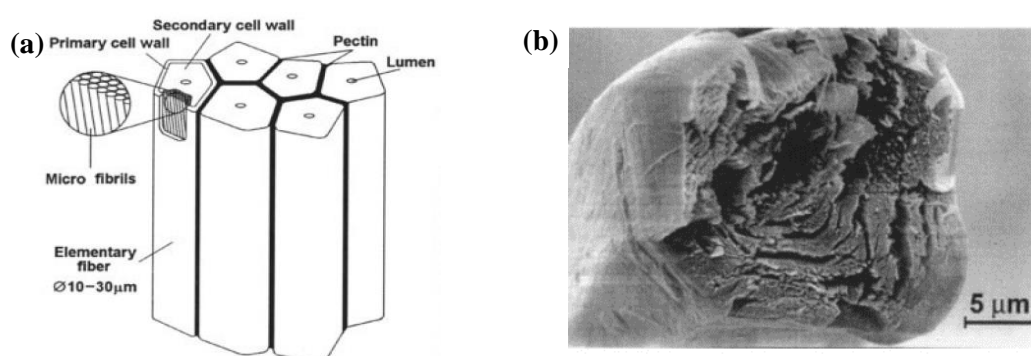


Figure 2.3. (a) Technical and elementary fiber; (b) SEM image of an elementary fiber. Copyright (2003) Wiley. Used with permission from [21]

Internal structure of an elementary fiber consists cellulose, hemicellulose, lignin, pectin, waxes and other components. Main constituent, which provide the actual stiffness, is cellulose in the form crystalline cellulose.

Table 2.3. *Chemical Composition of some common natural fibers [10].*

Fiber	Cellulose (%)	Hemicellulose (%)	Lignin (%)	Waxes (%)
Flax	71	18.6-20.6	2.2	1.5
Kenaf	72	20.3	9	-
Jute	61-71	14-20	12-13	0.5
Hemp	68	15	10	0.8
Ramie	68.6-76.2	13-16	0.6-0.7	0.3
Abaca	56-63	20-25	7-9	3
Sisal	65	12	9.9	2
Coir	32-43	0.15-0.25	40-45	-

The fiber does have non-crystalline cellulose as well, but in terms of intermolecular bonds it is inferior compared to crystalline. Cellulose molecules are helically wound around the cell walls with a certain angle. This helix angle is called micro fibril angle and it affects the tensile properties profoundly [11]. Another parameter affecting the performance of a natural fiber is the aspect (length-to-diameter) ratio. Long fibers are better at stress transfer when they are used in a composite laminate. This phenomenon is explained as an uncut fiber acts like a continuous beam. If the same length is replaced by bunch of a short fibers, at each transition region, a stress concentration point is created and strength of the overall structure diminishes. Therefore, fibers with high length and small diameter are preferred to be used in structural applications [5, 22-24]. Some of the mentioned parameters for natural fibers are listed in Table 2.4

Table 2.4. *Structural Parameters of Several Natural Fibers [11, 18, 24-29]*

Fiber	Cellulose Content (wt %)	Cellulose Crystallinity (%)	Micro fibril Angle (degree)	Aspect Ratio (Length/Diameter)	Luminal Porosity (%)
Bast					
Flax	64-71	50-90	5-10	1750	2-11
Hemp	70-74	50-90	2-6	900	2-11
Jute	61-72	50-80	8	100	10-16
Leaf					
Sisal	66-78	50-70	10-25	100	10-22
Pineapple	70-82	44-60	10-15	450	10-22
Banana	44-64	45-55	10-12	150	35-53
Seed					
Cotton	85-93	50-90	46	1000	5
Coir	32-43	27-33	30-49	35	30-50
Oil Palm	40-50	20-30	42-46	100	5-10

2.1.1.2. Matrix

Matrix materials in NFPCs can be thermoplastic, thermoset, rubber or biodegradable. Molecular structure of the thermoplastic matrix is suitable for becoming softer at elevated temperatures and return to its original form when it is cooled down. Contrary to this, thermoset resins have strong chemical bonds, which makes them amenable to be treated in relatively low temperatures. The most commonly used thermoplastic matrix types in NFPCs are polypropylene (PP), polyethylene, poly vinyl chloride (PVC); whereas phenolic, epoxy and polyesters are the thermoset resins [30, 31].

Shah et. al (2013) explain that natural composites with an aim of utilization in structural applications generally have thermoset matrices owing to three main reasons [11]. First, mechanical properties of thermoset matrices are superior due to their inherent molecular structure compared to thermoplastics. After curing process, they develop a highly rigid network of covalent molecular structures. Due to that, they show better performance in tensile loading. Second reason is easy application potential because of low processing temperatures and low viscosity. Unlike the thermoplastic curing, process temperatures typically below 100°C do not damage and degrade the natural reinforcement at the end; either no or little performance loss is observed. Low

viscosity makes the composite manufacturing process more versatile. In such case, liquid composite molding techniques could be used and high performance material requirements can be satisfied due to error-free manufacturing. Third reason is the shear properties caused by chemical interface which is formed with natural fibers. Thermoset resins are polar in nature like plant fibers. This feature makes them to be compatible with reinforcing fibers unlike thermoplastics which tend to be nonpolar.

There are other types of matrices used in natural fibers. Rubber matrices are one of them. Primary rubber matrices are natural rubber (NR-most common one), styrene butadiene rubber (SBR), butyl rubber (IIR), butadiene rubber (BR), nitrile rubber (NBR), chloroprene rubber (CR), ethylene propylene diene rubber (EPDM), polyurethane and silicon rubbers [32]. Use of bio-degradable matrices is a rather new development in the content of NFPCs. The idea of using a natural resin together with a natural reinforcement draw attention of many authors. In their work O'Donnell et. al [33] examined the plant oil-based natural composites (acrylated epoxidized soy bean oil). They successfully achieved to produce laminates with mechanical strengths enough to be employed in housing and automotive applications. Oksman et.al [34] in their work, demonstrated the PLA (Poly Lactic Acid) based flax composites have 50% increased performance compared to thermoplastic polypropylene matrix and indicated that PLA based composites could replace conventional thermoplastic composites. Girones et. al [35] examined corn starch based sisal and hemp composites and reported promising results in terms of performance increase. In their work, Pickering et. al. [32] summarized some of the natural and biodegradable matrices that can be seen in Table 2.5

Table 2.5. *Natural and Biodegradable Matrices* [32].

Natural Substances	Synthetic Substances
Polysaccharides	Poly(amides)
Starch	Poly(anhydrides)
Cellulose	Poly(amide-enamines)
Chitin	Poly(vinyl alcohol)
Proteins	Poly(vinyl acetate)

Collagen/gelatin	Polyesters
Casein, albumin, fibrogen, silks	Poly(glycolic acid)
Polyhydroxyalkanoates	Poly(lactic acid)
Lignin	Poly(caprolactone)
Lipids	Poly(orthoesters)
Shellac	Poly(ethylene oxides)
Natural Rubber	Poly(phosphazines)

The matrices used with natural reinforcing fibers can be enhanced in terms of mechanical performance by using certain chemical and physical methods, which is explained in the upcoming sections.

2.1.2. Mechanical Properties of NFPCs

Natural fiber composites draw great interest due to their advantages over conventional composite materials like low cost, high specific strength, high strength-to-weight ratio, relatively good mechanical properties, non-abrasive nature and biodegradability [30]. However, these materials are not free from problems. In this section, mechanical properties of NFPCs are explained.

In terms of structural applications, mechanical properties of NFPCs are driven by several parameters, such as fiber type, pre-process of the fiber, fiber-matrix interface, fiber volume fraction, and manufacturing method.

Fiber type is the dominant element, which affects the tensile properties of NFPCs. As it is indicated in Section 1.1.1, Natural fibers can be classified as bast, leaf, core, grass, and reed fibers. Bast fibers are the superior in terms of mechanical properties compared to other types due to their chemical composition and cellular structure [11]. These types of fiber are rich in terms of crystalline cellulose content. Cellulose gives strength and rigidity to the fiber, therefore tensile properties of a fiber is proportional to cellulose content. Other properties related to fiber type are micro-fibril angle and aspect ratio.

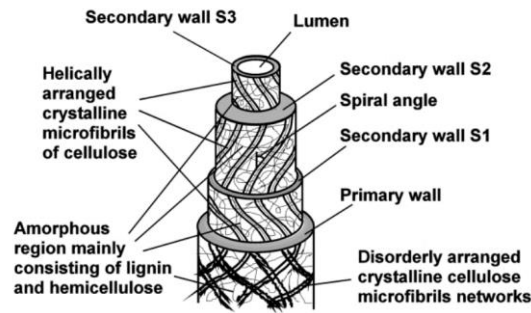


Figure 2.4. Schematical representation of plant cell structure. (Reprinted from [36] with permission from Elsevier)

Micro-fibril angle (MFA) is the angle between helically wound micro-fibrils at S2-layer and the longitudinal direction of the fiber. As this angle gets smaller, crystalline cellulose aligns with fiber and the loading direction in the composite which increases tensile strength at the end.

Aspect ratio is the ratio of fiber length-to-diameter. High aspect ratio is favorable in terms of strength of a natural fiber. This is because long fibers with small cross-section are better at stress transfer. Liu et. al [37] investigated the length effect of kenaf fiber reinforced plastics under impact loading and concluded that as the fiber length increases impact strength of the composite increases as well due to increasing fiber bridging effect. Bridging effect is a phenomenon that occurs during delamination of fiber-reinforced composites in which fibers form bridge like structures on the crack opening and slow down the crack growth. Therefore, fiber aspect ratio is an important parameter of a NFPC.

In order to use a natural fiber in a composite application, it must go through an extraction and preparation process. Fiber quality is highly variable due to this process and it affects the mechanical properties profoundly. The final product is special to the application that it will be used. The fibers could be in the forms of mats, unidirectional preregs, woven fabrics, non-woven fabrics etc. Retting is the initial operation of extracting bast fiber from woody substance and cellular tissues where the fibers reside

in the plant stem [38]. Whole process can be seen in Figure 2.5. Process parameters are effective on mechanical properties of the final product as well. The purpose of the whole operation is to obtain uniform, long, and undamaged fiber bundles to be used in consolidated composite forms. As it is indicated, process may show some difference from producer to producer but in order to ensure a consistent quality suppliers use batch mixing across several crops, harvests, and years [11].

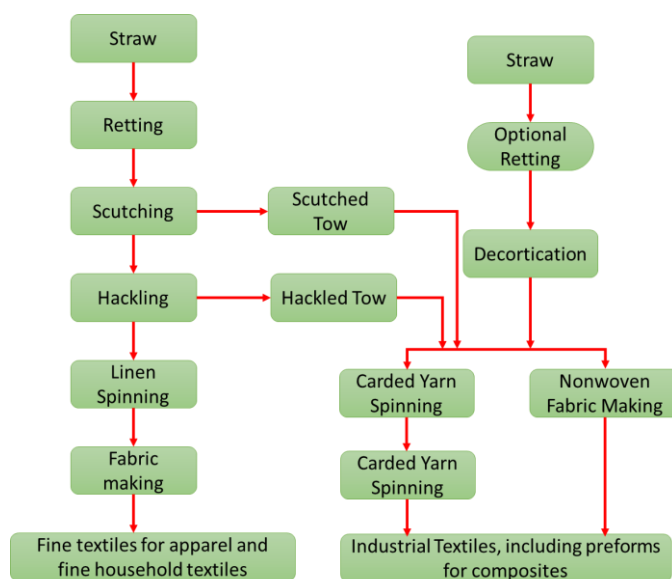


Figure 2.5. Bast fiber extraction & production stages [38]

Another performance driving parameter is fiber-matrix interface. As it is indicated in Section 1.1.1, the most commonly used matrix types are thermosets and thermoplastics. Among them, thermosets are more suitable for structural applications due to load bearing capacity to be used in high performance composite applications, low processing temperatures, low viscosity for different type of consolidation methods, and better compatibility with plant fibers. Polymer matrices are nonpolar and hydrophobic in nature, since the natural fibers consists polar hydrophilic substances like cellulose, inferior stress transfer issues arise [5]. The very first

performance treatment starts from this interface. Fiber-matrix adhesion could be improved using several chemical and physical techniques. These methods focus on cleaning fiber surface and removing impurities to assure better adhesion. Besides, some of the techniques abrade the fiber surface in micro level. By doing so, bonding between matrix and fiber further strengthens. Some of treated and untreated fiber composite properties can be seen in Figure 2.6.

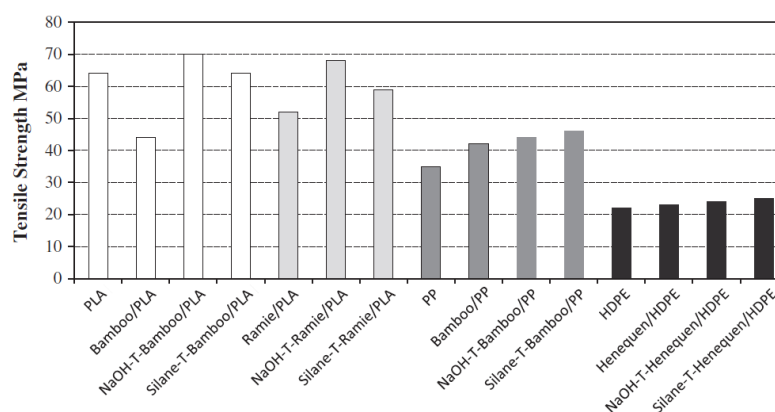


Figure 2.6. Tensile strength of NFPCs with or without treatment [5, 39, 40] (Reprinted from [5] with permission from Elsevier)

Haque et. al investigated chemical treatment of palm and coir reinforced polypropylene composites [41]. He used benzene diazonium salt to increase compatibility of fibers with the matrix. Hydroxyl group in the natural fiber, which is responsible for high water absorption, is converted to diazo group, by doing so better mechanical properties are obtained. Cantero used various chemical treatments including maleic anhydride (MA), maleic anhydride-polypropylene copolymer (MAPP), vinyl trimethoxy silane (VTMO) to enhance adhesion characteristics of flax fibers to the polypropylene matrix [42]. At the end of his work, he observed wettability characteristics, flexural and tensile strength properties was improved. Saha [43] conducted a study regarding treatment of jute fibers with alkali (NaOH) solution. He

dipped the fibers 0.5% alkali solution followed by a 30 minutes alkali stream. The indicated results were quite satisfactory in which uniaxial tensile strength has been increased up to 65%. The physico-chemical characterization of fibers that he made revealed that non-cellulosic matters that are removed properly with the aid of this process gave rise to an increase in tensile strength. Fiber volume fraction is the next parameter which affect mechanical properties of NFPCs. Shalwan et. al [5] classified the effect of volume fraction into two categories: theoretical and experimental. Theoretical models, which include rule of mixtures (ROM), have proportional relation with volume fraction and tensile strength. Real case is not alike. Up to certain limit, tensile strength of a composite increases with increasing fiber volume fraction. Yet, excessive amount of fiber in a composite laminate may deteriorate the fiber matrix interface and diminishes the stress transfer rate, at the end, results in an inferior structural composite. In their work, Brahim et. al [44] investigated influence of volume fraction in unidirectional Alfa/Polyester composite. They prepared specimens with 12, 21, 32 and 44 % volume ratios. What they observed was a direct proportion between increasing volume ratio and longitudinal modulus. Jacob [45] studied mechanical properties of Sisal/Oil Palm hybrid natural fiber composite. He found out that increase of fiber concentration resulted with an increase in elastic modulus of the composite. But tensile strength and tear strength diminished after a specific value. Shibata et. al [24] conveyed in their work that volume fraction increase up to 60% in kenaf and 66% in bagasse increased the flexural modulus. After that, due to insufficient resin, it was reported that flexural modulus diminished.

Each NFPC system exhibit different behavior due to highly scattering parameters related to manufacturing, harvesting, processing and design. The optimum values could only be reached via theoretical and experimental efforts. Some of the optimum fiber concentrations that give rise to maximum tensile properties can be observed from Table 2.6.

Table 2.6. *Optimum fiber volume ratios for different NFPCs [5, 24, 30, 41, 44-51]*

Material	Optimum Fiber Concentration (%)
Sisal-oil palm/natural rubber	≈ 30
Coir/PP	≈ 15
Palm/PP	≈ 15
Hemp/PP	≈ 40-50
Flax/HDPE	≈ 20
Rice/HDPE	≈ 5-10
Kenaf/PP	≈ 40
Jute/PP	≈ 40
Hemp/PLA	≈ 35
Jute/PBS	≈ 20
Alfa/polyester	≈ 44
Sisal/rubber	≈ 30
Oil palm/rubber	≈ 30
Kenaf/corn-starch	≈ 50
Bagase/corn-starch	≈ 50
Ramie cloth/polyester	≈ 30

Manufacturing method of natural fiber composite systems is quite effective on the performance. As the fiber content increases, it becomes harder to consolidate the NFPC [11]. Common methods for NFPC manufacturing is injection molding, compression molding, vacuum infusion, hand layup, prepregging and resin transfer molding (RTM). The system to be used changes mostly according to matrix type as viscosity and cure temperature are the key factors. Among the mentioned manufacturing methods, compression molding is the most common one which can be used with both thermoplastic and thermoset resins. Due to mentioned compaction difficulties, composites with desirable volume fractions and mechanical properties sometimes could not be manufactured. Other techniques which utilize liquid resins could defect the composite because of porosities as well. Therefore, the method to be used for NFPC production is vital in terms of performance.

Natural fiber reinforced polymers are not free from problems for sure. To summarize these merits; water absorption characteristics, poor dimensional stability, poor thermal

performance, unknown long term properties like fatigue and impact strength can be counted.

2.1.3. Selection of Natural Fiber and Matrix Assembly

General performance parameters of natural fiber composites are mentioned in the previous section. As it is indicated, mechanical properties show great scatter considering consolidated forms of fibers with resin due to various reasons. Thinking of the task in which NFPC will be employed, like structural applications, one shall have deep knowledge of fiber's properties. Therefore, the fiber and its matrix assembly have to be scrutinized profoundly.

Among the all types of natural fibers, bast fibers are known to perform best in loading applications. Since a structural task will mainly include a loading application, the fiber to be selected shall be one of them. In this sense, flax fiber comes into prominence considering the literature. Some properties of flax are quite competitive compared to synthetic fibers which can be observed in Table 2.7. Especially E-Glass is thought to be replaced by flax fiber in certain structural applications.

Table 2.7. *Some Properties of flax and synthetic fibers [11, 17, 30]*

Fiber	Density (g/cm³)	Elongation (%)	Tensile Strength (MPa)	Elastic Modulus (GPa)
Flax	1.45-1.55	2.7-3.2	500-1500	28-100
E-Glass	2.5	0.5	2000-3000	70
S-Glass	2.5	2.8	4570	86
Aramid	1.4	3.3-3.7	3000-3150	63-67
Carbon (PAN-based)	1.4	1.4-1.8	400	230-240

Due to its superior properties, flax fiber is selected to be investigated in this thesis. Its mechanical properties are further explored in Section 2.2.

Epoxy as a thermoset matrix is quite handy in terms of processing and is very versatile. Its elastic-plastic properties are explored many times by various authors. Available data in the literature is enough to model it mathematically. Therefore, the matrix is selected as epoxy to be used in this study.

2.2. Flax Fiber and Its Composites

In this section, natural composites reinforced with flax fibers and the fiber itself are elaborated

2.2.1. Flax Fiber: an introduction

Flax (*Linum usitatissimum*) is a member of *Linaceae* family. Its cultivated plants grow up to 1.2 meters having slender stems. The leaves of the plant are glaucous green, slender lanceolate, 20-40 mm long and 3 mm wide. The flowers are blue, about 20 mm in diameter. The plant is known to be used ever since ancient times, even dated back up to 36,000 years ago [52]. It is mainly grown for its seeds to be used in foods and for its oil apart from reinforcement.



Figure 2.7. (a) Flax field with flowers; (b) Retting of a flax field [53].

The extraction of flax fiber requires series of operations. The very first operation is dew-retting which can be seen in Figure 2.7-b. The plant is placed in the field for a

certain period of time in order to loosen and get the fiber bundles separated from the stem. During this phase, plant is rotated to be exposed to sun light in both sides. As it is indicated in section 2.1.2, retting is effective on fiber's mechanical performance. Upon completion of retting process, the stem and woody core are segmented and some of the loosened long fibers are extracted. This process is called scotching. The next step is to clean and form the thick, rough fibers in order to obtain high quality technical fibers. Long and short fibers are separated for different uses, like prepregs, woven and non-woven forms [20].

2.2.1.1. Flax Fiber Composition and Morphology

As in the case of other natural fibers, flax is composed of fiber bundles. These bundles consist of technical fibers and the technical fibers contain elementary fibers as shown in Figure 2.8. Technical fibers are thin long fibers containing 10 to 40 elementary fibers; elementary fibers are single plant cells mostly between 10 to 25 μm in diameter; 20 to 50 mm in length [25].

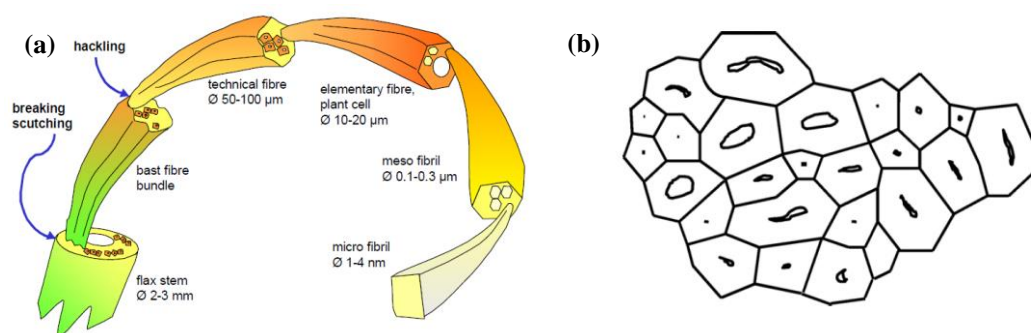


Figure 2.8. (a) Schematic representation of flax fibre [25]; (b) Flax fiber bundle (Reprinted from [54] with permission from Elsevier)

Internal structure of flax fiber is no different compared to general natural fiber structures. It is composed of primary and secondary cell walls. Secondary cell walls are named as S1, S2, and S3 respectively. Inter-cell walls are filled with lumen. The secondary wall includes high percentage and crystalline cellulose which is responsible

for stiffness and strength. The cellulose is helically wound around S2 layer at an MFA about 10 degrees [55]. The orientation angle affects the response of the fiber under loading which is elaborated in upcoming sections thoroughly. The other materials present in the flax fiber's internal structure together with cellulose (64.1-75%) are hemicellulose (11-20.6 %), pectin (1.8-2.3%), lignin (2-2.5%), waxes (1.5-1.7%), lipids and ashes [20, 56]. Representation of an elementary fiber's core structure could be observed in Figure 2.9.

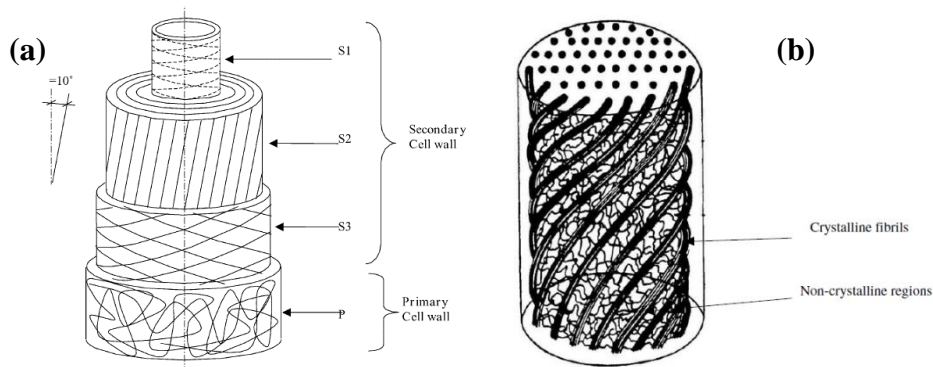


Figure 2.9. (a) Internal structure of elementary flax fiber (Reprinted from [55] with permission from Elsevier); (b) Representation of crystalline and amorphous cellulose. Copyright (1963) Wiley. Used with permission from [57]

2.2.1.2. Flax Fiber Mechanical Properties

The characterization of flax fiber is more or less similar to the other natural fibers. Yet, properties like chemical composition, cellulose content and crystallinity, length, shape, diameter, strength and stiffness values scatter vastly from fiber to fiber depending on the growing and harvesting conditions.

Tensile properties of flax fibers are superior to other types of natural fibers which make them great candidates to replace E-Glass in certain applications [25, 58]. The major problem regarding the flax fibers is that strength and stiffness values of elementary and technical fibers are not alike. As it is defined previous section,

technical fiber is a group in which certain amount of elementary fibers are resident. Strength and elastic modulus values of elementary fibers are 1500-1800 MPa and 60-80 GPa respectively, yet these properties are about 800-1500 MPa and 55-75 GPa in technical fibers [56, 59]. This is mainly due to the fact that layers of low strength pectin are filled in between elementary fibers inside of the technical fibers. As a result, load bearing capacity of technical fibers diminishes.

The very first step to understand the mechanical behavior of a material is to perform testing. Many authors used different techniques to obtain stress-strain behavior of the flax fiber like single fiber test (SFT), dry fiber bundle test, and impregnated fiber bundle test (IFBT) [60]. Each test has its own difficulties and advantages. For example, in SFT, it is cumbersome to obtain and prepare a single fiber. IFBT requires a decent micromechanical model and several assumptions to calculate single fiber's mechanical properties. Charlet [61] used MTS type electromechanical testing equipment to obtain stress-strain curve of an elementary flax fibre. He found out that stress-strain curve had three sections: first linear part until 0.3% of deformation, a nonlinear part between 0.3 and 1.5%, then a second linear part until the rupture (Figure 2.10). He explained this duality with the inherent structure of the fiber: in the first part due to global loading of the fiber each cell wall is deformed, then second nonlinear zone could be associated with elasto-visco-plastic deformation of the fiber caused by the possible re-arrangement of the amorphous cell materials like pectins and hemicellulose, meanwhile microfibrils align with loading direction. Afterwards, in the final region, linear elastic response of aligned microfibrils could be observed.

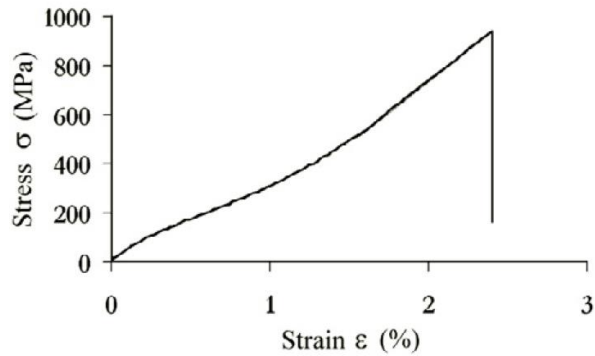


Figure 2.10. Stress-Strain curve of an elementary flax fiber (Reprinted from [61] with permission from Elsevier)

In another study of the author, he obtained mean tensile properties of a set of 90 elementary flax fibers with large scatters. Strength value, ultimate strain, initial modulus, and final modulus values are found to be 1256 ± 619 MPa, 2.5 ± 1.1 , 54 ± 29 GPa, 62 ± 32 GPa respectively [59]. Coroller et. al. [62] tested three different originated elementary flax fibers and an E-Glass fiber. They reported that while glass fiber exhibited a quasi-linear behavior, all flax fibers' stress-strain curves were divided into 3 sections, two linear and a nonlinear in between. Figure 2.11 depicts the behavior of the fibers.

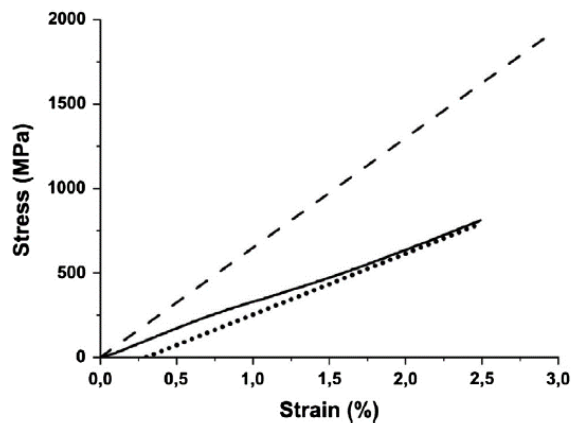


Figure 2.11. Stress-strain curve of E-Glass and elementary flax fibers (Dashed line: E-Glass; Straight Line: Hermes Flax; Dotted Lines: linear part of the curve where Young's modulus is measured) (Reprinted from [62] with permission from Elsevier)

In their work, they also calculated the tensile properties of elementary flax and E-glass fibers. From the values, it is obvious that origin of the plant has tremendous effect on tensile characteristics which could be observed in Table 2.8.

Table 2.8. *Tensile properties of elementary fibers [62].*

Fiber	Young's Modulus (GPa)	Stress at break (MPa)	Strain at break (%)	Fiber Diameter (μm)
Hermes Flax	48.9 ± 12.0	1066 ± 342	2.8 ± 0.8	18.6 ± 3.9
Andrea Flax	48.3 ± 13.8	841 ± 300	2.2 ± 0.8	18.1 ± 3.9
Marilyn Flax	57.1 ± 15.5	1135 ± 495	2.1 ± 0.6	13.9 ± 2.7
E-Glass	70.3 ± 5.8	1765 ± 432	2.9 ± 1.0	17.9 ± 1.9

Bensadoun et.al. [60] tested the elementary flax fibers in accordance with NF EN 1007-4 standard for advanced technical ceramics and obtained the stress-strain curve. What they observed was a behavior which includes two linear zones and a nonlinear zone in between. The first elastic modulus of the fiber (57.0 ± 13 GPa) is measured at approximately 0.3% strain; whereas secondary modulus is calculated at about 1% (44.5 ± 14 GPa). The scatter of the values is not low due to highly variable properties of the plant fiber itself.

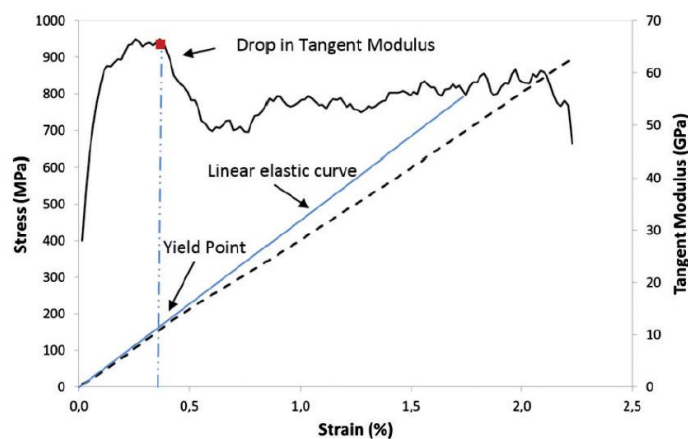


Figure 2.12. Tensile test results on elementary flax fiber. Dotted line represents stress-strain curve, full line is tangent modulus. [60]

Since it is quite cumbersome to execute dry fiber bundle test on elementary fibers and discontinuities of technical fibers create difficulty on uniform loading, impregnated fiber bundle tests are utilized [60]. Arbelaiz et. al. [63] investigated short flax fiber bundle/polypropylene composites. They used different fiber volume fractions in their specimens. Tensile and three-point bending tests were carried out. Stress strain curve they obtained is presented in Figure 2.13. Linear and nonlinear trend can also be seen in the plot. In this method fiber's tensile properties are back calculated making use of micromechanical theoretical models.

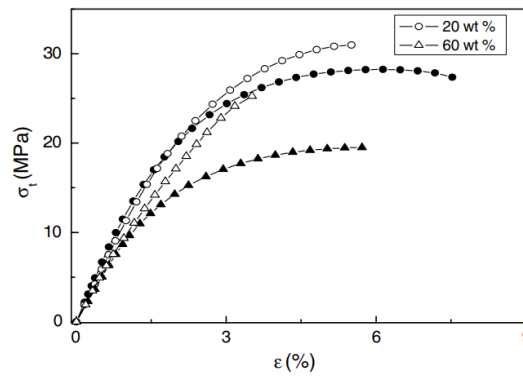


Figure 2.13. Tensile stress vs strain curve of flax fiber bundle/PP composite with chemical treated (hollow shape) and untreated (solid shapes) fibers. (Reprinted from [63] with permission from Elsevier)

Mechanical properties of flax fiber can also be determined via impregnated fiber bundle testing. The fiber itself is not directly tested in this method; instead, consolidated composite specimens are employed. Obtained results are utilized in order to calculate the single fibers properties making use of micromechanical theoretical models. In this method calculated values are dependent on the validity and power of the used micromechanical equations. Bensadoun et. al. [60] asserted that it is not a blocking factor for stiffness determination but for the strength, local fiber misorientations, fiber-matrix adhesion and fiber volume fraction have to be

considered. They calculated strength and stiffness of the fibers via following equations:

$$E_f = \frac{E_c - E_m(1 - v_f)}{v_f} \quad (\text{Eq. 1})$$

$$\sigma_{u,f} = \frac{\sigma_c - \sigma'_m(1 - v_f)}{v_f} \quad (\text{Eq. 2})$$

where E_m is the elastic modulus of the matrix, E_f is the longitudinal modulus, v_f is the volume fraction ratio, and $\sigma_{u,f}$ is the longitudinal strength of the fiber. Whole “c” subscripted parameters are related to composite specimens whereas σ'_m is calculated from the equation below:

$$\sigma'_m = E_m \varepsilon_{u,c} \quad (\text{Eq. 3})$$

The authors’ findings as the result of the study are initial and secondary longitudinal modulus which were found to be 59.8 ± 2.4 GPa; 40.8 ± 3.5 GPa respectively. The ultimate strength of the flax fiber was calculated as 527 ± 138 MPa.

The key note to be deduced from these studies is that flax fibers do not exhibit fully linear behavior up to rupture when they are loaded in tensile unlike synthetic fibers. Due to their natural cell structure, they show elasto-viscoplastic material responses.

2.2.2. Flax Fiber Composites Mechanical Properties

Previous section has focused on stress-strain behavior of elementary and technical flax fibers. In this section, mechanical properties of flax fiber and its matrix assembly are elaborated.

Flax fiber reinforced composites are not only in the form of monofilament configurations. These fibers also exist in the forms of mats, rovings, fabrics and yarns. Each type of architecture form has its own manufacturing methods like film stacking, hand lay-up, compression molding, filament winding, manual winding, resin transfer molding, injection molding and pultrusion [56].

Flax fiber composites in the form of mats are the most primitive examples of composite forms and they are used with thermoplastic matrices. Garkhail et. al. [64] compared the flax fiber mat-polypropylene composite with glass mat reinforced thermoplastics. They also investigated the fiber length and fiber volume ratio effect on the performance. The conclusion they reached was stiffness of flax fiber composites were comparable to E-glass, but strength of the flax fiber reinforced composite was far below the E-glass counterpart. That is mainly due to random distribution and low aspect ratio of the fibers making the matrix to carry the most of the load. In order to prevent this, different fiber architectures are introduced. Unidirectional (UD) fiber composites having high stiffness in longitudinal direction make possible to design the structure in a more customized fashion. These kinds of composites are advantageous in terms of strength and stiffness. Yet, limitations in manufacturing of curved surfaces cause further type of fabric architectures to be introduced. Examples of different textile architectures could be seen in Figure 2.14

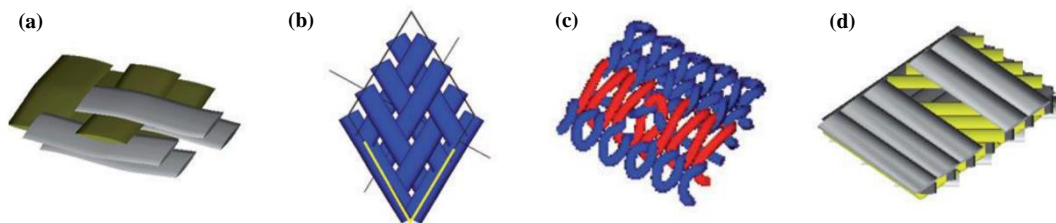


Figure 2.14. Textile architecture forms used in flax fiber composites, (a) woven, (b) braided, (c) knitted, (d) non-crimp fabric [20]

Fabric type reinforcements are good for dimensional stability and easy handling, with inferior properties compared to UD composites [20]. Tailorable structure allows designers to create laminates that are reinforced for more than one principle directions. But due to crimping effects (bending of the fiber on top of each other) underneath each and every fiber group, the overall integrity in terms of stiffness and strength diminishes. Despite manufacturing limitations and difficulties, UD fiber composites are still favorable considering tensile properties. Besides, anisotropy of flax fiber structures requires laminated forms to be balanced and symmetric to have quasi-isotropic properties. Stress-strain curve of several UD and woven fabric composites are given in Figure 2.15. Intrinsic nature of flax fiber is also reflected to the composite laminates where there exist two linear regions and a nonlinear region in between. From Figure 2.15, it is clear that unidirectional forms have superior stiffness and strength compared to woven forms.

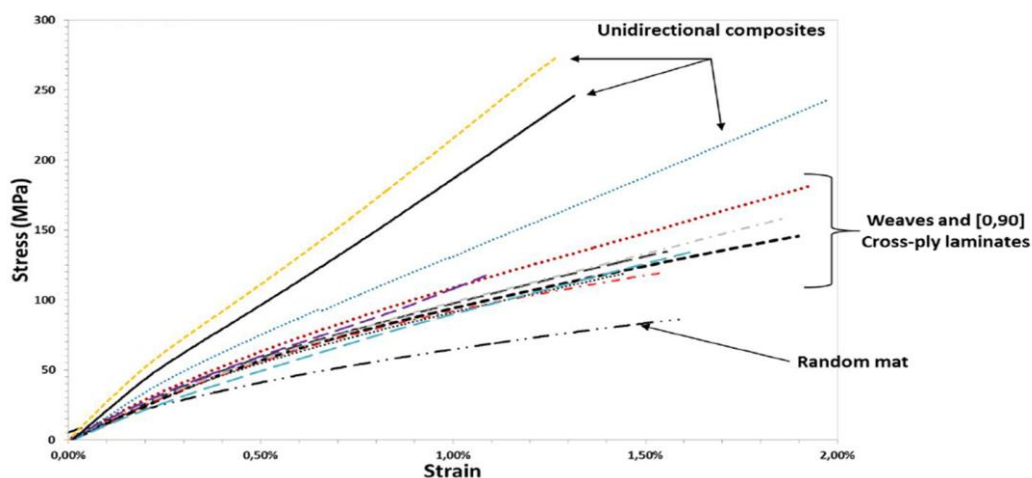


Figure 2.15. Stress-strain curves of various flax/epoxy composites with different forms [20]

Apart from textile architectures, properties which affect the mechanical performance of NFPCs are also valid for flax fiber composites like micro fibril angle (MFA), matrix fiber adhesion, matrix, fiber volume fraction etc. When MFA is oriented in loading

direction, composite will exhibit superior properties. Shah et. al. [65] investigated the MFA effect on tensile properties of flax-polyester composite. They showed that as the MFA converges to loading direction, in their case 0° , composite's elastic properties improved. The stress-strain curves could be seen in Figure 2.16.

Likewise, when matrix fiber adhesion is properly set up via certain chemical treatments, macro structure will be more sustainable in terms of mechanical strength. Considering the matrix itself; either thermoset, thermoplastic or natural resins, the compatibility with fiber or elastic-plastic properties are key parameters for structural composites.

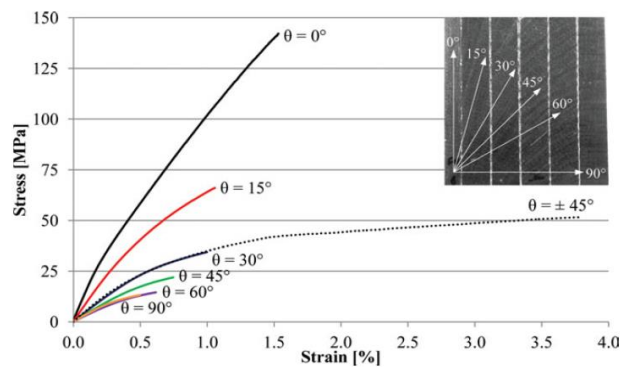


Figure 2.16. Stress-strain curve for various MFAs in flax-polyester composite (Copyright (2012) Wiley. Used with permission from [65])

Volume fraction of fiber in the composite laminate is another critical design parameter as mentioned earlier. As this ratio increases up to a limit, tensile properties of the composites enhance. But after this limit, due to lack of resin in the laminate, poor wetting conditions or voids, structural parameters are badly influenced; consequently, one ends with an inferior composite assembly.

2.3. Finite Element and Micromechanical Modeling of Flax Fiber Composites

Previous sections focused on general properties of natural fibers and flax fibers and their composites. As indicated in section 1.3, flax fiber and epoxy matrix is selected as composite assembly. In this section, models developed in the literature are examined which are about prediction of elastic properties, development of finite element models based on unit cell, and constitutive models. This classification is made considering the historical development of the studies.

2.3.1. Prediction of Elastic Properties

In order to use a material in engineering applications, the very first step is to determine its mechanical properties like Young's modulus, Poisson ratio, strain-stress at failure, stress strain plots, fracture toughness etc. Studies conducted within this frame mainly include an experimental procedure and a basic linear model to correlate. For this purpose, rule mixtures and reverse rule of mixture equations are vastly used. In this approach there are several assumptions like fibers are uniformly distributed throughout the matrix, matrix is free of voids, perfect bonding is assured between matrix and fibers, applied loads are either parallel or normal to the fiber direction, no residual stress in the lamina, and both fiber and matrix behave as linearly elastic material.

Baley [55] tested flax fiber/epoxy composite under tensile loading then tried to predict the Young's modulus considering volume fraction ratio and evolution of MFA during testing. He used Halpin-Tsai equations to calculate longitudinal elastic modulus of flax fiber:

$$\frac{M}{M_m} = \frac{1 + \xi\eta V_f}{1 - \eta V_f} \quad (\text{Eq. 4})$$

where

$$\eta = \frac{\frac{M_f}{M_m} - 1}{\frac{M_f}{M_m} + \xi} \quad (\text{Eq. 5})$$

M stands for E_L , E_T or G_{LT} ; M_f is E_f , E_m or G_f ; and M_m is E_m or G_m . The subscripts m, f, L, T represent matrix, fiber, longitudinal and transverse respectively. V_f is volume fraction of fiber and ξ is the shape factor. After some mathematical manipulations, he obtained modulus of elasticity in x-direction loading:

$$E_x = \left(\frac{1}{E_L} + \frac{\theta^2}{G_{LT}} \right)^{-1} \quad (\text{Eq. 6})$$

For a fiber volume fraction of 73.8%, calculated modulus of elasticity value is 99.940 GPa where the test result was 91.803 GPa which is quite similar to experimental values considering an elementary linear model.

Shah et. al. [65] investigated flax fiber composites subjected to off-axis loading. They used conventional rule of mixtures and Chamis formulae to calculate longitudinal and transverse modulus of elementary flax fiber, where “c” and “ θ ” stands for composite and loading direction, respectively:

$$E_{c,\theta} = \left[\frac{1}{E_{c,\theta}} \cos^4 \theta + \left(\frac{1}{G_{c12}} - \frac{2\nu_{c12}}{E_{c,0}} \right) \cos^2 \theta \sin^2 \theta + \frac{1}{E_{c,90}} \sin^4 \theta \right]^{-1} \quad (\text{Eq. 7})$$

In order to calculate shear modulus, they used Halpin-Tsai equation:

$$G_{c12} = \frac{G_m(1 + \xi\eta V_f)}{(1 - \eta V_f)} \quad (\text{Eq. 8})$$

where

$$\eta = \frac{\frac{G_f}{G_m} - 1}{\frac{G_f}{G_m} + \xi} \quad (\text{Eq. 9})$$

In order to calculate flax fiber's longitudinal tensile modulus, rule of mixtures was used:

$$E_{f,0} = \frac{1}{V_f} [E_{c,0} - V_m E_m] \quad (\text{Eq. 10})$$

The results they obtained were stated to be in agreement with experiments. They calculated fiber's longitudinal modulus as 45.8 GPa. Furthermore, they also calculated shear modulus and transverse modulus of flax fiber as 2.0 GPa and 3.9 GPa respectively.

Kersani et. al.[66] studied the damage initiation and development in flax/epoxy composites under quasi-static tension. The authors prepared different laminate configurations including $[0^\circ]_8$, $[0^\circ, 90^\circ]_{2S}$, $[-45^\circ, +45^\circ]_{2S}$ and $[0^\circ, 90^\circ, +45^\circ, -45^\circ]_S$ to obtain tensile properties of flax fiber and its composites. The specimens were tested in tensile loading in which they exhibit mostly brittle behavior except for $[-45^\circ, +45^\circ]_{2S}$ laminate. Bilinear zone was also evident in his results (Figure 2.17) which was attributed to intrinsic change of stiffness of flax fibers with deformation. In order to model the laminates mathematically, he used classical laminate theory with ply idealizations and Chamis formulae. Flax fiber's longitudinal and transversal moduli values were calculated as $E_L = 70$ GPa; $E_T = 8$ GPa respectively; whereas Poisson coefficients were found as $\nu_{LT} = \nu_{TT} = 0.25$. One of the most important deductions they made was absence of transverse cracks in flax reinforced composite. They explained this phenomenon making use of low stiffness contrast between epoxy and flax fibers.

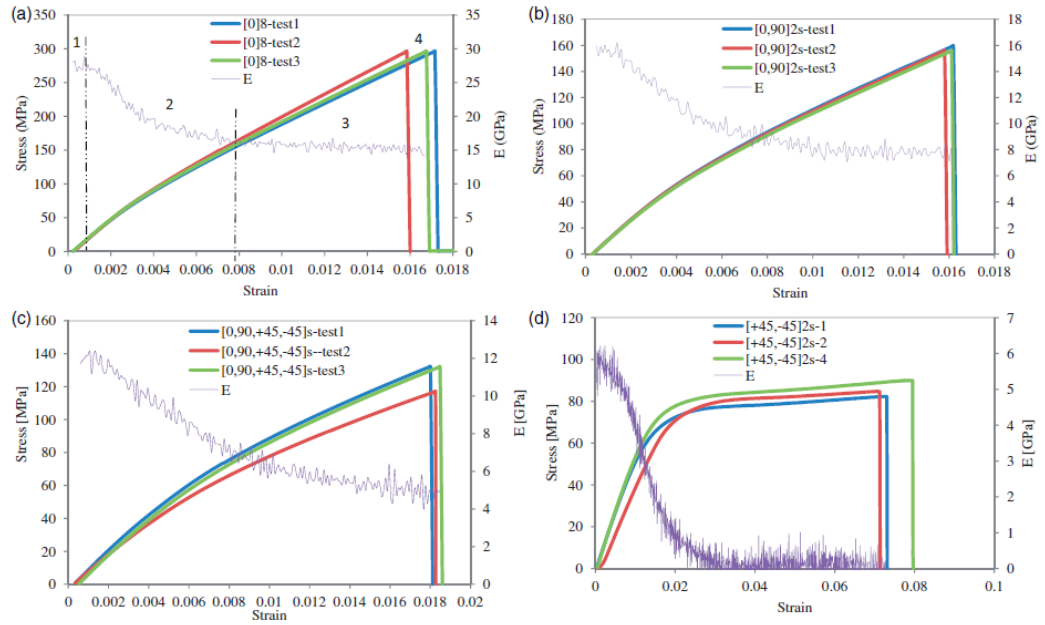


Figure 2.17. Stress-strain curves for laminates (a) $[0^\circ]_8$, (b) $[0^\circ,90^\circ]_{2S}$, (c) $[0^\circ,90^\circ,+45^\circ,-45^\circ]_S$, (d) $[-45^\circ,+45^\circ]_{2S}$ [66]

Baiardo et. al. [67] studied composites of flax fiber with polyester resin. They investigated change in tensile modulus with fiber content. They found out that tensile modulus increases with increasing fiber content then he fitted the results using modified rule of mixture:

$$E = \eta_0 \eta_1 V_f E_f + (1 - V_f) E_m \quad (\text{Eq. 11})$$

where E , E_f , E_m are moduli of composite, fiber and matrix respectively, V_f is fibre volume fraction and η_0 and η_1 are fiber fibre orientation and length efficiency factors. The authors defined length efficiency factor considering Cox Shear Lag model [68] as:

$$\eta_1 = \left[1 - \frac{\tanh(na)}{na} \right] \quad (\text{Eq. 12})$$

where

$$n = \sqrt{\left[\frac{2G_m}{E_f \ln(2R/d)} \right]} \quad (\text{Eq. 13})$$

a is the aspect ratio, G_m is the matrix shear modulus, and $2R$ is the distance between each fiber and its nearest neighbor. Calculated values $E_f = 27$ GPa, $E_m = 0.446$ GPa, and $G_m = 165$ MPa with $\eta_0 = 0.194$ showed parallelism with experimental values shown in Figure 2.18.

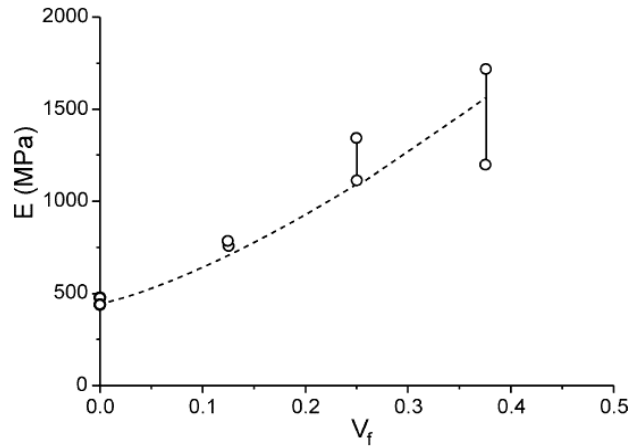


Figure 2.18. Variation of Young's Modulus with changing volume fraction ratio (hollow circles: experimental values; dashed line: equation results) (Reprinted from [67] with permission from Elsevier)

One of the earliest studies made in this field is conducted by Lamy et. al. [69]. In their work, they attempted to predict stiffness of flax fiber-epoxy composites using a mathematical formulation based on an averaging technique among 12 class of fibers with diameters from $5\mu\text{m}$ to $35\mu\text{m}$. Longitudinal elastic modulus of UD composite is proposed to be calculated via equation below:

$$E_L = \sum_{i=1}^n V_{fi} E_i + (1 - V_f) E_m \quad (\text{Eq. 14})$$

where i is class number, V_{fi} is fiber volume fraction of diameter d_i . Authors claimed V_{fi} to be proportional to the cross section of the fiber which at the end leads to $V_{fi} = n_i d_i^2$, where n_i is the number of fibers in each class. Then, Eq.14 took the form:

$$E_L = V_f \sum_{i=1}^n \frac{n_i d_i^2}{\sum_{i=1}^n n_i d_i^2} E_i + (1 - V_f) E_m \quad (\text{Eq. 15})$$

The results obtained from the mathematical model were compared with experimental results which could be observed in Figure 2.19. Authors, to conclude, made a correlation in between fiber diameter, fiber volume fraction, and matrix modulus and stated that as the fiber diameter increases, elastic modulus decreases.

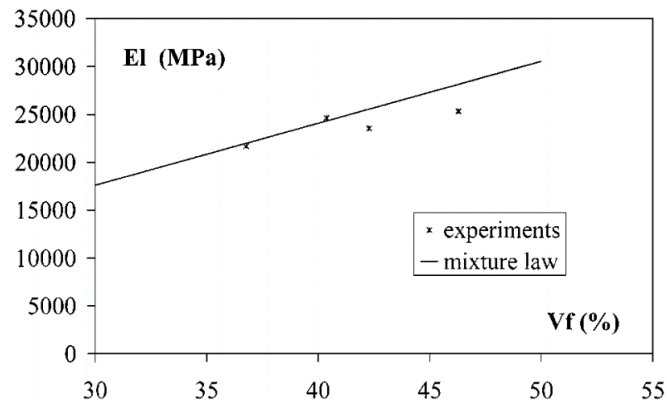


Figure 2.19. Evolution of stiffness with volume fraction ratio (Reprinted by permission from Springer Nature: [69])

Similar study is conducted by Garkhail et. al. [64] which was also mentioned in previous chapters with a different aspect. They used rule of mixtures and Cox Shear

Lag model to predict tensile modulus and strength of the flax/PP and flax/MAPP, as well. The results they obtained are presented in Figure 2.20:

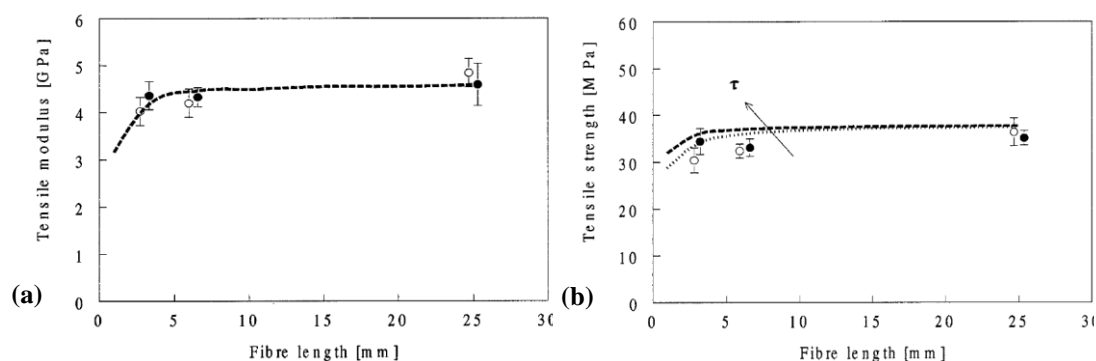


Figure 2.20. (a) Tensile modulus vs fiber length curve, (b) Tensile strength vs fiber length curve hollow and solid points represent flax/PP and flax/MAPP respectively. (Reprinted by permission from Springer Nature: [64])

Madsen et. al. [70] investigated the effect of porosity unlike all the other studies which idealize the composite assembly as void free. They created a theoretical model by taking the porosities that are caused by production and structurally aspects into account. The anisotropy of the flax fiber was also taken into account while creating the modified form of rule of mixture. The theoretical model used was derived as follows:

$$v_c = v_f + v_m + v_p \quad (\text{Eq. 16})$$

where c, f, m, p represent composite, fiber, matrix and porosity respectively. Then Eq.16 could be rewritten using volume and weight fractions:

$$v_c = \frac{m \cdot W_f}{\rho_f} + \frac{m \cdot W_m}{\rho_m} + V_p \cdot v_c$$

$$v_c = \frac{\frac{m \cdot W_f}{\rho_f} + \frac{m \cdot W_m}{\rho_m}}{1 - V_p} \quad (\text{Eq.17})$$

where m , ρ , W , V describe mass of composite, density, weight fraction and volume fraction respectively. Volume fractions for fiber and matrix were evaluated by the authors as:

$$V_f = \frac{v_f}{v_c} = \frac{\frac{W_f}{\rho_f}}{\frac{W_f}{\rho_f} + \frac{W_m}{\rho_m}} (1 - V_p) \quad (\text{Eq. 18})$$

$$V_m = \frac{v_m}{v_c} = \frac{\frac{W_m}{\rho_m}}{\frac{W_f}{\rho_f} + \frac{W_m}{\rho_m}} (1 - V_p) \quad (\text{Eq. 19})$$

As it is indicated earlier, the authors modeled porosity in two components namely $V_{p(proc)}$ and $V_{p(struc)}$ which indicate porosities caused by manufacturing process and structural aspects such as fiber type and orientation. Afterwards, a new function based on fibre weight fraction was introduced:

$$\alpha = \frac{(1 - W_f)\rho_f}{W_f\rho_m} \quad (\text{Eq. 20})$$

$$V_f = \frac{1}{1 + \alpha} \left(1 - (V_{p(proc)} + V_{p(struc)}) \right) \quad (\text{Eq. 21})$$

$$V_m = \frac{1}{1 + \alpha} \left(1 - (V_{p(proc)} + V_{p(struc)}) \right) \quad (\text{Eq. 22})$$

In order to calculate longitudinal (E_1) and transverse (E_2) moduli values, rule of mixture was used with fibre anisotropy ratio (α):

$$E_1 = (V_f + E_f + (1 - V_f)E_m)(1 - V_p)^2 \quad (\text{Eq. 23})$$

$$E_2 = \left(\frac{(E_f f a)E_m}{((1 - V_f)(E_f f a) + V_f E_m)} \right) (1 - V_p)^2 \quad (\text{Eq. 24})$$

Then process and structural void terms were formulated as below:

$$V_{p(proc)} = 0.06 W_f \quad (\text{Eq. 25})$$

$$V_{p(struc)} = 0.32 W_f - 0.20 \text{ for } W_f > 0.625$$

$$\text{else } V_{p(struc)} = 0 \quad (\text{Eq. 26})$$

Longitudinal and transverse moduli values were calculated using (Eq.23) and (Eq.24). The authors fitted theoretical model to the experimental data and the results they reached are presented in the Figure 2.21.

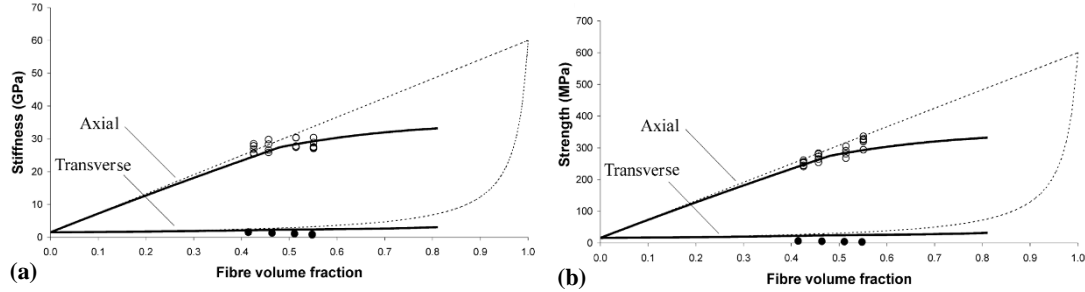


Figure 2.21. (a) Stiffness and (b) Strength vs fibre volume fraction plots; hollow points: axial experimental results; full points: transverse experimental results; dotted lines uncorrected rule of mixture data; full lines: corrected rule of mixture and anisotropy included data. (Reprinted from [70] with permission from Elsevier)

In the content of elastic property prediction, several publications are investigated. Since these are the early studies in this field, they mostly contain experiments and theoretical models to fit the trend of the behavior of flax fiber composites. Again, most of the studies focuses on longitudinal behavior and lack the transverse properties. One

vital deduction from this section is done by Kersani implying the transverse moduli mismatch between matrix and the fiber is low which contradicts with the case in synthetic fibers [66].

2.3.2. Development of Finite Element Models

After determination of elastic properties phase, development of finite element models to simulate the behavior of flax fiber composites under loading conditions is the next step. To fulfil this task, various authors created micromechanical models based on reproducibility of a unit cell and solve the problems with the predetermined boundary conditions. In this type of studies, a supplementary theoretical model is sometimes derived and compared with the results obtained from FEM simulations.

Straumit et. al. [71] investigated the flax fiber and flax/epoxy composite moduli making use of a finite element model. Different from the other works, they took fiber misalignment into account while creating the FE model. The 3D model was created using X-Ray computed tomography images. By doing so, a complete and realistic geometry was assured which is shown in Figure 2.22. 8-node linear brick elements (C3D8) are used in FE model. The material properties were input to ABAQUS® software in the form of engineering constants.

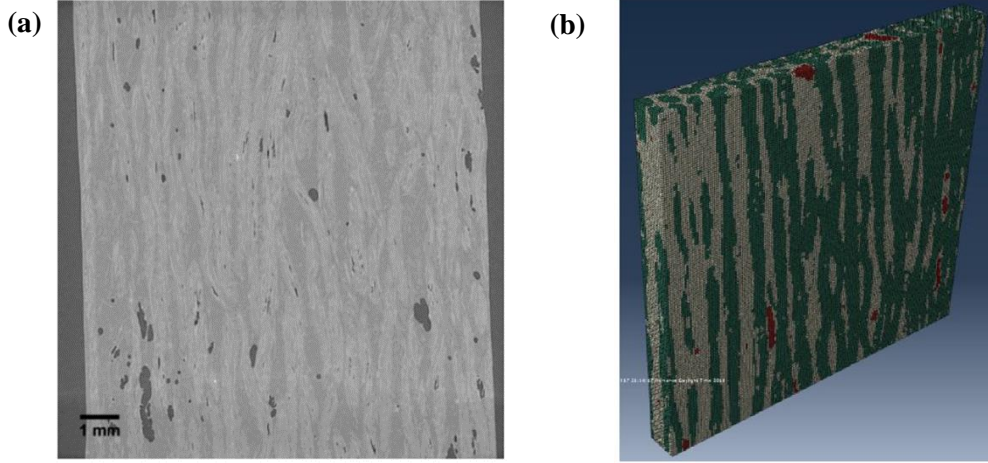


Figure 2.22. (a) X-Ray imaging and (b) FE Model of quasi-UD flax/epoxy composite [71].

Properties of matrix and fiber were taken as follows: $E_m = 2.7$ GPa, $\nu_m = 0.23$, $E_{f,T} = 10$ GPa, $\nu_f = 0.25$. After simulations and a series of experimental procedures, they calculated flax fiber's modulus 63.0 ± 1.46 GPa, which is consistent with the experimental results: 62.4 ± 2.87 GPa.

Modniks et. al. [72] modeled short flax fiber reinforced polymer composite using a unit cell to reproduce the tensile stress-strain behavior. They performed numerical studies on flax/polypropylene (PP) and flax/maleic-anhydride-grafted polypropylene (PPM). Orientation averaging approach was used in the model starting from the equation:

$$\sigma_{ij}^c(\boldsymbol{\varepsilon}^c) = \frac{1}{4\pi} \int_0^{2\pi} \int_0^\pi \sigma_{ij}^{UD}(\boldsymbol{\varepsilon}^c, \varphi, \theta) f(\varphi, \theta) \sin \theta d\theta d\varphi \quad (\text{Eq. 27})$$

where $f(\varphi, \theta)$ represents fiber orientation distribution density as function of φ and θ angles. $\sigma_{ij}^{UD}(\boldsymbol{\varepsilon}^c, \varphi, \theta)$ designates the stress under a prescribed strain in a UD composite's unit cell. The theoretical model used in matrix was Ramberg-Osgood equation:

$$\varepsilon = \frac{\sigma}{E} \left(1 + a \left(\frac{\sigma}{\sigma_0} \right)^{n-1} \right) \quad (\text{Eq. 28})$$

where E is the Young's modulus, a , σ_0 , and n stand for model parameters. The FE model was created using 20-node quadratic brick elements (C3D20) with symmetry boundary conditions which could be seen in Figure 2.23.

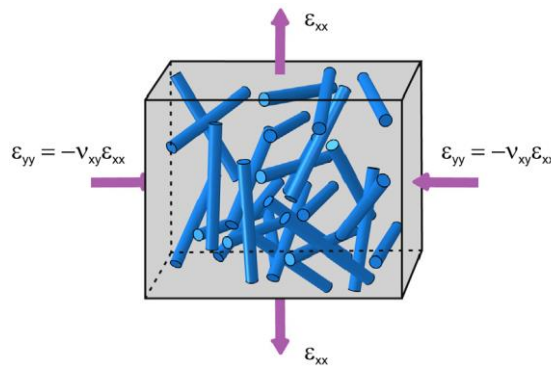


Figure 2.23. Representative unit cell in uniaxial tension. (Reprinted from [72] with permission from Elsevier)

Material properties were input as: $E_m = 1.6$ GPa, $\nu = 0.4$, $\sigma_0 = 16$ MPa, $a = 0.235$, and $n = 5.44$. The authors assumed flax fiber to be linear elastic with a modulus of 69 GPa and 1.21 mm long. The results obtained from FEM were agreeing with the theoretical model and presented for volume fraction of 0.20 in the Figure 2.24. The solid lines represent the experimental results whereas dashed lines represents the theoretical model used in FEM. They concluded that predicted diagrams were found to be in reasonable agreement with the experimental data up to 1.5 % strain.

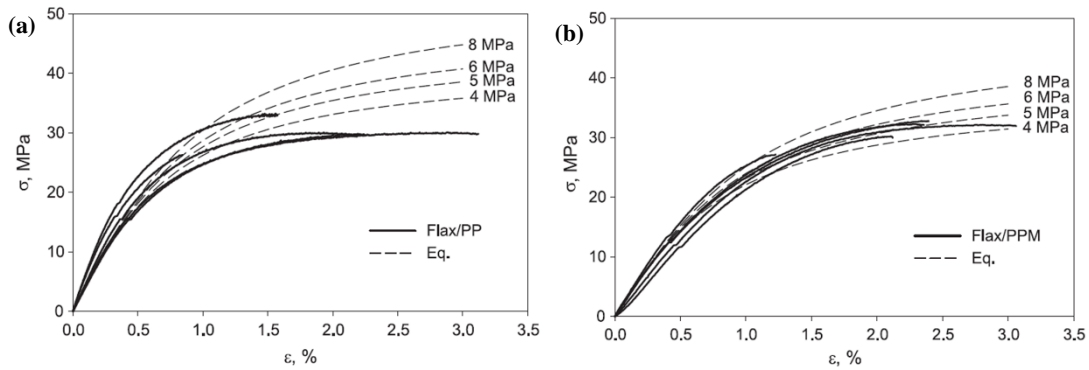


Figure 2.24. Stress-strain diagrams with volume fraction ratio of 0.2 for (a) Flax/PP and (b) Flax/PPM. Reprinted from [72] with permission from Elsevier)

Beakou et. al. [73] studied tensile strength flax fiber bundles. In their work, they modeled the fiber bundles in FE modeling tool. Based on optical micrographs, they recreated the bundle geometry. The key point of their study was to investigate middle lamella which is the zone in between two elementary fibers. Middle lamella was represented using bilinear cohesive zone model. In order to reduce of the computational cost, one quarter of the bundle (Figure 2.25) geometry was considered by the authors. Discretization was made with elements having 20 nodes and 3 DOF per node.

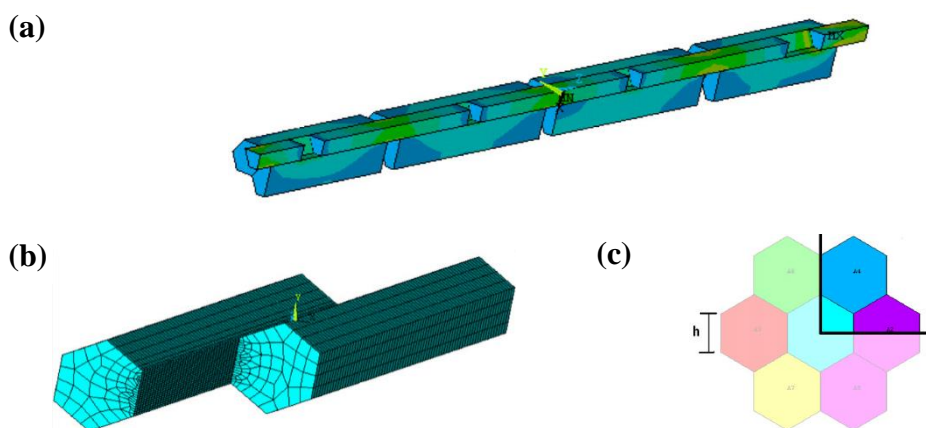


Figure 2.25. (a) Staggered geometry of post processed FEM, (b) Discretized fibers, (c) Idealized schematic lamella representation (Reprinted from [73] with permission from Elsevier)

Elastic properties were taken as: $E_L = 48.48$ GPa, $E_T = 13.29$ GPa, $G_{LT} = G_{TT} = 2.95$ GPa, and $\nu_{LT} = 0.183$. After simulations, it was determined that middle lamella region is critical in terms of load carrying capacity of fiber bundle. The experimental, simulation, and literature data results regarding bundle strength could be seen in Figure 2.26.

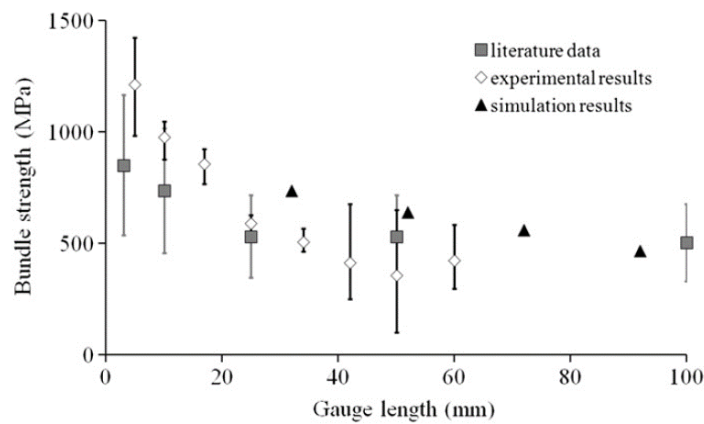


Figure 2.26. Bundle strength vs Gauge length plot. (Reprinted from [73] with permission from Elsevier)

Another numerical modeling study of flax fiber reinforced polymer composite was performed by Sliseris et. al. [74]. They created representative volume elements filled with short flax fibers having different aspect ratios making use of an algorithm. FE model of flax fibers was discretized with tetrahedron elements as shown in Figure 2.27. The study included 4 main material models for fibers, defects of fibers, interface zones in fiber bundles, and matrix. They modeled fiber with linear elastic, isotropy with a Young's modulus of 54 GPa, and Poisson's ratio of 0.2. Defects of the fibers were modeled with brittle material constitutive law and a transverse modulus of 2 GPa. In the interface zone, brittle material law was utilized as well with 1.627 GPa, Poisson ratio of 0.35 and transverse modulus of 0.3 GPa. Finally, polypropylene matrix was

modeled using plasticity with isotropic hardening having a tensile modulus of 1.627 GPa, Poisson's ratio of 0.35 and yield strength of 1.627 MPa.

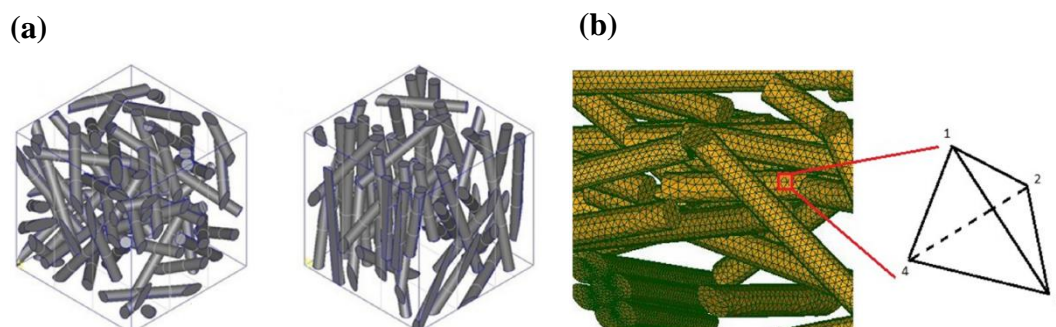


Figure 2.27. (a) Microstructures with different orientations; (b) Discretization of flax fibers with tetrahedron elements (Reprinted from [74] with permission from Elsevier)

Then, numerical model was compared with experimental data which seemed to be in fairly good agreement. Stress-strain behavior and tensile modulus according to aspect ratios can be seen in Figure 2.28.

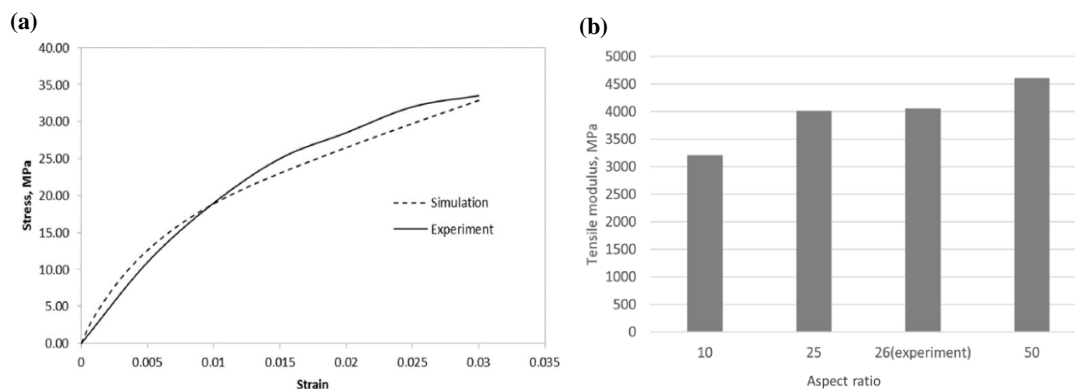


Figure 2.28. (a) Stress-Strain curve with simulation and experimental values; (b) Variation of tensile modulus with respect to aspect ratio (Reprinted from [74] with permission from Elsevier)

Thuault et. al. [75] modeled elementary flax fiber and simulated numerically to explore tensile mechanical behavior using finite element analysis. They made use of experimental data to develop a numerical multilayer model of flax fiber. In their model, flax fiber was assumed to be a 20 μm in diameter and 800 μm long cylinder. S1, S2, S3 layers were modeled with hollow cylinders and lumen is modeled in the central cavity (Figure 2.29). Quadratic 3D elements were used in finite element modeling. The MFA and S2 layer effects on tensile modulus were tried to be explored in detail. Young's moduli values of cellulose and hemicellulose were input as 134 and 16 GPa, respectively. Poisson's ratios were selected as 0.1 and 0.2.

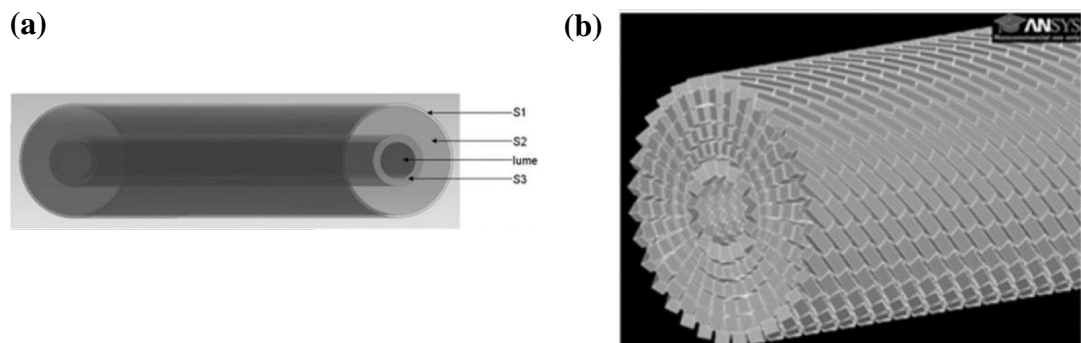


Figure 2.29. (a) FE modeling of elementary flax fiber; (b) micro fibril arrangement [75]

Finally, simulations showed that fiber mechanical properties are dramatically affected by S2 layer and MFA, cellulose content has an influence on fiber mechanical properties, and fiber ultrastructure drastically influence flax fiber longitudinal modulus values.

2.3.3. Constitutive Models

In this section, studies including a constitutive model are mentioned. These types of studies can be considered as the most advanced and current type of studies made in this field. Authors make use of a continuum mechanics approach to fully represent the mechanical properties of the flax fibers and compare simulation results with the

experimental data. For this purpose, rheological models are utilized which are based on elastic, plastic and viscous aspects.

Andersons et. al. [76] studied the quasi-UD flax fiber/epoxy composite based on orthotropy assumption. In their work, they used a semi empirical tensor-linear model to describe the nonlinear deformation under combined loading. They combined the deformation of UD ply with an elementary laminate theory to characterize stress-strain diagrams of laminated composites under tension. The governing theoretical model used is as follows:

$$\varepsilon_{\varphi} = a_{\varphi} \sigma_{\varphi} \sinh(p(\boldsymbol{\sigma})) / p(\boldsymbol{\sigma}) \quad (\text{Eq. 29})$$

where p is a nonnegative scalar function of the stress tensor and P is a continuous, strictly increasing function whose inverse function of $p(P)$ could be expressed in finite analytical form. For a nonlinear response in both tension and compression, authors used Lagzdins [77] form for $p = p(\boldsymbol{\sigma})$ as:

$$p(\boldsymbol{\sigma}) = (b_{ijkl} \sigma_{ij} \sigma_{kl})^{1/2} \quad (\text{Eq. 30})$$

ε_{φ} and σ_{φ} stand for the strain and stress in the loading direction, and b is nonnegative definite tensor. a_{φ} is respective compliance which is expressed as:

$$a_{\varphi} = \frac{\cos^4 \varphi}{E_1} + \frac{\sin^4 \varphi}{E_2} + \left(\frac{1}{G_{12}} - \frac{2\nu_{12}}{E_1} \right) \sin^2 \varphi \cos^2 \varphi \quad (\text{Eq. 31})$$

The theoretical model was compared with experimental data by the authors, as well for different loading directions:

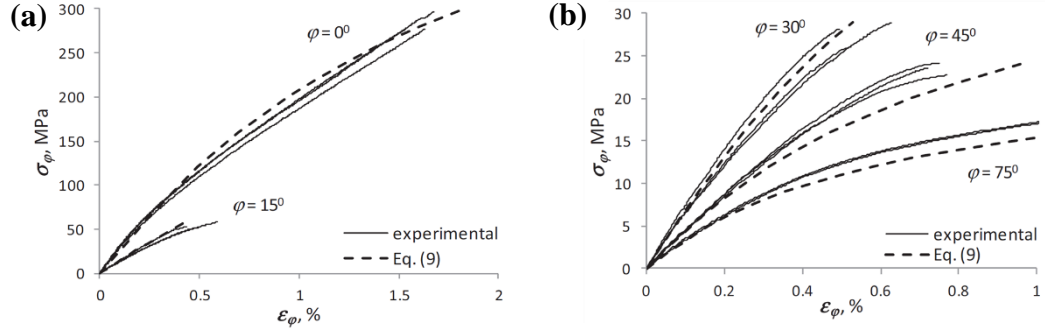


Figure 2.30. Stress-Strain diagrams for loading angles (a) 0°, 15°; (b) 30°, 45°, 75° (Reprinted from [76] with permission from Elsevier)

The close agreement between dashed and full lines is obvious from stress-strain curves of Figure 2.30 that theoretical modeling of the authors was accurate.

Poilâne et. al.[78] investigated flax fiber reinforced polymers under uniaxial loading in terms of volume fraction, titration of yarn reinforcement and temperature. In order to have a full understanding of the specimens in terms of elasticity, viscoelasticity, and viscoplasticity, they developed a phenomenological model based on eight independent parameters. They claimed that nonlinear behavior could only be attributed to viscoplastic effects and the model was created based on two hardening modes: linear and nonlinear. Material and mechanical behavior model could be explained briefly: the authors partitioned the total strain into two parts elastic (reversible strain) and inelastic (viscoelastic and viscoplastic):

$$\varepsilon = \varepsilon^e + \varepsilon^{in} = \varepsilon^e + \varepsilon^{ve} + \varepsilon^{vp} \quad (\text{Eq. 32})$$

Then state equations are written as:

$$\sigma = \rho \frac{\partial \psi}{\partial \varepsilon^e} \quad (\text{Eq. 33})$$

$$\chi_i = \rho \frac{\partial \psi}{\partial \alpha_i} \quad (\text{Eq. 34})$$

where χ_i and α_i stand for inelastic parameters, ρ is density, and σ is the Cauchy's stress. Then internal variable evolution is:

$$\dot{\varepsilon}^{in} = \frac{\partial \Omega}{\partial \sigma} = \dot{\varepsilon}^{ve} + \dot{\varepsilon}^{vp} \quad (\text{Eq. 35})$$

$$\dot{\alpha}_i = -\frac{\partial \Omega}{\partial X_i} \quad (\text{Eq. 36})$$

Then inelastic parameters were determined and system of equations were solved to get viscoelastic and viscoplastic responses. Finally, they obtained a repetitive stress-strain curve from simulations based on developed constitutive model and compared with experimental data:

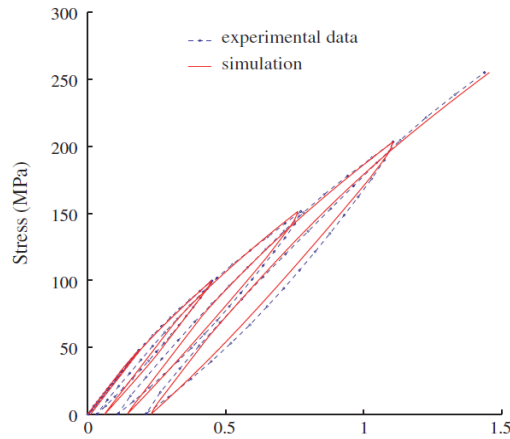


Figure 2.31. Stress-strain plot with experimental data and simulation (Reprinted from [78] with permission from Elsevier)

Rubio-Lopez et. al. [79] studied a rheological model to predict viscoplastic behavior of NFRCs. Their model was based on utilization of elastic, plastic, and viscous elements to determine mechanical response of the material under certain loading conditions. The model consisted of three branches in parallel: nonlinear elastic behavior of the material was modeled with Yeoh model, viscous behavior was

modeled with Maxwell model, and plasticity was represented by frictional analogy to the Maxwell model:

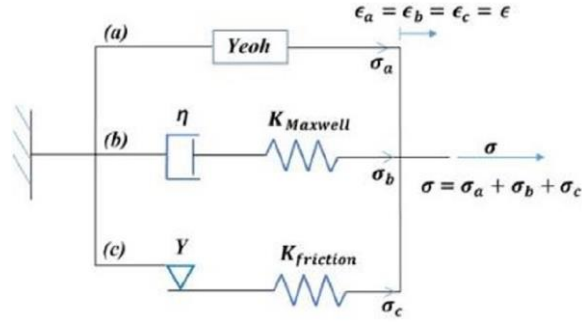


Figure 2.32. Author's philosophy of modeling NFPCs. (Reprinted from [79] with permission from Elsevier)

Governing equation for nonlinear Yeoh model under uniaxial tension is given below:

$$\sigma_{yeoh} = \frac{2\epsilon(3 + \epsilon(3 + \epsilon))((1 + \epsilon)^2 C_1 + \epsilon^2(3 + \epsilon)(2(1 + \epsilon)C_2 + 3\epsilon^2(3 + \epsilon)C_3))}{(1 + \epsilon)^2} \quad (\text{Eq. 37})$$

where C_1 , C_2 , C_3 are the elastic constants. The viscous behavior was introduced with Maxwell model as indicated. This analogy includes a series spring damper system of which stress is the same but strain is the sum of each component. From spring definition:

$$\sigma = K \cdot \epsilon \quad (\text{Eq. 38})$$

where K is spring constant and from viscous damper definition:

$$\sigma = \eta \frac{d\epsilon}{dt} \quad (\text{Eq. 39})$$

where η is damping constant, strain rate equation takes the form:

$$\dot{\sigma}_{Maxwell} + \frac{K}{\eta} \cdot \sigma_{Maxwell} = K \cdot \dot{\epsilon} \quad (\text{Eq. 40})$$

The plasticity was introduced via third branch which is the spring and a frictional element in series. This equation is 2 phase, at first model stiffness is dominated by the spring element up to activation of frictional element whose role is to set up a limit for the stress:

$$\begin{aligned} \text{if } \epsilon < \epsilon_y &\rightarrow \sigma_{friction} = K_{friction} \cdot \epsilon \\ \text{if } \epsilon \geq \epsilon_y &\rightarrow \sigma_{friction} = Y \end{aligned} \quad (\text{Eq. 41})$$

Then the constitutive equation of the global model becomes:

$$\sigma = \sigma_{Yeoh} + \sigma_{Maxwell} + \sigma_{Friction} \quad (\text{Eq. 42})$$

After derivation of global model, authors calibrated their model for unknown parameters. Finally, the comparison of experimental data (redline) and theoretical model (dotted line) for flax/PLA composite with different strain rates is presented in Figure 2.33.

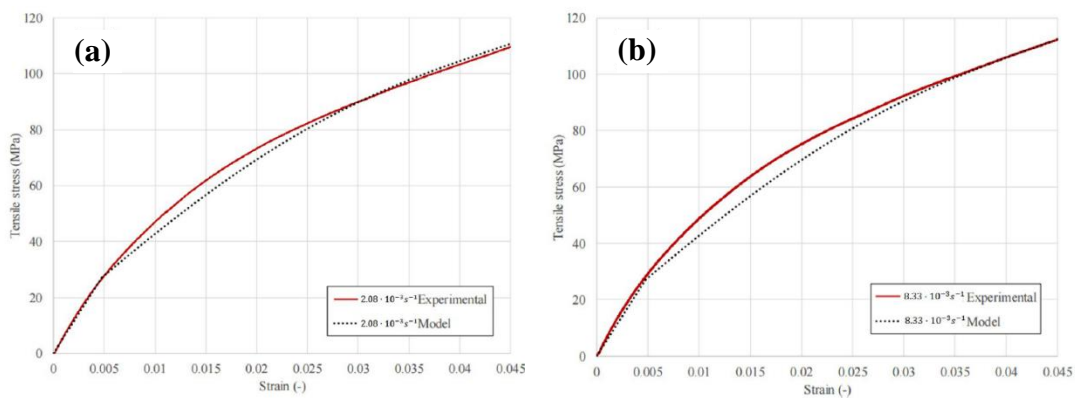


Figure 2.33. Comparison of experimental results and theoretical model of Flax/PLA composite for (a) small and (b) high strain rates (Reprinted from [79] with permission from Elsevier)

Studies including constitutive models of flax fiber composites are rather new field. Since parameters needed to create the models require extensive testing and not readily found in the literature, there are not many works published by authors. As it is explained above, most of the models are based on phenomenological models, which include a constitutive relation simulation on each aspect of the subject.

To sum up, this section mainly focused on material and finite element modeling studies published on the area of flax fiber composites. Studies are classified according to their advancement level. In the Section 2.3.1, preliminary studies conducted in this field are illustrated. Experiments to determine Young's modulus of the flax fiber and stress-strain behavior of both flax fiber and its composite were the main subjects. After determination of modulus (mostly longitudinal) then by using a linear micromechanical model, authors tried to predict this value without any simulations. What authors lacked were the transverse moduli, which is quite difficult to measure through the experiments. In the second part Section 2.3.2, somewhat more advanced studies are scanned. These studies include a FEM together with a theoretical micromechanical model. Developed FEMs benefit from the reproducibility of a RVE (representative volume element). Some of them contain results which were also correlated using experimental data. The last section addresses a few constitutive models for flax fiber composites. Investigated studies in this section contain computational mechanics models that are the most advanced type found in the literature. Yet, as indicated previously, since this is a relatively recent field, one could not find a wealth of information on many aspects. In general, having recognized the nonlinear and inelastic nature of deformation, authors created phenomenological constitutive models and calculated the stress-strain responses of various strain rate inputs.

CHAPTER 3

OBJECTIVE OF THE THESIS

In this chapter, objective and motivation of the thesis is elaborated and literature survey is summarized.

Use of NFRCs in structural application is a recent development. As indicated earlier, to be able to use these materials in dedicated applications, the material itself must be explored thoroughly. In this content, authors made several investigations to reveal the materials' intrinsic mechanical properties. Among the others, flax fiber and its composites came to the forefront with its superior characteristics. As a first step, experiments to predict elastic properties are conducted. Many authors tried to predict the mechanical behavior with a basic linear mathematical expression. Later on, as the know-how increased, detailed modeling and simulation works started. Flax fiber and its composites are modeled with FEM tools and modeling studies are supported with experiments. Furthermore, these models are used to fit a theoretical equation. Afterwards, constitutive phenomenological models are created which show the most advanced and recent status of this field. In the majority of the studies examined, the fiber and composites are explored under longitudinal tensile loading conditions which is the stiffest direction of the fiber. With its good specific properties, flax fibers are thought to replace some synthetic fibers like E-glass, yet only longitudinal merits are not enough. Glass fibers are isotropic materials whose properties are direction-independent. When used in composites under transverse loading, due to very high stiffness contrast with resins, probability of crack formation and a possible following failure is imminent [66]. For this very reason, the substitute material should overcome this weakness. Transverse stiffness of flax fiber is not as much as its longitudinal stiffness so that it has the potential to be introduced as this "substitute" material. In some of the publications, authors claimed that absence of

transverse crack needs to be investigated in detail [65, 66]. Transverse properties and response under high strain of flax fiber and its composites have to be scrutinized further to gain this know-how.

Currently, what exist in the literature could be shortly listed as well evaluated elastic properties of natural fibers including flax; stress-strain diagrams, micromechanical RVE based FE analyses and phenomenological models based on constitutive relations. What does not exist but needed for this “substitute” material is a material model and a complete FEA so that stress concentrations under transverse loading with high deformations can be examined. Similar studies are conducted in the literature but for different materials and focus points. In their work Sabuncuoglu and his co-workers [80] studied the stress concentrations in steel fiber composites having a hexagonal cross section under transverse loading conditions, and compared with conventional materials. Different volume fractions and multiple fiber packaging types were used in their RVEs. The obtained results demonstrate how stress concentrations change under transverse loading for different fiber geometries, volume fractions and packaging types.

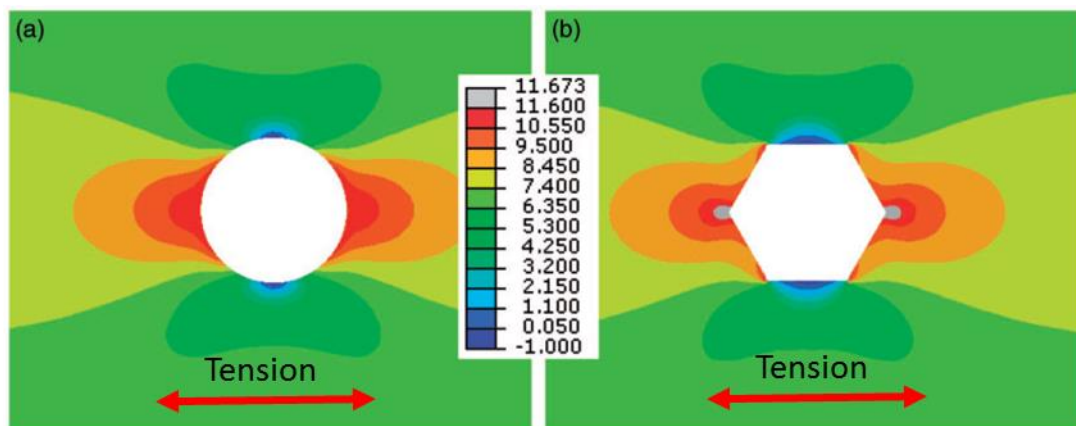


Figure 3.1. Max. principal stress distribution in the matrix with (a) circular and (b) hexagonal fiber cross sections [80]

In this thesis flax/epoxy composite is modeled and subjected to transverse loading conditions to investigate the stress concentrations including high strain inputs.

Comparisons with conventional synthetic fibers, namely carbon and glass fibers is done, as well. Modeling and material details are explained in forthcoming sections.

A Short summary of the publications that is reviewed is given in Table 3.1. As indicated earlier, RVE under transverse loading conditions is not common in literature especially in the flax fiber composites field.

Table 3.1. Literature review summary

Method	Author	Notes	Reference
Prediction of Elastic Properties	Baley, 2006	Longitudinal elastic modulus of flax fiber composite is determined using Halpin-Tsai equations and compared with experiments	[54]
	Shah, 2012	Flax fiber's longitudinal modulus is calculated using ROM and compared with experiments.	[65]
	Kersani, 2015	Longitudinal and transverse moduli values are calculated using Chamis formulate and experiments are conducted to compare theoretical data with various specimens.	[66]
	Baiardo, 2004	Tensile and shear modulus are calculated using ROM and Cox Shear Lag model. Then results are compared with experiments.	[67]
	Lamy, 2000	Stiffness of the flax-epoxy composite is predicted using ROM and compared with experiments.	[69]
	Garkhail, 2000	Elastic moduli of flax/PP and Flax/MAPP composites are determined using ROM and Cox Shear Lag model.	[64]
	Madsen, 2003	Longitudinal and transverse moduli of flax fiber composites are calculated with porosity assumptions.	[70]
	Straumit, 2017	Flax-Epoxy composite is modeled in finite element making use of X-Ray images and solved for fiber Young's modulus, then compared with experiments	[71]
	Modniks, 2013	Randomly distributed short flax fibers in RVE is investigated and elastic modulus is calculated, then results are compared with experiments showing close relation.	[72]
	Beakou, 2013	Flax fiber bundle is modeled in finite element methods, stiffness and strength properties are investigated.	[73]
FEM Models	Sliseris, 2016	Flax fibers are modeled in FEM tools in a RVE to study effect of different loading directions, then stiffness properties are predicted.	[74]
	Thauault, 2014	Flax fiber itself is modeled in FEM. The effect of MFA, S1, S2 and S3 layer is investigated.	[75]
	Anderson, 2015	A semi-empirical tensor-linear model for quasi-UD flax fiber-epoxy is created and solved for various loading directions.	[76]
	Poilane, 2014	A nonlinear constitutive model is created and solved for different strain rate inputs	[78]
Constitutive Models	Rubio-Lopez, 2016	Rheological model based on viscous behavior is created and solved for different strain rate inputs	[79]

CHAPTER 4

MATERIAL MODELING OF THE FLAX FIBER COMPOSITE

In this section, material modeling philosophy used in FE analyses in the content of the thesis is elaborated. Material model for each composite constituent is mentioned and methods are explained thoroughly. As indicated in previous sections, selected natural fiber and resin are flax and epoxy, respectively.

4.1. Flax Fiber Material Model

Being one of the stiffest bast fiber, flax fiber is known to have good mechanical properties. But its stress-strain behavior under tensile loading is quite different compared to classical synthetic fibers such as glass and carbon. In the previous part, the methods to obtain fiber's elastic properties are mentioned. In order to model the flax fiber for FEA, main approaches are observed to be based on linear elasticity and hyperelasticity [20, 74, 78, 92].

4.1.1. Flax Modeling Using Linear Elastic Approach

The mechanical behavior of solids is driven by constitutive stress-strain relations. These equations express the stress as a function of strain, strain rate, strain history, temperature and material properties. Elastic models do not include rate or history effects. The models can be defined as deformable continua which retract to their original shapes when deformation inducing loads are removed. In the linear elastic approach, constitutive stress-strain law is restricted to be linear. Most of the materials such as metals, plastics, ceramics, rock, concrete exhibit linear behavior under small deformations [81]. In linear elastic approach, material is assumed to be either isotropic or anisotropic. Isotropy is a fundamental material property which is related to directional independent mechanical behavior.

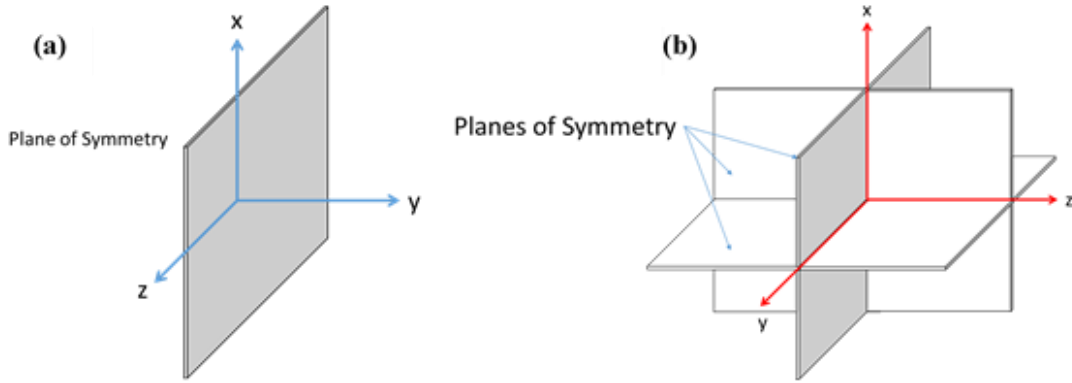


Figure 4.1. (a) Plane of symmetry, (b) planes of symmetry of orthotropic materials

Isotropic materials have infinite number of symmetry planes whereas anisotropic materials have a limited number of material symmetry. Isotropic elastic behavior can be modeled with two independent elastic constant: Young's modulus, E , and Poisson's ratio, ν . In the case of orthotropy, required independent elastic constants to represent material behavior is 9. Elastic compliance can be written as:

$$\begin{Bmatrix} \varepsilon_{11} \\ \varepsilon_{22} \\ \varepsilon_{33} \\ \gamma_{12} \\ \gamma_{13} \\ \gamma_{23} \end{Bmatrix} = \begin{bmatrix} 1/E_1 & -\nu_{21}/E_2 & -\nu_{31}/E_3 & 0 & 0 & 0 \\ -\nu_{12}/E_1 & 1/E_2 & -\nu_{32}/E_3 & 0 & 0 & 0 \\ -\nu_{13}/E_1 & -\nu_{23}/E_2 & 1/E_3 & 0 & 0 & 0 \\ 0 & 0 & 0 & 1/G_{12} & 0 & 0 \\ 0 & 0 & 0 & 0 & 1/G_{13} & 0 \\ 0 & 0 & 0 & 0 & 0 & 1/G_{23} \end{bmatrix} \begin{Bmatrix} \sigma_{11} \\ \sigma_{22} \\ \sigma_{33} \\ \sigma_{12} \\ \sigma_{13} \\ \sigma_{23} \end{Bmatrix} \quad (\text{Eq. 43})$$

Complete representation of flax fiber is assumed to be done making use of transversely isotropic material model which is a special subclass of orthotropy. This case characterizes plane of isotropy at every point in the material. In order to determine the material parameters, assuming 1-2 plane to be the plane of isotropy, one can write,

$$E_1 = E_2 = E_p \quad (\text{Eq. 44})$$

$$\nu_{31} = \nu_{32} = \nu_{tp} \quad (\text{Eq. 45})$$

$$\nu_{13} = \nu_{23} = \nu_{pt} \quad (\text{Eq. 46})$$

$$G_{13} = G_{23} = G_t \quad (\text{Eq. 47})$$

$$\frac{\nu_{tp}}{E_t} = \frac{\nu_{pt}}{E_p} \quad (\text{Eq. 48})$$

$$G_p = \frac{E_p}{2(1 + \nu_p)} \quad (\text{Eq. 49})$$

where p and t stand for in-plane and transverse, respectively. The resulting tensor consists of 5 independent elastic constants to characterize the behavior of transversely isotropic material. Then, elastic compliance takes the form

$$\begin{Bmatrix} \varepsilon_{11} \\ \varepsilon_{22} \\ \varepsilon_{33} \\ \gamma_{12} \\ \gamma_{13} \\ \gamma_{23} \end{Bmatrix} = \begin{bmatrix} 1/E_p & -\nu_p/E_p & -\nu_{tp}/E_t & 0 & 0 & 0 \\ -\nu_p/E_p & 1/E_p & -\nu_{tp}/E_t & 0 & 0 & 0 \\ -\nu_{pt}/E_p & -\nu_{pt}/E_p & 1/E_t & 0 & 0 & 0 \\ 0 & 0 & 0 & 1/G_p & 0 & 0 \\ 0 & 0 & 0 & 0 & 1/G_t & 0 \\ 0 & 0 & 0 & 0 & 0 & 1/G_t \end{bmatrix} \begin{Bmatrix} \sigma_{11} \\ \sigma_{22} \\ \sigma_{33} \\ \sigma_{12} \\ \sigma_{13} \\ \sigma_{23} \end{Bmatrix} \quad (\text{Eq. 50})$$

In order to model flax fiber as orthotropic material with transverse isotropy, these constants have to be found. Yet, constants must satisfy the stability requirements [82] provided below as well,

$$E_1, E_2, E_3, G_{12}, G_{13}, G_{23} > 0 \quad (\text{Eq. 51})$$

$$|\nu_{12}| < (E_1/E_2)^{1/2} \quad (\text{Eq. 52})$$

$$|\nu_{13}| < (E_1/E_3)^{1/2} \quad (\text{Eq. 53})$$

$$|\nu_{23}| < (E_2/E_3)^{1/2} \quad (\text{Eq. 54})$$

$$1 - \nu_{12}\nu_{21} - \nu_{23}\nu_{32} - \nu_{31}\nu_{13} - 2\nu_{21}\nu_{32}\nu_{13} > 0 \quad (\text{Eq. 55})$$

where 1-2 plane is plane of isotropy and 3 is the direction perpendicular to it. (Eq. 55) is the inequality which assures compressible material behavior. As the left-hand side approaches zero, material exhibits incompressible behavior [82]. These constants are selected from literature, i.e. mostly cited publications in flax fiber field of study. Three

candidate sets of constants to be used in FE analyses are selected. These parameters given in Table 4.1

Table 4.1. *Flax fiber orthotropic constants, compiled from literature*

Elastic Constant	Dataset#1	REF	Dataset #2	REF	Dataset #3	REF
E_3	70.0 GPa	[66]	62.3 GPa	[60]	70.0 GPa	[66]
E_1	8.0 GPa	[66]	5.8 GPa	[60]	8.0 GPa	[66]
G_{31}	4.6 GPa	[20]	4.6 GPa	[20]	4.6 GPa	[20]
G_{12}	1.9 GPa	[83]	1.87 GPa	[84]	2.5 GPa	[85]
ν_{31}	0.25	[66]	0.25	[66]	0.25	[66]

Each set is tested with given stability requirements using equations 51-55. The only dataset that satisfies the stability conditions is number 3. Therefore, these 5 independent material parameters are selected to be used in orthotropic material modeling of flax fiber under transverse isotropy assumption.

4.1.2. Flax Modeling Using Hyperelastic Approach

Hyperelastic approach to model flax fiber is an alternative method in the study. As it is mentioned in literature review section, actual response of the flax under loading is inelastic, visco-elastic plastic. But it is quite complex and cumbersome to model this material with those mechanical aspects and the readily available knowledge in the literature. Recalling the stress-strain curve of flax fiber, the bilinear and a nonlinear zone indicate that modeling flax fiber requires a different treatment.

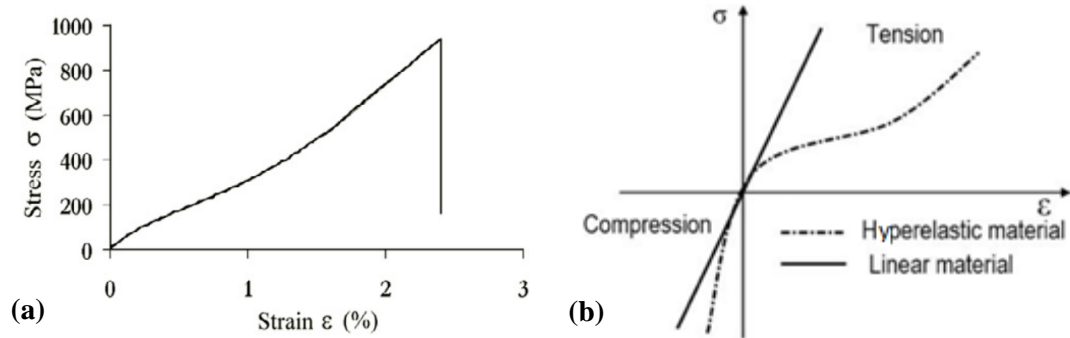


Figure 4.2. (a) Flax fiber stress-strain curve (Reprinted from [61] with permission from Elsevier) ; (b) representative linear and hyperelastic stress-strain curve [86]

From Figure 4.2, behavior of flax fiber subjected to tension shows some resemblance with hyperelastic material behavior which is isotropic and nonlinear. Yet, although the stress strain curves are similar, the behavior of flax fiber depicted in Figure 4.2 occurs at much smaller strain values compared to most of the hyperelastic materials. In order to use this material model properly in FEA, parameters have to be determined in advance. To do so, material test data module of ABAQUS® is used. In this module, several types of test data including uniaxial, biaxial, planar, and volumetric need to be input, then these experimental data are fit to a strain energy potential by the software. Convergence information of input data is presented at the end to select the most appropriate strain energy potential with its parameters to model the subject as closely as in the real case. In this study, particularly for flax fiber, only available test data is uniaxial test which is in fact not fully accessible. The data points to be used in material modeling are extracted from a frequently cited stress-strain curve taken from literature [61]. An open-source software is used to extract the data points from the stress-strain curve. Due to lack of test data regarding biaxial, planar and volumetric, only uniaxial test data is used.

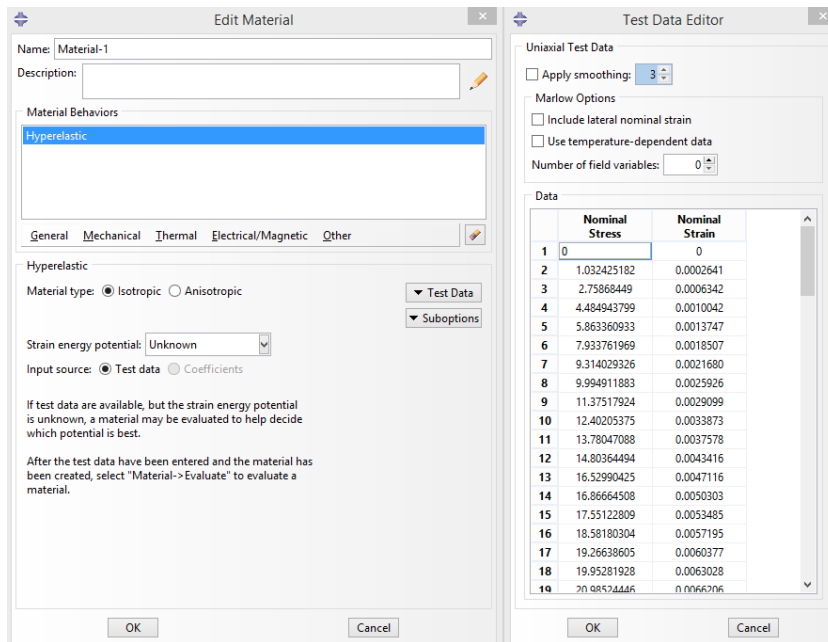


Figure 4.3. Test data input to ABAQUS®

Since transverse tensile test of a single fiber is very hard to conduct, an assumption is made using the information on the literature. The obtained data points are scaled 1-to-10 [23] in terms of stress and stress-strain curve is reconstructed (Figure 4.4), and input to software is done using scaled data points. The reason of this scaling is that transverse tensile testing of a single elementary fiber is quite troublesome, and nearly impossible. Due lack of knowledge in the literature about transverse testing, this assumption is made based on reviewed publications.

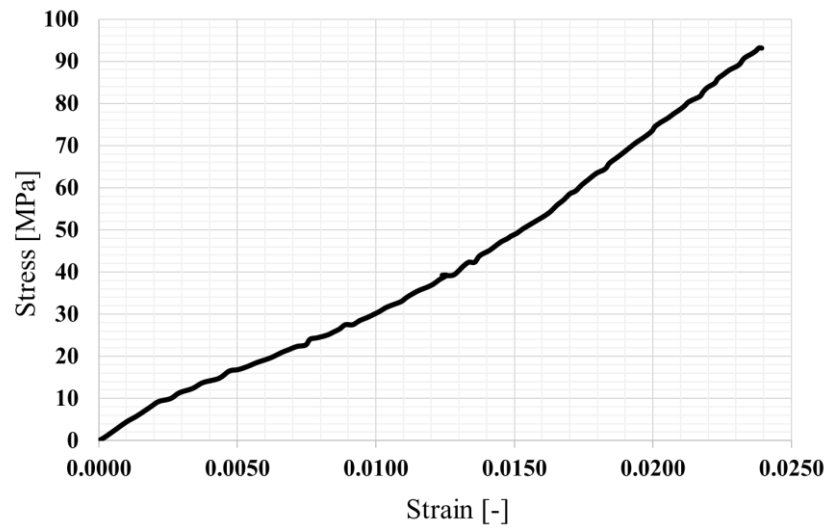


Figure 4.4. Scaled Stress-Strain curve used for the transverse load application

As explained above, scaled data points are input to software as shown in Figure 4.3. After an evaluation, software suggests different strain energy potentials which could be used in modeling, yet, with different stability results. The models suggested by the software are Mooney-Rivlin, Polynomial, Reduced Polynomial, Ogden, Arrude-Boyce, Van Der Waals and Marlov. Two models showing a good agreement with the test data is selected, namely, Ogden and Reduced Polynomial strain energy functions. Stability limit information of these both functions is shown in Figure 4.5.

(a) HYPERELASTICITY - OGDEN STRAIN ENERGY FUNCTION WITH N = 3

I	MU_I	ALPHA_I	D_I
1	-1642855.60	2.00011336	0.00000000
2	1075069.76	4.00011164	0.00000000
3	568991.065	-1.99988301	0.00000000

STABILITY LIMIT INFORMATION

UNIAXIAL TENSION: STABLE FOR ALL STRAINS
 UNIAXIAL COMPRESSION: STABLE FOR ALL STRAINS
 BIAxIAL TENSION: STABLE FOR ALL STRAINS
 BIAxIAL COMPRESSION: STABLE FOR ALL STRAINS
 PLANAR TENSION: STABLE FOR ALL STRAINS
 PLANAR COMPRESSION: STABLE FOR ALL STRAINS
 VOLUMETRIC TENSION: STABLE FOR ALL VOLUME RATIOS
 VOLUMETRIC COMPRESSION: STABLE FOR ALL VOLUME RATIOS

(b) HYPERELASTICITY - POLYNOMIAL STRAIN ENERGY FUNCTION WITH N = 3

D1	C10	C01	C02	C03
D2	C20	C11	C12	
D3	C30	C21	C22	
0.00000000	555.808942	0.00000000		
0.00000000	-41831.1876	0.00000000	0.00000000	
0.00000000	34467917.0	0.00000000	0.00000000	0.00000000

STABILITY LIMIT INFORMATION

UNIAXIAL TENSION: STABLE FOR ALL STRAINS
 UNIAXIAL COMPRESSION: STABLE FOR ALL STRAINS
 BIAxIAL TENSION: STABLE FOR ALL STRAINS
 BIAxIAL COMPRESSION: STABLE FOR ALL STRAINS
 PLANAR TENSION: STABLE FOR ALL STRAINS
 PLANAR COMPRESSION: STABLE FOR ALL STRAINS
 VOLUMETRIC TENSION: STABLE FOR ALL VOLUME RATIOS
 VOLUMETRIC COMPRESSION: STABLE FOR ALL VOLUME RATIOS

Figure 4.5. Output of (a) Ogden; (b) Reduced polynomial strain energy functions

The analysis results suggest the Ogden and Reduced Polynomial strain energy functions are suitable for input data to be used to model the hyperelastic behavior. The formulation of these models are as follows,

$$U_{OGDEN} = \sum_{i=1}^N \frac{2\mu_i}{\alpha_i} (\bar{\lambda}_1^{\alpha_i} + \bar{\lambda}_2^{\alpha_i} + \bar{\lambda}_3^{\alpha_i} - 3) + \sum_{i=1}^N \frac{1}{D_i} (J^{el} - 1)^{2i} \quad (\text{Eq. 56})$$

where $\bar{\lambda}_i$ are the deviatoric principal stretches $\bar{\lambda}_i = J^{-\frac{1}{3}} \lambda_i$; λ_i are the principal stretches; N is strain energy function order; and μ_i, α_i, D_i are the material parameters.

$$U_{R,Poly} = \sum_{i+j=1}^N C_{ij} (\bar{I}_1 - 3)^i (\bar{I}_2 - 3)^j + \sum_{i=1}^N \frac{1}{D_i} (J^{el} - 1)^{2i} \quad (\text{Eq. 57})$$

where C_{ij} and D_i are material parameters; \bar{I}_1 and \bar{I}_2 are the first and second deviatoric strain invariants defined as:

$$\begin{aligned} \bar{I}_1 &= \bar{\lambda}_1^2 + \bar{\lambda}_2^2 + \bar{\lambda}_3^2 \\ \bar{I}_2 &= \bar{\lambda}_1^{-2} + \bar{\lambda}_2^{-2} + \bar{\lambda}_3^{-2} \end{aligned} \quad (\text{Eq.58})$$

Parameters calculated via the software is presented in Table 4.2 and Table 4.3

Table 4.2. *Ogden Strain Energy Function Parameters Calculated by ABAQUS®*

μ_1	α_1	μ_2	α_2	μ_3	α_3	D_1	D_2	D_3
-1642856	2.000113	1075070	4.000112	568991.1	-1.99988	0	0	0

Table 4.3. *Reduced Polynomial Strain Energy Function Parameters Calculated by ABAQUS®*

c_{10}	c_{20}	c_{30}	d_1	d_2	d_3
555.8089	-41831.2	34467917	0	0	0

Stress-strain curve is reconstructed with literature data points and strain energy function parameters to see the agreement, which could be observed in Figure 4.6.

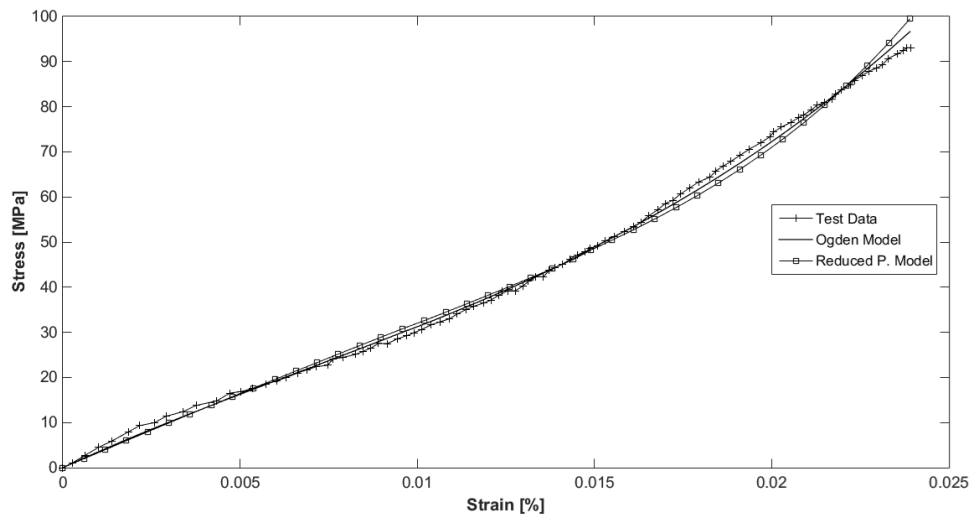


Figure 4.6. Stress-strain plot of evaluated hyperelastic potential functions and the literature test data

From the plot it is clear that Ogden strain energy function shows quite similar behavior compared to the test data. Therefore, it is eligible to be used in FEA as flax fiber material model. Note that while hyperelastic model gives a stress strain behavior similar to that of flax fiber, the transverse isotropic nature of fibers is not represented.

4.2. Epoxy Matrix Material Modeling

Epoxy is a commonly used thermoset type resin. In this study epoxy is modeled as elastoplastic material. Materials elastic properties and plastic strain data are selected from literature [87].

Table 4.4. *Epoxy matrix elastic properties*

Material Property	Value
Young's Modulus, E	2.95 GPa
Poisson's Ratio, ν	0.4

Isotropic hardening is employed for plastic region. Strain input as material property is total strain, which is calculated as:

$$\varepsilon^{total} = \varepsilon^{el} + \varepsilon^{pl} \quad (\text{Eq. 59})$$

where ε^{el} is the elastic strain, $\varepsilon^{el} = \sigma/E$; ε^{pl} is the plastic strain which is taken from [87]. With all this information, stress-strain diagram of epoxy is constructed in Figure 4.7:

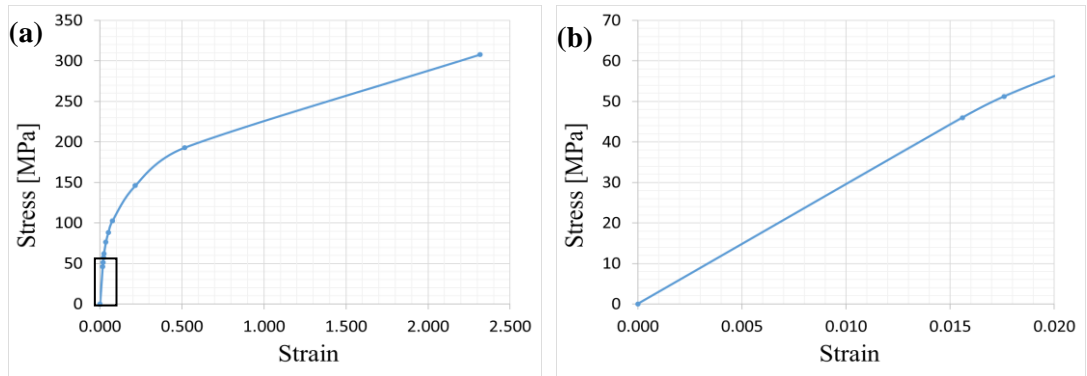


Figure 4.7. Epoxy matrix total stress-strain: (a) the entire curve; (b) zoomed view up to 0.02 strain [87]

4.3. Material Models Used in Thesis

To model the flax fiber, two alternative approaches seem to be appropriate for the analyses. These are orthotropy with transverse elasticity and hyperelasticity. Considering nature of the fiber, anisotropic and nonlinear behavior, both models have deficiencies. In linear elastic approach, material itself does not behave linearly under high deformations. Yet, for small strains, these nonlinear behavior does not make much difference. Additionally, directional dependent properties are better emphasized and reflected to models via orthotropic elastic approach. On the other hand, since material response is nonlinear, inelastic approach seems to be more appropriate at first glance. But, Ogden strain energy function is valid for isotropic materials and direction-dependent behavior would be lacked if this model was selected. To reflect anisotropy, 4th order strain potentials are needed which cannot be found in the literature. Considering the main focus in this study, transverse behavior is more crucial and is a

reason of choice in itself. Elastic properties of synthetic fibers used in this study for comparison also presented in Table 4.5 (L and T represent longitudinal and transverse respectively):

Table 4.5. *Elastic properties of synthetic fibers*

Glass	Carbon
$E = 72 \text{ GPa}$	$E_L = 276 \text{ GPa}$
$\nu = 0.25$	$E_T = 10.3 \text{ GPa}$
	$G_{TT} = 3.8 \text{ GPa}$
	$G_{LT} = 27.9 \text{ GPa}$
	$\nu_{LT} = 0.26$

In summary, considering their advantages and disadvantages, flax fiber is decided to be modeled using orthotropic elastic approach. However, the validity of this choice will be checked by analyzing stresses on the flax fiber itself in Appendix A. By doing so, all five independent elastic constants are selected from literature given in section 4.1.1 on Table 4.1, dataset number 3. As mentioned, epoxy is modeled by elasto-plastic approach.

CHAPTER 5

FEM DESCRIPTION OF THE FLAX FIBER COMPOSITE

In this chapter, finite element models are created to investigate stress concentrations in the flax fiber composite. Three types of RVEs (Representative Volume Element) are used through the evolution of the study, namely; single RVE, hexagon RVE and random RVE. Analysis models, discretization, mesh structure, material models, element types, geometric constraints, boundary conditions, and post-processing methods are mentioned. All these aspects are created via Python® scripts and calculations are performed in Abaqus® finite element software.

RVE is a statistical representation of the typical material properties [88]. In order to simulate the material properly, there are some criteria to be satisfied within the concept of RVE. RVE should be selected sufficiently large with respect to micromechanical model. Furthermore, the information it contains has to well reflect the microstructure, and shall be a good representation of a continuum [88]. Elementary flax fiber shape is assumed to be circular, and diameter is taken 25 μm as determined for the average value of flax fibers [89]. The bonding between fiber and the matrix is assumed perfect. Several authors also made this assumption as indicated in Section 2.3.1. Most of the studies including this assumption is based on linear elastic modeling approaches [54, 65, 67, 69]. A mesh sensitivity study is also conducted and presented in the results section. Hereinafter, RVEs containing the information of conducted research are used in FEA.

5.1. Single Fiber RVE of Flax-Epoxy Composite

Initially, single fiber model is constructed to observe stress concentrations on the vicinity of fiber itself without the effect of other fibers. For this purpose, a square RVE (Figure 5.1) is created with edge dimensions 15 times diameter of the fiber, which is

375 μm with a thickness of 37.5 μm , to prevent the edge effect on the stress distribution. With this representation, fiber is assumed to be in an infinite medium.

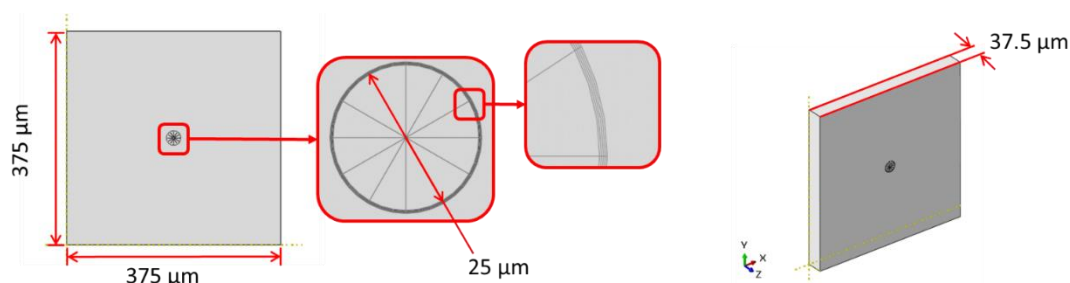


Figure 5.1. Single fiber RVE dimensions

After creation of geometry, material properties and boundary conditions are assigned respectively. As it is explained in previous chapter, flax fiber is modeled as orthotropic with transverse elasticity and epoxy matrix is modeled elasto-plastic. Next step is discretization. The model is meshed considering proper calculation of stresses around the fibers accurately, meaning that interface regions between fiber and matrix is modeled with denser meshes as shown in Figure 5.2. The thickness and width of those elements are assigned as 0.01 and 0.005 of fiber diameter, respectively. A sensitivity analysis is conducted as well, showing that assigned mesh size is dense enough to obtain accurate results with reasonable computational cost. Since the model includes some nonlinearity the element type used in analyses is C3D8R for both fiber and matrix, eight-node with reduced integration. Then, boundary conditions are assigned to the analysis model.

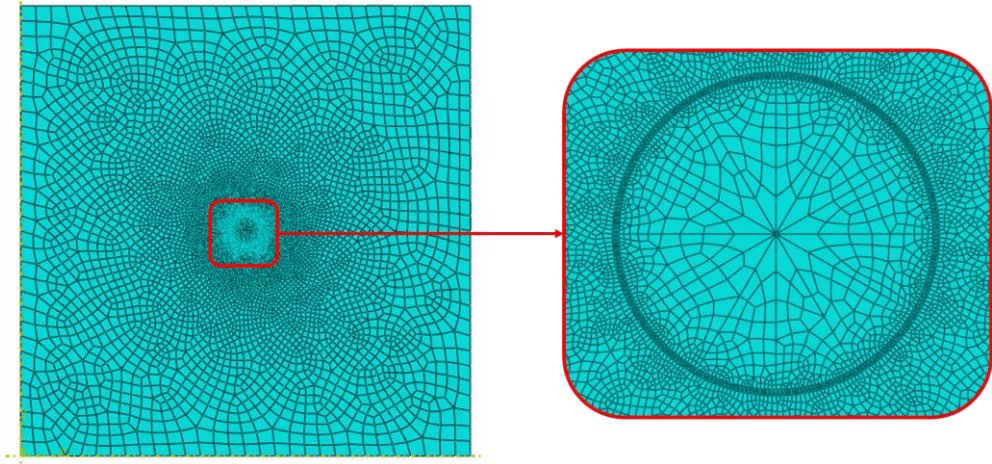


Figure 5.2. Single RVE mesh structure

The RVE is exposed to transverse strain from right and left surfaces, which is x-direction (direction-1). Top and bottom surfaces in y-direction (direction-2) are kept free, whereas front and back surfaces in z-direction (direction-3) are constrained so as not to move (Figure 5.3). List of boundary conditions could be seen in Table 5.1

Table 5.1. *Single RVE boundary conditions*

Surface	Displacement	Value
Right	U_1	$\varepsilon_0/2 \times RVE \text{ Side Length}$
Left	U_2	$-\varepsilon_0/2 \times RVE \text{ Side Length}$
Front	U_3	0
Back	U_4	0
Top	U_5	Free
Bottom	U_6	Free

After assigning boundary condition, analyses are run with various transverse strain values. Then, normal and shear stress concentrations around the fiber itself, and horizontal stress concentrations from the surface of the fiber to the RVE edge is obtained in the post process stage.

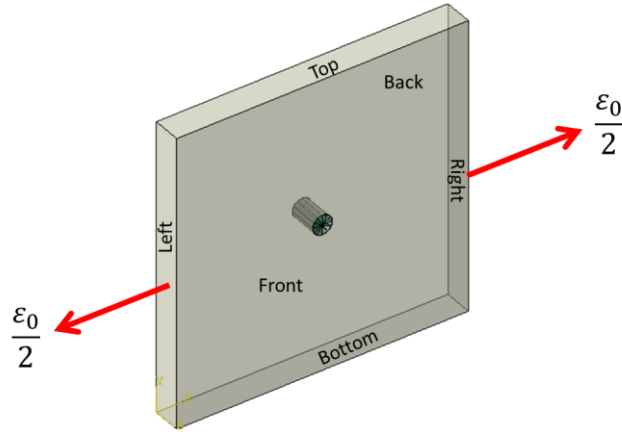


Figure 5.3. Boundary conditions shown on the RVE

5.2. Hexagon RVE of Flax-Epoxy Composite

After completion of single fiber RVE, hexagon RVE is created as second step. One reason to use hexagon RVE is that it gives more accurate and credible results compared to other regular packing types like square [90]. Just like single fiber RVE, vicinity of central fiber is properly seeded to obtain 2 layers of finer meshes. Being different from the previous case, fiber volume ratios are introduced to the analysis model. Model dimensions are determined with respect to fiber diameter and volume fraction ratio. Short edge of RVE is A , long edge is B and r_f is the fiber radius (Figure 5.4). Making use of fiber volume ratio, geometry and constant thickness, dimensions of RVE are calculated as:

$$v_f = \frac{A_{fiber}t}{A_{RVE}t} = \frac{2\pi r_f^2}{AB}, \quad B = A\sqrt{3} \rightarrow A = \sqrt{\frac{2\pi r_f^2}{v_f\sqrt{3}}} \quad (\text{Eq. 60})$$

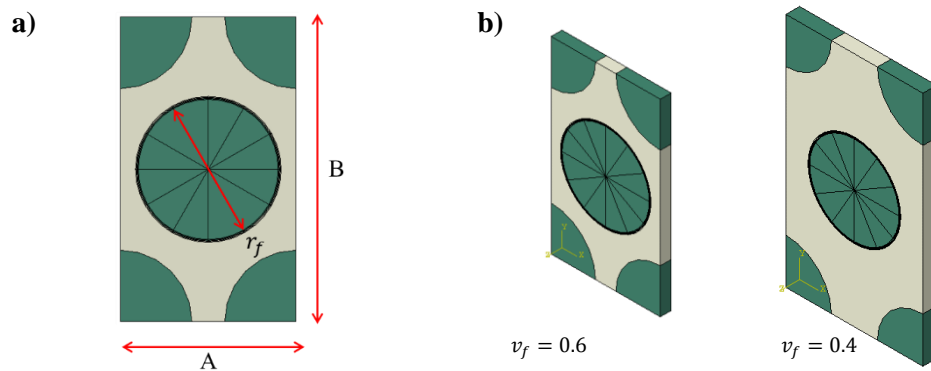


Figure 5.4. Hexagon RVE: a) Dimensions, b) isometric view with 0.4 and 0.6 fiber volume fractions with the same fiber diameter

Then material properties are assigned to related regions including central fiber, quarter fibers and the matrix. Boundary conditions are defined as follows: transverse strain is applied in x -direction and Poisson contraction is applied for the other directions. After that, RVE is discretized with C3D8R type elements, 8-node reduced integration with hourglass control. Fine mesh density in the vicinity of the central fiber is essential to obtain stresses properly. Boundary conditions are shown and listed in Figure 5.6 and Table 5.2 respectively, indices T stands for transverse, whereas L stands for longitudinal.

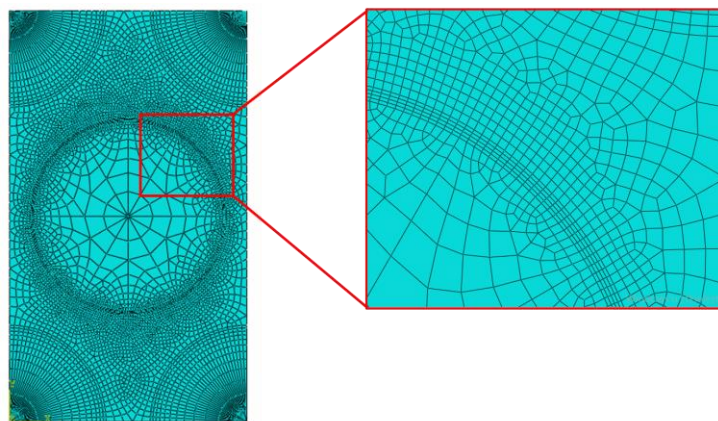


Figure 5.5. Mesh structure of hexagon RVE

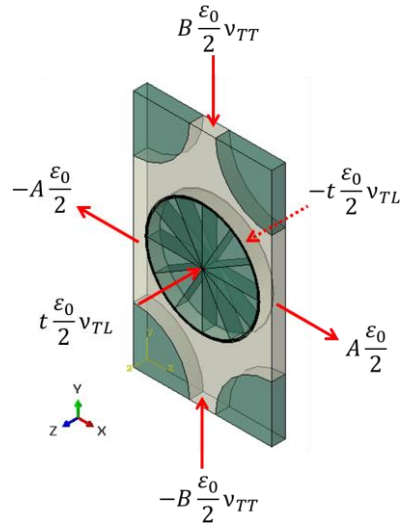


Figure 5.6. Boundary conditions shown in hexagon RVE

Table 5.2. Boundary conditions for hexagon RVE

Side	Displacement	Value
X1	U_x	$A \frac{\epsilon_0}{2}$
X2	U_x	$-A \frac{\epsilon_0}{2}$
Y1	U_y	$B \frac{\epsilon_0}{2} \nu_{TT}$
Y2	U_y	$-B \frac{\epsilon_0}{2} \nu_{TT}$
Z1	U_z	$t \frac{\epsilon_0}{2} \nu_{TL}$
Z2	U_z	$-t \frac{\epsilon_0}{2} \nu_{TL}$

5.3. Random RVE of Flax-Epoxy Composite

Random is the third and final type of RVE that is investigated in the content of the thesis. Due to inherent nature of the flax fibers, whether they are used in UD forms or others, random distribution is quite appropriate for simulations. As in the case of previous ones, RVE is created with calculated dimensions, but since multiple fibers

are modeled, a distribution technique is required. For this purpose, a randomization algorithm is taken from literature that is developed by Melro et. al. [91] and implemented to the model. The code randomly distributes fibers in a certain RVE according to the fiber diameter and requested fiber volume ratio. Fiber volume fraction is also introduced to analysis models. Assigned boundary conditions are the same with hexagon RVE as shown in figure below:

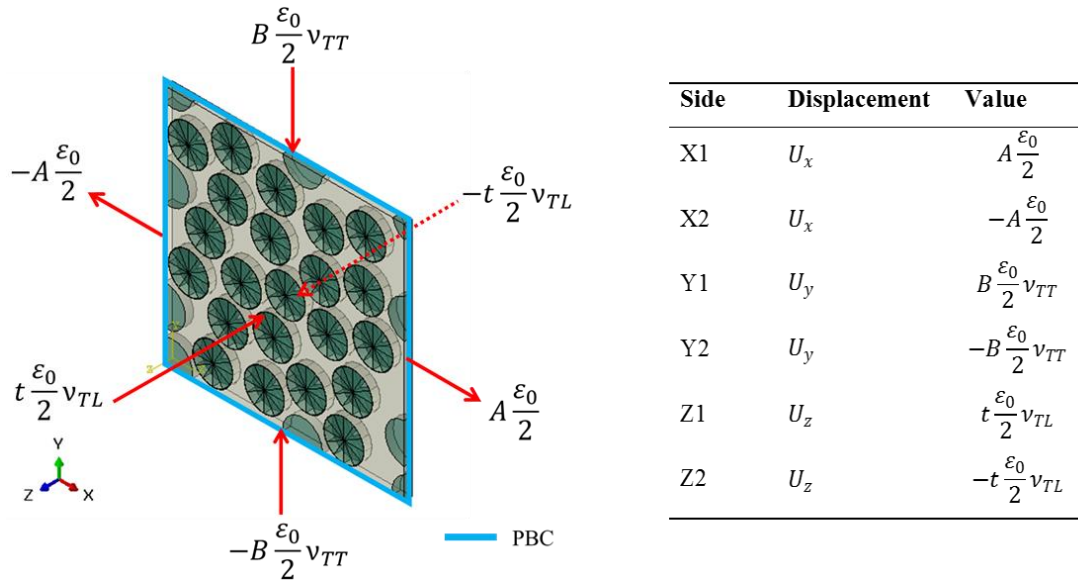


Figure 5.7. Boundary conditions for random RVE

Being different from hexagon RVE, periodic boundary conditions (PBC) are applied to random distribution as well in order to simulate a large system by using the unit cell. In the PBC, each nodes on sides of the RVE is connected to a symmetric hypothetical counter node. By doing so, computational cost is avoided and the response of the large model is representatively calculated.

The mathematical explanation of PBC is as following. The displacement field for the periodic structure can be written as:

$$u_i(x_1, x_2, x_3) = \varepsilon_{ij}^0 x_j + u_i^*(x_1, x_2, x_3) \quad (\text{Eq. 61})$$

where ε_{ij}^0 is the global strain tensor and $\varepsilon_{ij}^0 x_j$ is the linear distributed displacement field, and $u_i^*(x_1, x_2, x_3)$ is the periodic function from one unit cell to the another one which stands for a modification to the linear displacement field due to the heterogeneous structure of the composite. Because the periodic array of the repeated unit cells represents a continuous body, conditions of continuous displacements and same traction distributions at the opposite parallel boundaries, have to be satisfied at the neighboring unit cell boundaries. Eq. 61 could satisfy the continuous displacement related requirement but it cannot hold for the latter since the term $u_i^*(x_1, x_2, x_3)$ is not known. Each unit cell boundary surface have to be seen in parallel pairs, and the displacement of these opposite boundaries can be written as:

$$u_i^{k+} = \varepsilon_{ij}^0 x_j^{k+} + u_i^* \quad (\text{Eq. 62})$$

$$u_i^{k-} = \varepsilon_{ij}^0 x_j^{k-} + u_i^* \quad (\text{Eq. 63})$$

where k^+ and k^- depict the k^{th} couple of two opposite parallel boundary surfaces of a repeated unit cell. Taking into account $u_i^*(x_1, x_2, x_3)$ is the same at two parallel boundaries due to periodicity, the difference between Eq. 62 and Eq. 63 becomes

$$u_i^{k+} - u_i^{k-} = \varepsilon_{ik}^0 (x_j^{k+} - x_j^{k-}) = \varepsilon_{ij}^0 \Delta x_j^k \quad (\text{Eq. 64})$$

Δx_j^k is constant for each pair of the parallel boundary surfaces with specified ε_{ij}^0 , right hand side of the equation becomes constant [93]. The statement given in Eq. 64 is

defined to the finite element solver via tying node function and it specifies displacement difference between two opposite boundaries. Yet, Eq. 64 does not guarantee traction continuity conditions. The traction continuity condition can be written as

$$\sigma_n^{k+} - \sigma_n^{k-} = 0, \quad \sigma_t^{k+} - \sigma_t^{k-} = 0 \quad (\text{Eq. 65})$$

where n and t stand for normal and shear stresses at the corresponding parallel boundary surfaces. For general periodic boundary value problems, equations 64 and 65 are a complete set of boundary conditions. In order to reflect PBC defined in (Eq. 64) to the FEM, the meshing at each two paired boundary surfaces have to be the same. At each pairing node, only two displacement components coming from constraint equation (Eq. 64) is stored. Then it is reflected to FEM via a code.

In the RVE numerical analyses, average strain and stress over all elements are computed by taking the stress and strain from each and every element and multiplying them with the volume of that very element. The average stress and strain components are defined as:

$$\bar{\sigma}_{ij} = \frac{1}{V} \int_V \sigma_{ij} dV \quad (\text{Eq. 66})$$

$$\bar{\varepsilon}_{ij} = \frac{1}{V} \int_V \varepsilon_{ij} dV \quad (\text{Eq. 67})$$

The strain energies calculated by different boundary conditions have to satisfy the following inequality for the same value of $\bar{\varepsilon}_{ij}$

$$U^t \leq U^p \leq U^d \quad (\text{Eq. 68})$$

where t, p and d superscripts stand for homogeneous traction boundary conditions, periodic boundary conditions and displacement boundary conditions respectively [93]. It is obvious that homogeneous displacement boundary conditions overestimate the effective moduli which is calculated as:

$$C_{ijkl} = \frac{\sigma_{ij}}{\varepsilon_{kl}} \quad (\text{Eq. 69})$$

On the contrary, homogeneous traction boundary conditions underestimate it. The PBC illustration is depicted in Figure 5.8.

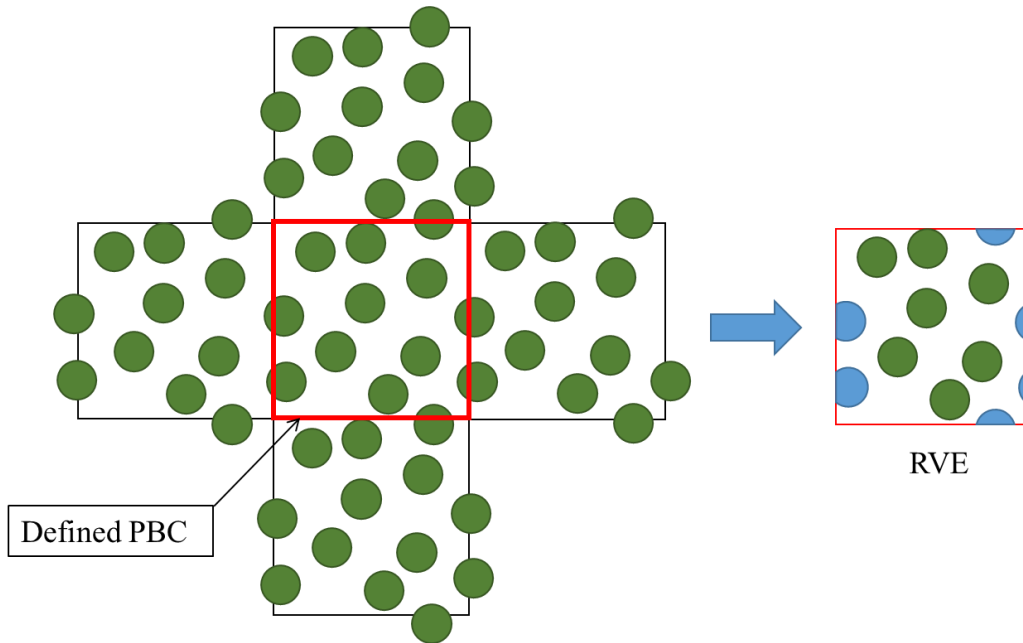


Figure 5.8. Representation PBC and Random RVE

Analysis models of 0.6 and 0.4 fiber volume fraction can be observed from Figure 5.9.

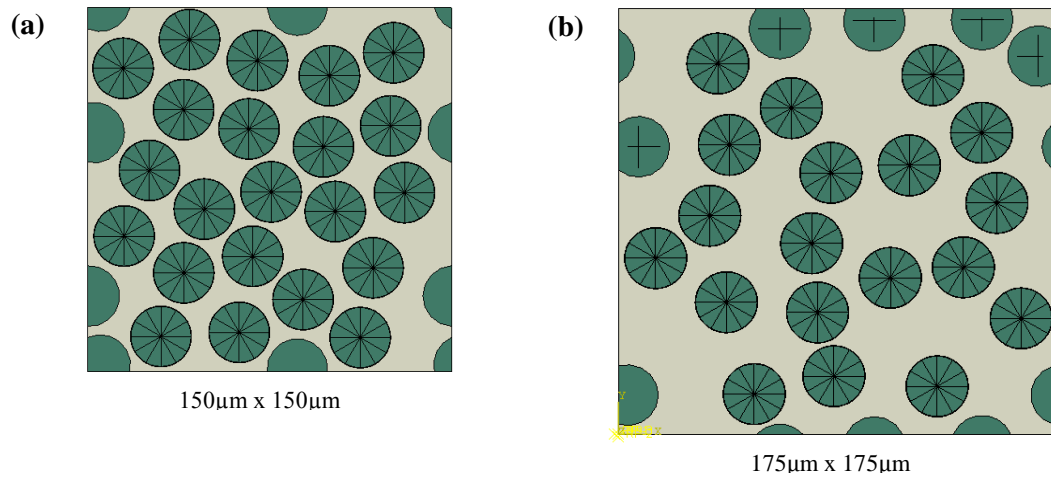


Figure 5.9. Random RVEs with fiber volume fraction of (a) 0.6 and (b) 0.4

Then, model is discretized with C3D8R elements considering the close vicinity of each fiber to obtain a proper stress distribution.

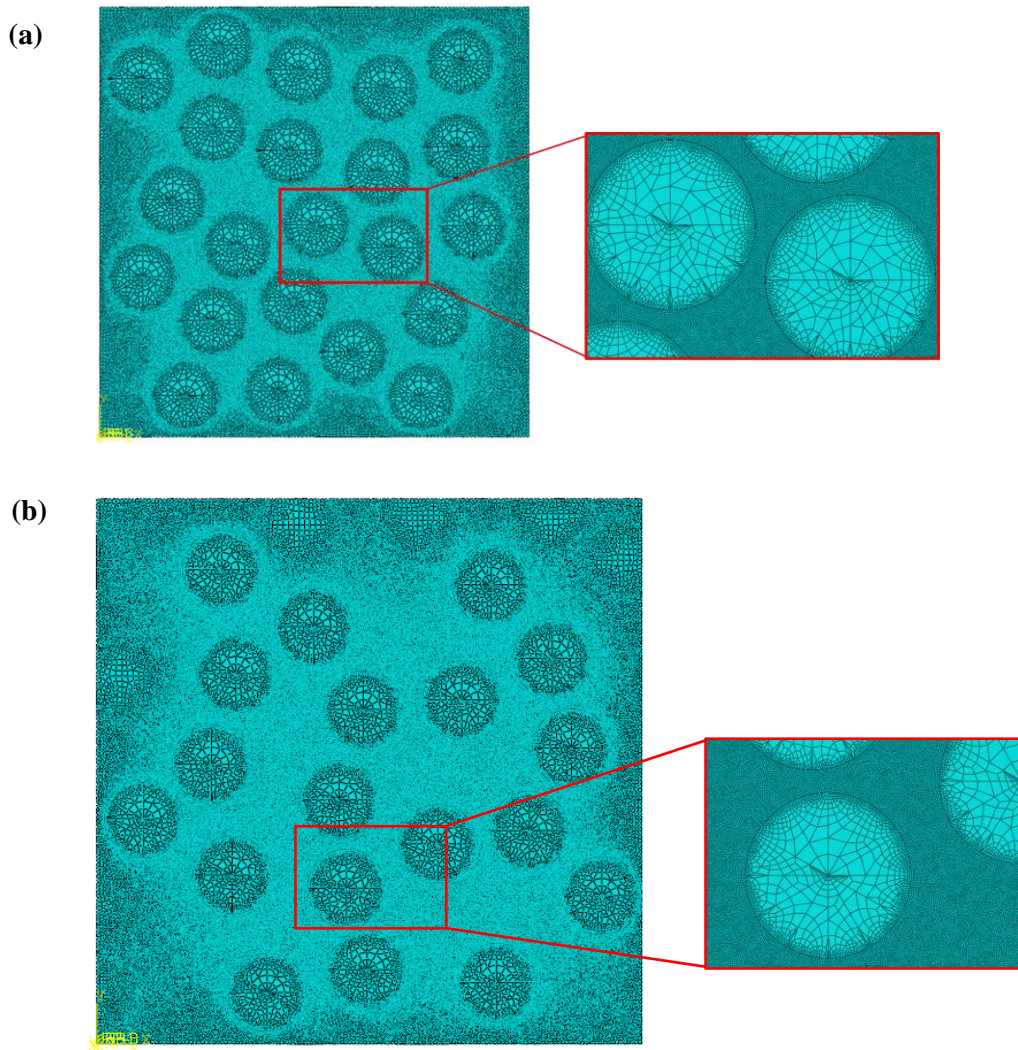


Figure 5.10. Mesh structures of random RVEs with fiber volume ratios of (a) 0.6 and (b) 0.4

5.4. Evaluation Method of Stress Outputs

After running the analyses with different parameter inputs, which is explained in next chapter, the stress outputs are obtained. In this part, methodology to evaluate the stress concentrations is explained.

At the end of each run maximum stress values, radial, shear stresses around the fiber within a predefined path are extracted and printed via Python® script. Then, these

values are normalized with average composite stress in load direction as given in (Eq. 70).

$$\begin{aligned}
 K_r &= \frac{\sigma_{rr}}{\sigma_{x_{ave}}} \\
 K_{r\theta} &= \frac{\sigma_{r\theta}}{\sigma_{x_{ave}}} \\
 K_x &= \frac{\sigma_x}{\sigma_{x_{ave}}}
 \end{aligned}
 \tag{Eq.70}$$

The schematical representations of radial, shear stresses around the fiber are given in Figure 5.11.

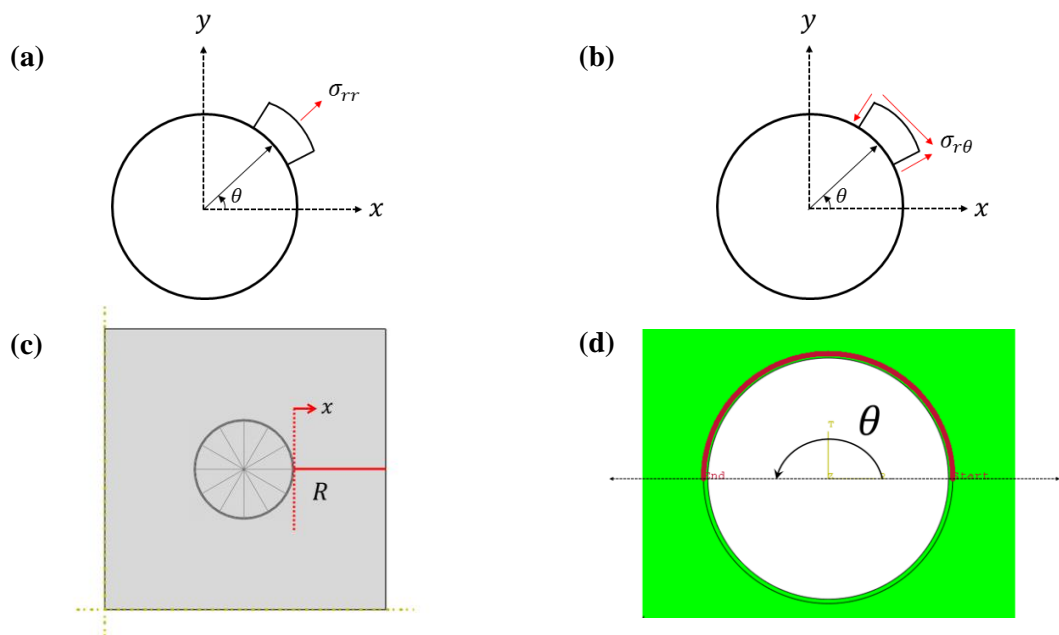


Figure 5.11. Calculated stress components for the thesis: (a) radial stress; (b) shear stress; (c) horizontal stress concentration measurement direction along RVE; (d) Path around the fiber from which stress concentration is measured

Bringing together all the outputs, stress concentrations around a single fiber starting from 0° to 180° (for single and hexagon RVE) and 360° (for random RVE) are created, results are presented in Chapter 6.

CHAPTER 6

ANALYSIS RESULTS

In this chapter, analysis results regarding single, hexagon and random RVEs are presented. All the post-process tasks are carried out via scripts. Upon completion of analyses, the output files are processed with Matlab® to present neat outputs regarding stress concentrations. The analysis durations for different type of RVEs are presented in the table below. Random RVE cases are solved in a super computer with 48 CPUs and 64 GB of memory whereas single and hexagon RVEs are solved in 4 CPUs with 6 GB of memory computer.

Table 6.1. *Flax Fiber RVE analyses solution times*

RVE	CPU Time (Sec)
Single Fiber RVE	363.50
Hexagon RVE ($v_f = 0.4$)	296.50
Hexagon RVE ($v_f = 0.6$)	129.50
Random RVE ($v_f = 0.4$)	384.40
Random RVE ($v_f = 0.6$)	202.30

As indicated previously, a mesh sensitivity analysis is conducted to observe if the results converge or not. The configuration is selected as hexagon RVE, maximum stress vs number of element curve is plotted. From the results of the analysis which is shown in Figure 6.1, it is apparent that results do converge. It is possible to state that the size and the configuration of the elements are proper and the analyses based on this mesh is reliable.

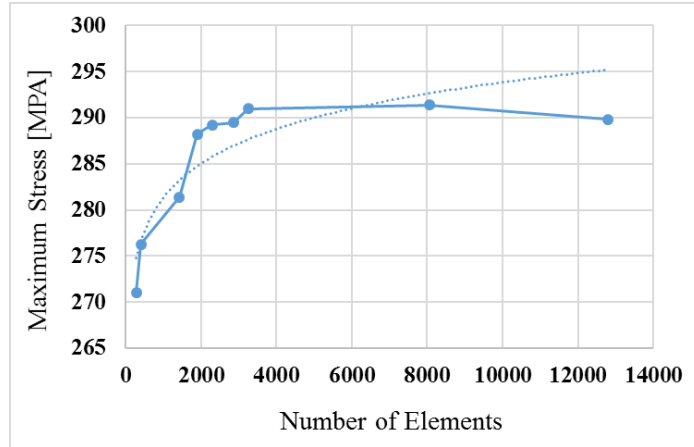


Figure 6.1. Mesh sensitivity analysis results

6.1. Single Fiber RVE Results

Section 6.1 focuses on stress concentration results of single RVE under prescribed boundary conditions that is mentioned in part 5.1. Initially, bilinear Young's modulus effect is investigated. Then material modeling approaches are compared (Section 6.1.2). Thirdly, the fiber is subjected to different transverse strains (Section 6.1.3) and last step is comparison with synthetic fibers like glass and carbon (Section 6.1.4).

6.1.1. Young's Modulus Duality Case Study

As explained in section 3, flax fiber stress-strain behavior is bilinear meaning that it does have two values of Young's modulus. Considering the material modeling approach in this study, that is orthotropic (Section 4.1.1); the effect of this duality should be further investigated. For this purpose, a comparison study is conducted. Bensadoun et. al. [60] studied this duality of elementary flax fiber. According to their test results, two elastic moduli are observed: $E_{f1} = 57.0$ GPa, and $E_{f2} = 44.5$ GPa for strain intervals of 0 to 0.001 and 0.003 to 0.005. Nevertheless, the problem here is that they are all in longitudinal direction. Since the focus point in this study is the transverse property, 1-to-10 scaling assumption is used [23] and moduli are taken as, $E_{T1} = 5.7$ GPa and $E_{T2} = 4.45$ GPa. Additionally, since it is a comparison study,

material is assumed as isotropic for the sake of simplicity. For an input strain of 0.2 %, the obtained results are presented in Figure 6.2, Figure 6.3 and Figure 6.4.

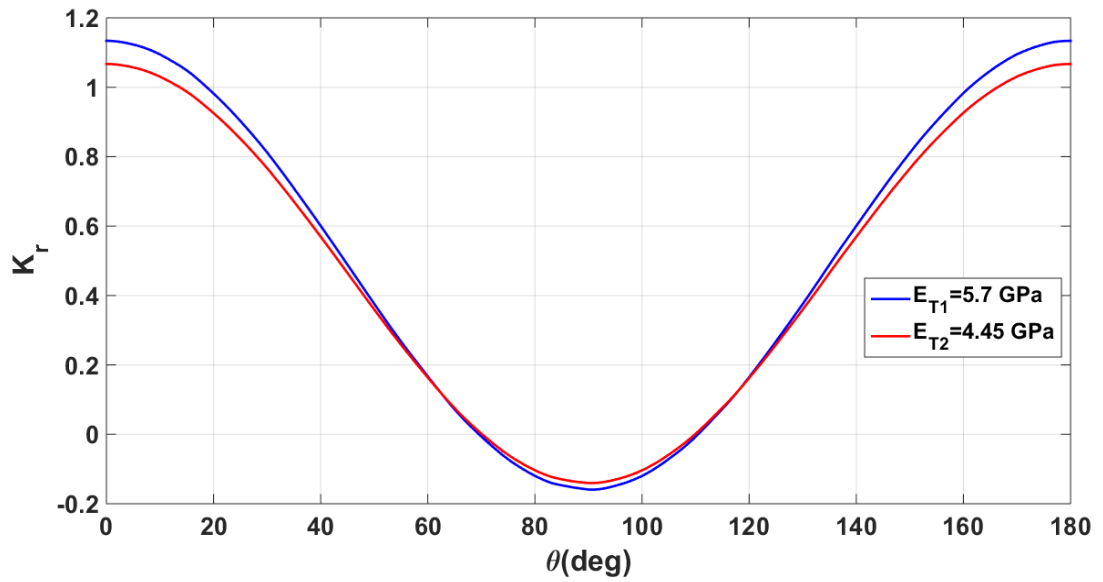


Figure 6.2. Single Fiber RVE Radial stress concentrations of along flax-matrix interface with dual transverse moduli for 0.2% strain input.

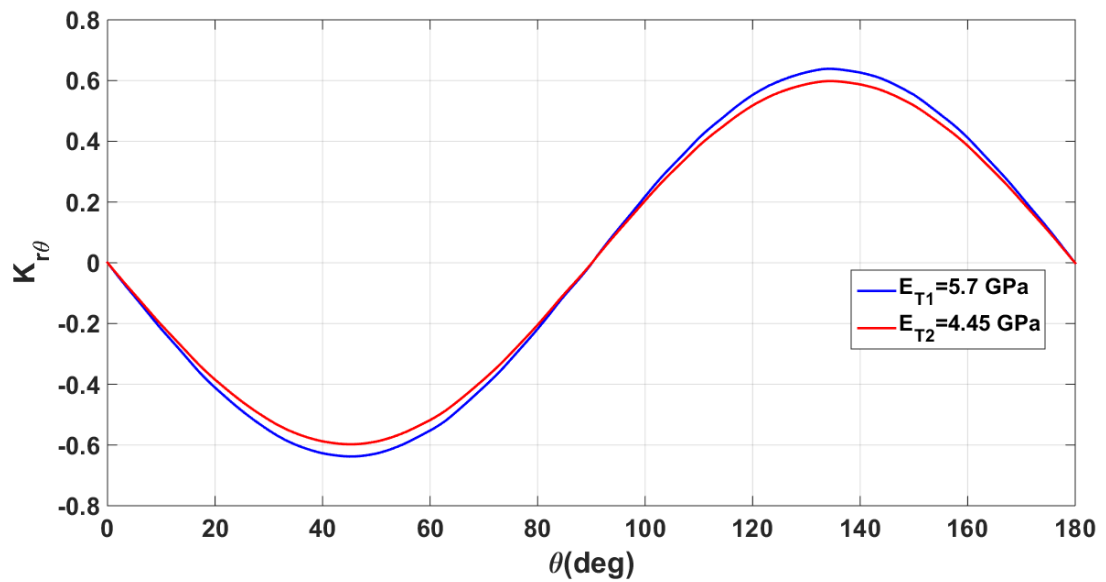


Figure 6.3. Single Fiber RVE Shear stress concentration along fiber matrix interface with dual transverse moduli 0.2% strain input.

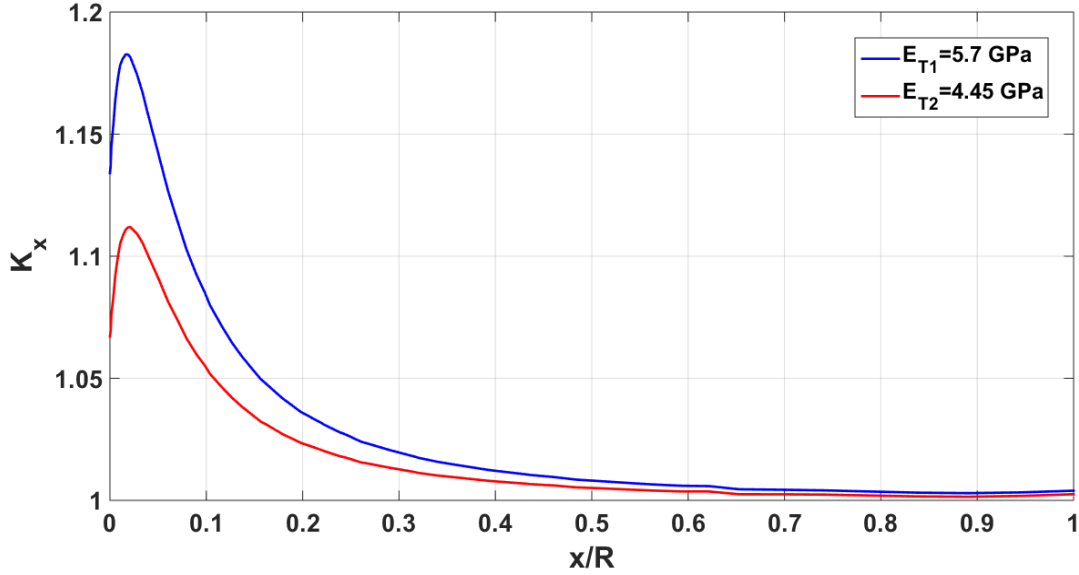


Figure 6.4. Single Fiber RVE horizontal stress concentration along the path between fiber and the model edge with dual transverse moduli 0.2% strain input.

Since the study is performed to have an idea about the effect of two different elastic moduli on stress concentrations, the flax material is assumed to be fully isotropic for the sake of simplicity. Two separate analyses are run and results are presented consecutively. In terms of radial stress concentrations around the fiber-matrix interface, the difference between reached maximum values is quite low. The model having transverse modulus $E_{T1} = 5.7$ GPa has maximum radial stress concentration, $K_r = 1.134$ whereas the one with second modulus value of $E_{T2} = 4.45$ GPa reaches $K_r = 1.067$ (Figure 6.2). The case in shear stress concentration is also similar. The difference between maximum shear stress concentrations is about 0.067 (Figure 6.3). Considering the horizontal stress concentrations from Figure 6.4, the variation is minimal as well. The difference between these two values is small enough to justify the utilization of a single Young's modulus value to obtain accurate results in terms of stress concentrations.

6.1.2. Comparison Case Study with Orthotropic and Hyperelastic Flax Fiber

Although selected material model to be used in analyses is orthotropic, in order to compare the stress concentrations in terms of order of magnitude and have a general idea, a comparison study is conducted. The inelastic modeling approach which uses Ogden strain energy function and the orthotropic elastic modeling approach are compared with respect to radial, shear and horizontal stress concentrations as presented in Figure 6.5, Figure 6.6 and Figure 6.7 for an input strain of 0.2 %.

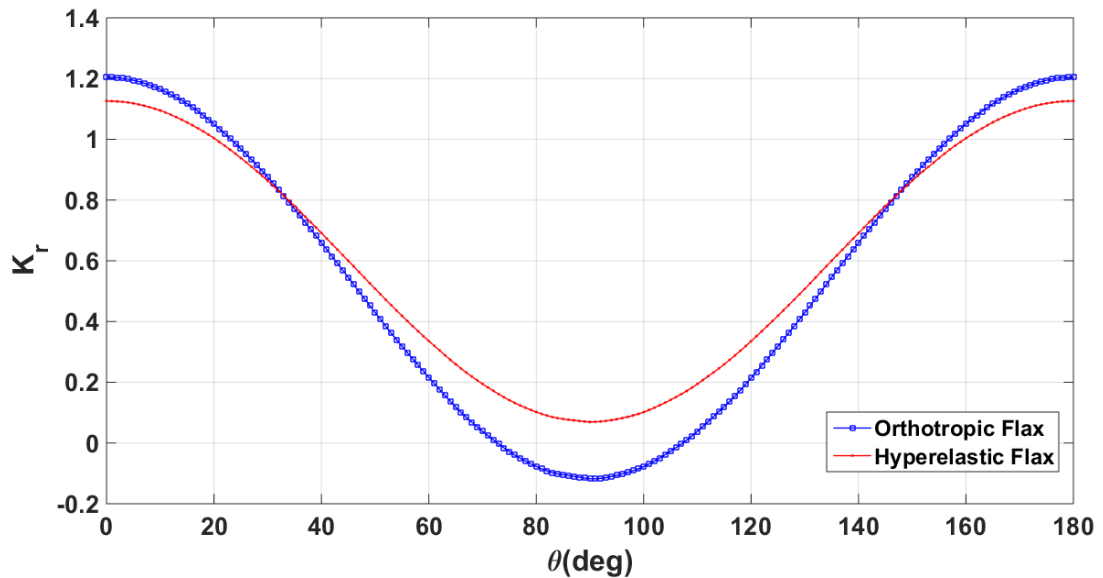


Figure 6.5. Single Fiber RVE Radial stress concentrations along flax-matrix interface for orthotropic (blue) and hyperelastic (red) modeling approaches for 0.2% strain input

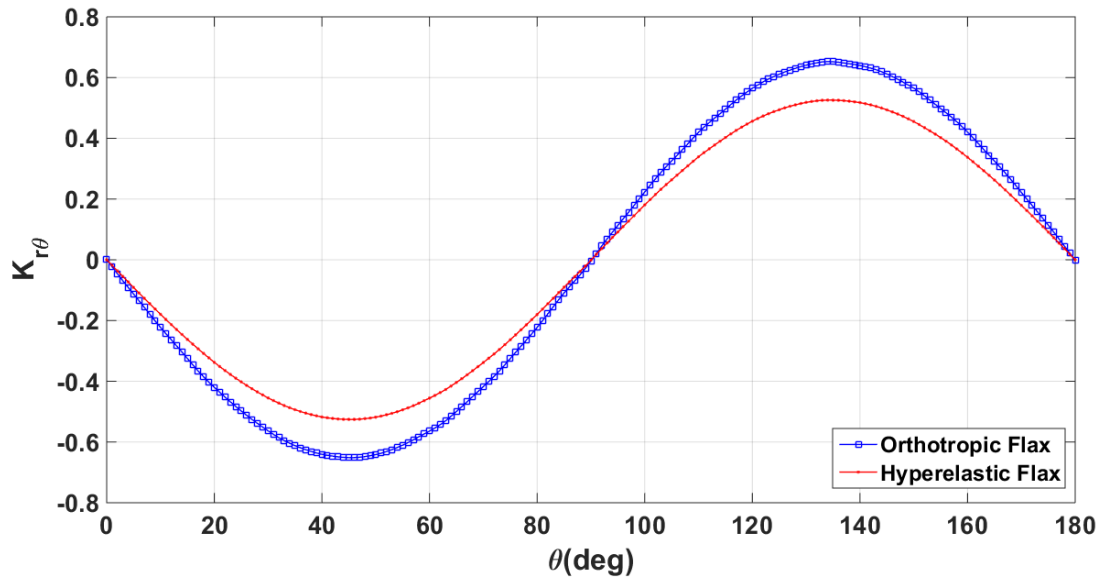


Figure 6.6. Single Fiber RVE shear stress concentrations along flax-matrix interface for orthotropic (blue) and hyperelastic (red) modeling approaches for 0.2% strain input.

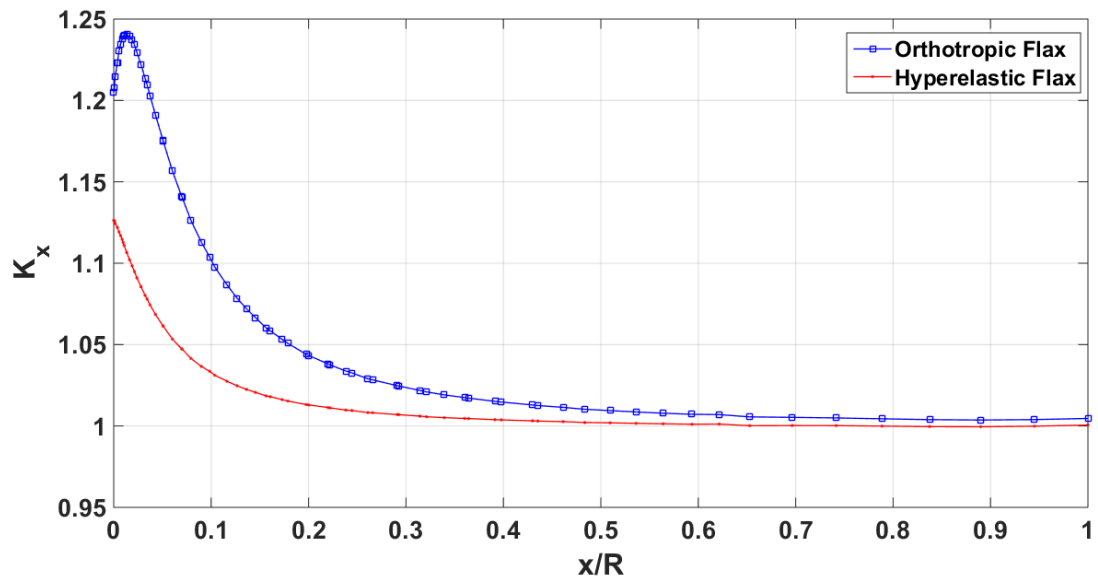


Figure 6.7. Single Fiber RVE horizontal stress concentration along the path between fiber and the model edge for orthotropic (blue) and hyperelastic (red) modeling approaches for 0.2% strain input.

Since the focal point in this study is the transverse aspects of the composite, hyperelastic approach is insufficient to characterize those features. The modeling approach, as mentioned in section 4.1.2, is based on scaling assumption due to lack of information to characterize transverse properties completely. Yet, in order to see the difference between two approaches, the comparison study is conducted. Considering radial stress concentration around the fiber-matrix interface (Figure 6.5), at the starting point of the radial path, i.e. 0° , the stress concentration difference is not so much. But, between 80° and 100° , the difference is about 0.2 which could be seen from the plot. By checking the shear stress concentration plot (Figure 6.6), one can see that towards to 45° and 135° , difference between two cases increases which is expected since the principle direction for the shear stress is highest in 45° . Finally, horizontal stress concentrations can be observed from Figure 6.7, which has the largest difference in terms of stress concentrations compared to others. Considering the results, hyperelastic and orthotropic modeling approaches do not give very different results, but due to mentioned reasons using hyperelastic approach may results with misleading outcomes.

6.1.3. Stress Concentrations for Varying Strains

Single fiber RVE model is subject to various strain values, starting from 0.1 % up to 5%. Contour plot of two strain values are presented in Figure 6.8 and stress concentration distributions in the fiber/matrix interface are given in Figure 6.9, Figure 6.10 and Figure 6.11.

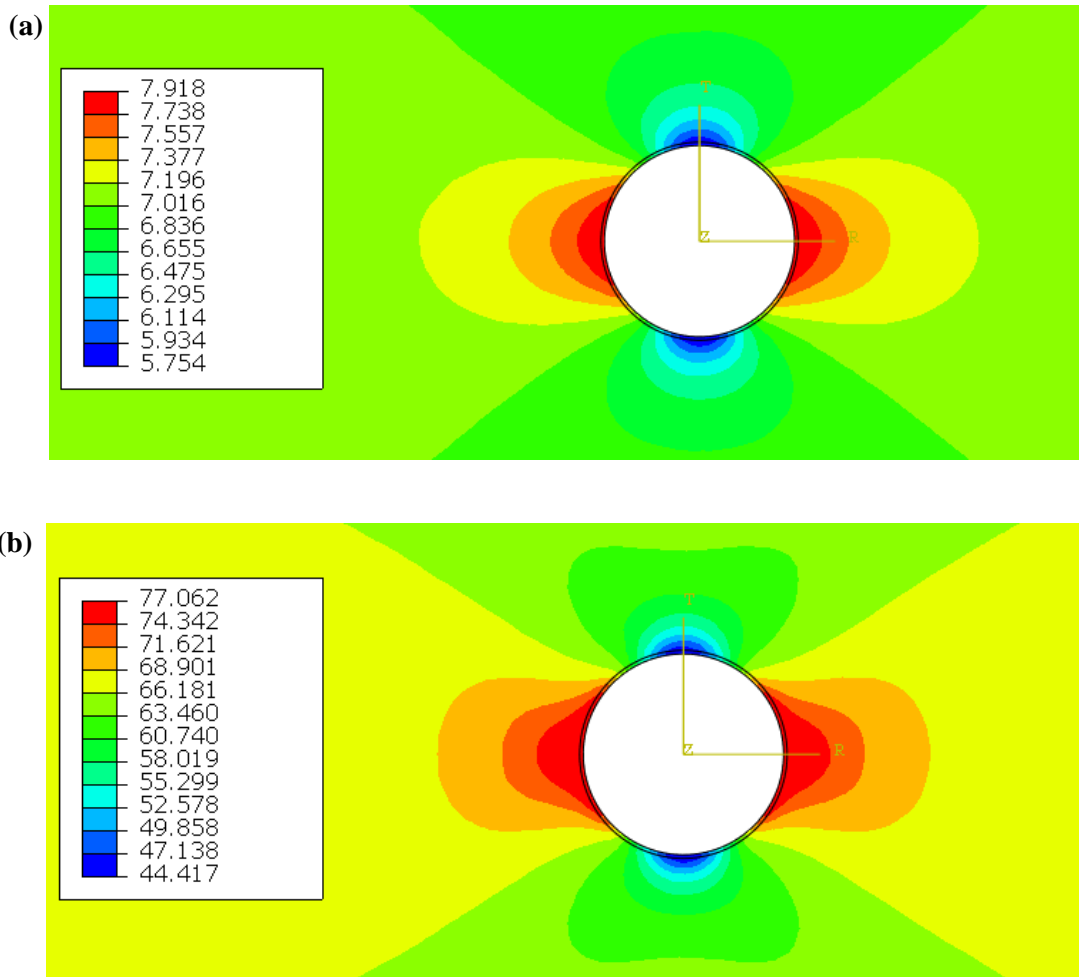


Figure 6.8. Distribution of maximum principle stress for the input strains values of (a) 0.2 %; (b) 2%

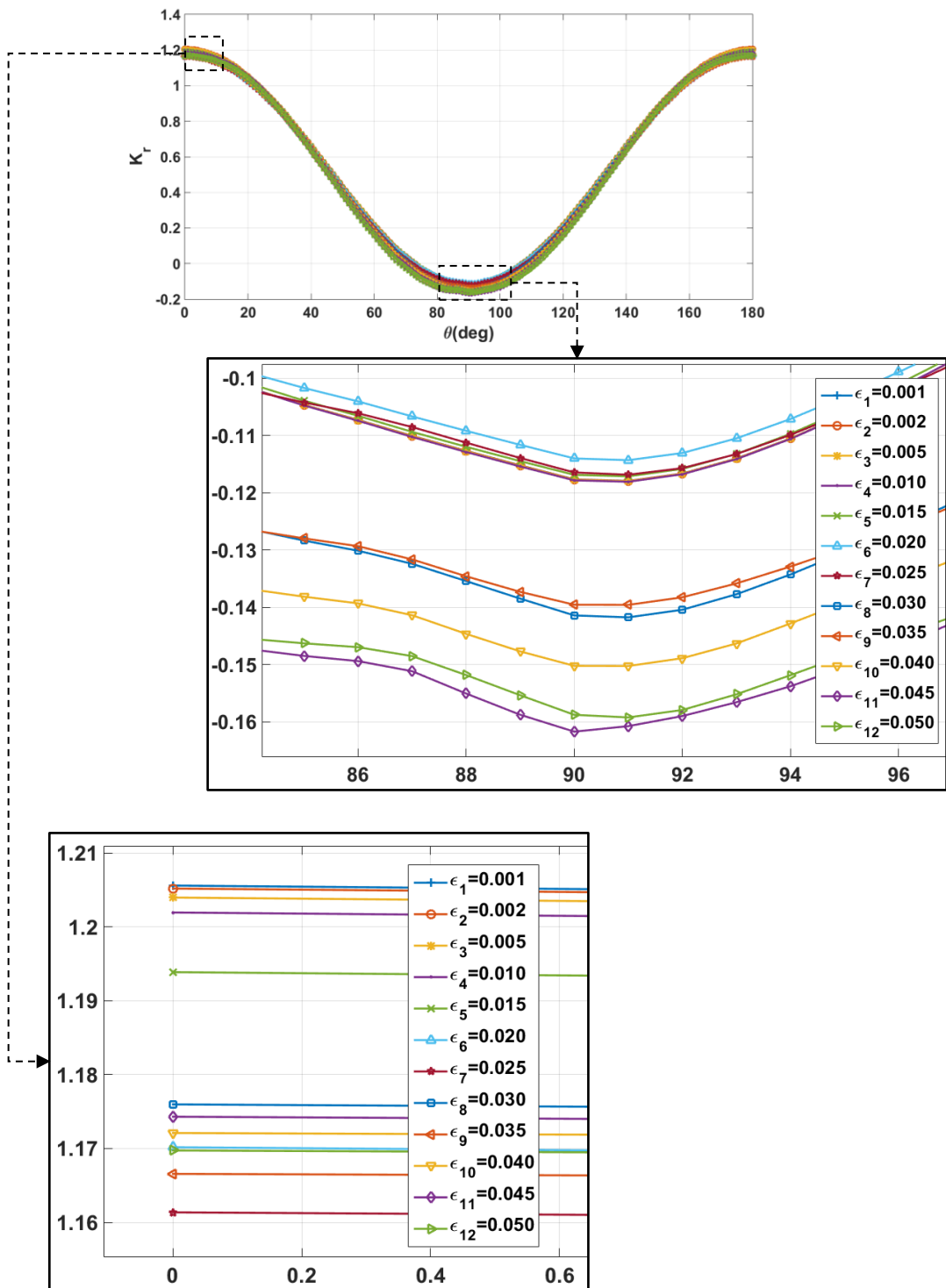


Figure 6.9. Single Fiber RVE radial stress concentrations along flax-matrix interface for various transverse strain inputs starting from 0.1% to 5%.

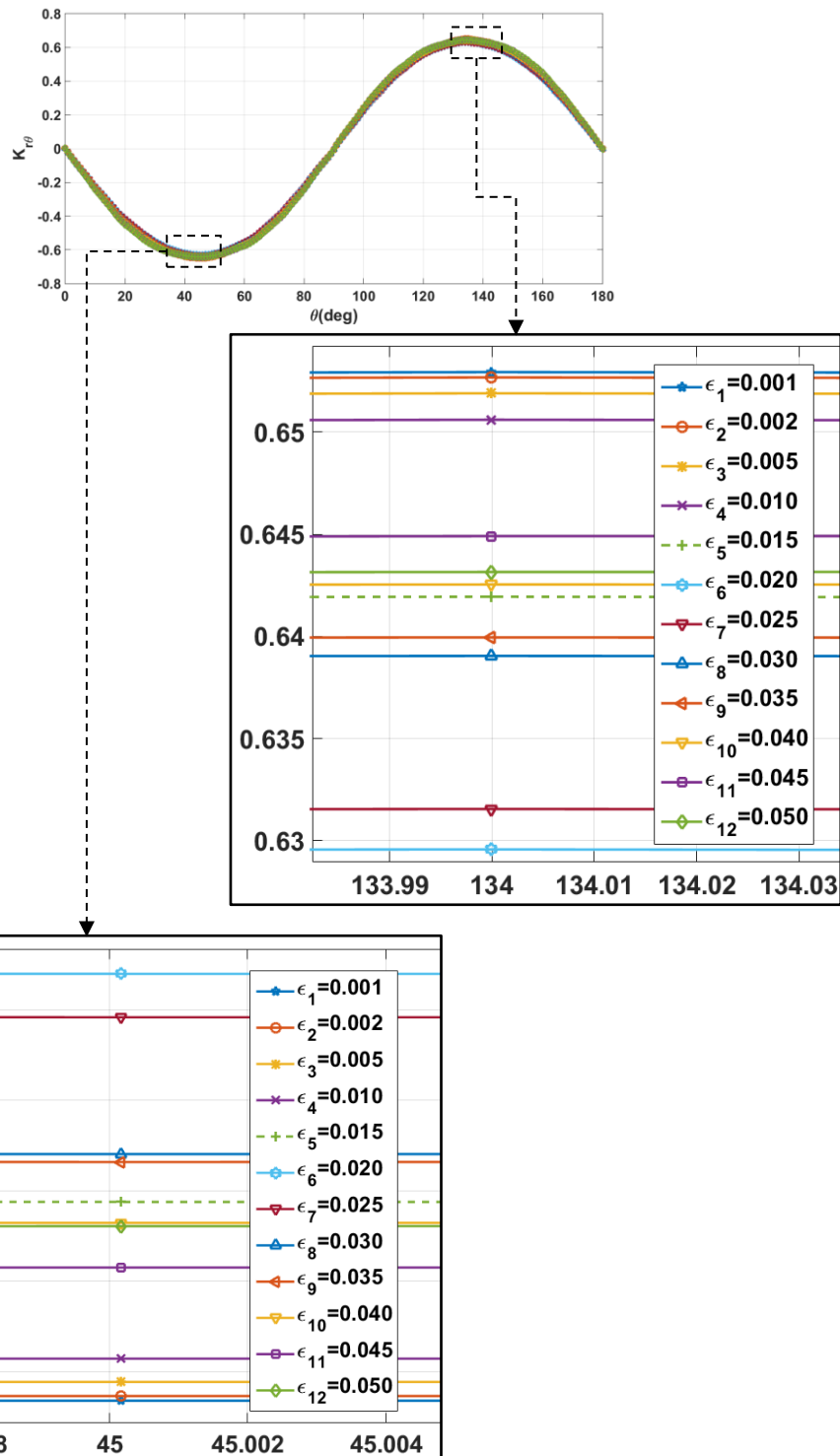


Figure 6.10. Single RVE shear stress concentrations along flax-matrix interface for various transverse strain inputs starting from 0.1% to 5%.

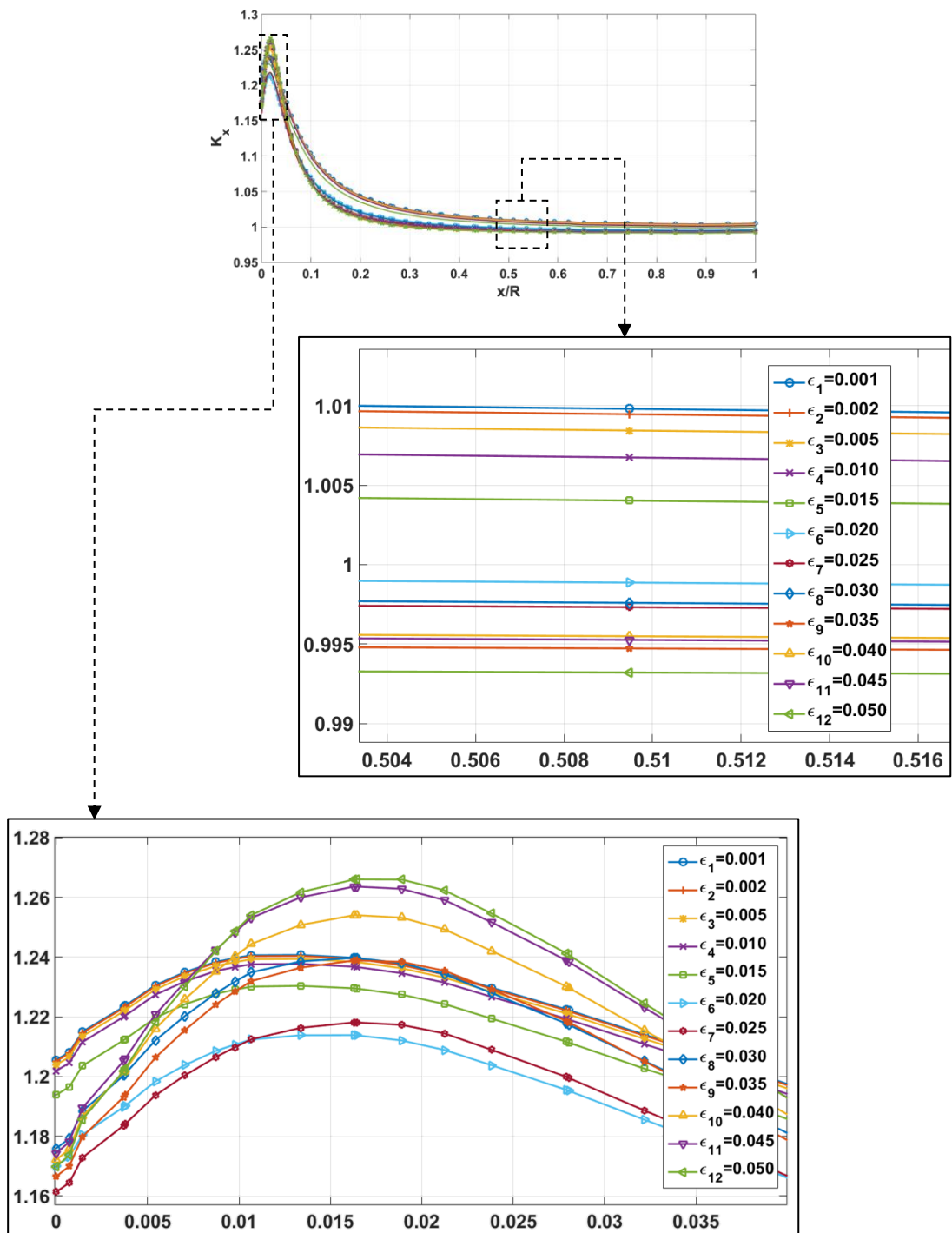


Figure 6.11. Single Fiber RVE horizontal stress concentration along the path between fiber and the model edge for various transverse strain inputs starting from 0.1% to 5%.

This case study is conducted to see the effect of strains from 0.1 % to 5%. In this analysis, the fiber is orthotropic flax and the matrix is elastoplastic epoxy. Starting from Figure 6.8, that color distribution is wider for the high strains meaning that stresses are created and distributed in a less concentrated manner. Radial stress concentration around fiber matrix interface proves this statement: stress concentrations decrease as the strain input increases which can be observed from Figure 6.9. Considering starting point of the path around the fiber, recall Figure 5.11, that is the 0° vicinity, highest concentration belong to 0.1 % strain case which is the same for shear stress concentrations (Figure 6.10). Horizontal stress concentrations have a little fluctuations just after the starting point of the path (Figure 6.11). However, at the fiber/matrix interface point and half of the RVE border, it is observed that increased strain inputs results with lower concentrations as well. Considering the elastic limit strain of the epoxy which is about 0.017, presented in Figure 4.7 (b), stress concentrations seen in single fiber RVE is are nearly the same up to this value. As the transverse strain input increases over this limit, especially for the radial and shear stress concentrations, starting from $\varepsilon_6 = 0.015$ stress concentrations starts to decrease. It is due to the fact that epoxy matrix yields and it passes to the plastic zone. High concentrations in the fiber/matrix interface generate a softening effect. This is an important deduction to be able to set a value to the onset of yielding caused by the matrix.

6.1.4. Comparison Case Study with Glass and Carbon Fiber

In this section flax fiber is compared with glass and carbon fiber with the same amount of transverse strain input which is 0.2 %. Radial, shear and horizontal stress distribution results are shown in Figure 6.12, Figure 6.13 and, Figure 6.14 respectively.

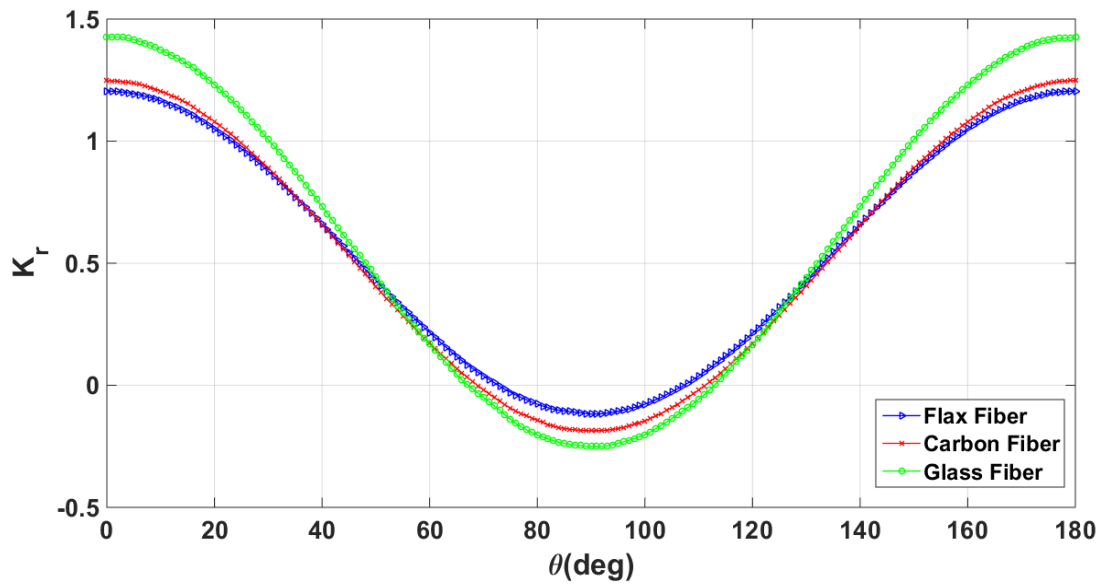


Figure 6.12. Single Fiber RVE radial stress concentrations along flax-matrix interface for flax (blue), carbon (red) and glass (green) fibers for 0.2% strain input.

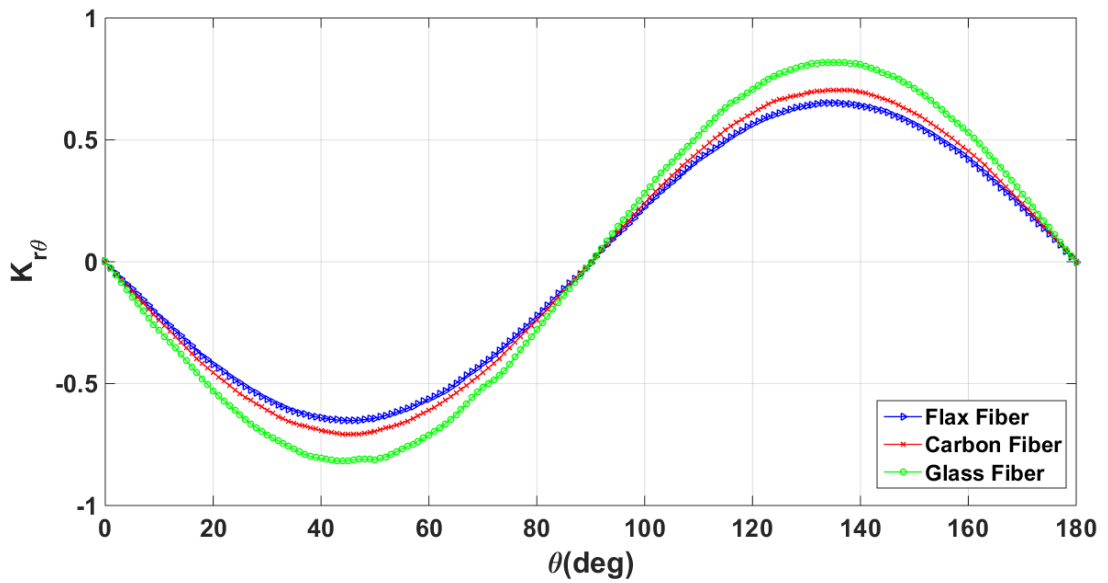


Figure 6.13. Single Fiber RVE shear stress concentrations along flax-matrix interface for flax (blue), carbon (red) and glass (green) fibers for 0.2% strain input.

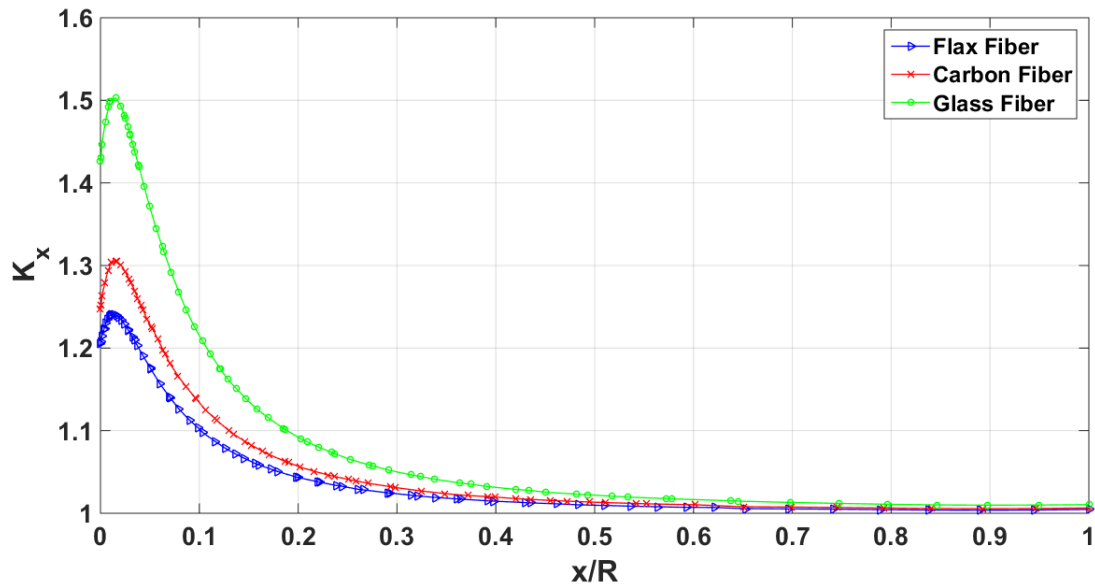


Figure 6.14. Single Fiber RVE horizontal stress concentration along the path between fiber and the model edge for flax (blue), carbon (red) and glass (green) fibers for 0.2% strain input.

This comparison case regarding flax, glass and carbon fibers the final case of single fiber RVE. In this analysis flax, carbon and glass fibers are subjected to transverse loading for a strain input of 0.2 % to evaluate the stress concentrations on the fiber-matrix interface. The radial and shear stress concentrations along the interface and horizontal stress concentrations from the fiber to the edge of RVE is presented in Figure 6.12, Figure 6.13, and Figure 6.14. The maximum stress concentrations are observed at a slight distance from the fiber matrix interface for horizontal stress concentrations. Considering radial stress concentrations, as expected, the highest concentration is observed in glass fiber, then comes carbon; and the least is the flax fiber. This is mainly due to large stiffness contrast between the fiber and the polymeric matrix. The glass fiber is a fully isotropic material meaning that transverse modulus is the same as longitudinal one, 72 GPa. The carbon fiber's transverse modulus is 10 GPa whereas flax fiber's is 8 GPa. This deduction is profoundly important for the study considering the idea that flax fiber composites may be used as a substitute for glass fibers. As indicated earlier, glass and flax fiber's longitudinal strengths are

comparable, but with this transverse property, it is apparent that flax fiber can be more promising in terms of mixed mode loading applications.

6.1.5. Element Type Comparison

This analysis is conducted to see if elements with reduced integration affect the results of the analyses. For this purpose 2 runs are performed with C3D8 and C3D8R elements. The CPU time durations for these analyses are presented in table below:

Table 6.2. CPU time for Single Fiber RVE with C3D8 and C3D8R elements

Element Type	Time (sec)
C3D8	439.90
C3D8R	363.50

The results of the analyses could also be seen from the radial, shear and horizontal stress concentration distribution plots:

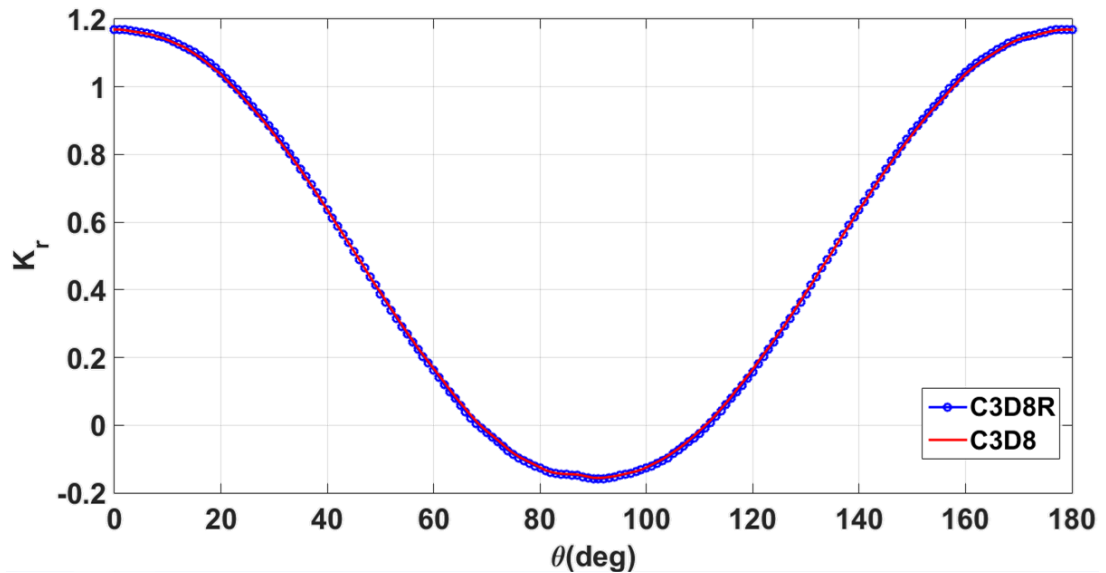


Figure 6.15. Radial stress concentration distribution for comparison with C3D8 and C3D8R type elements

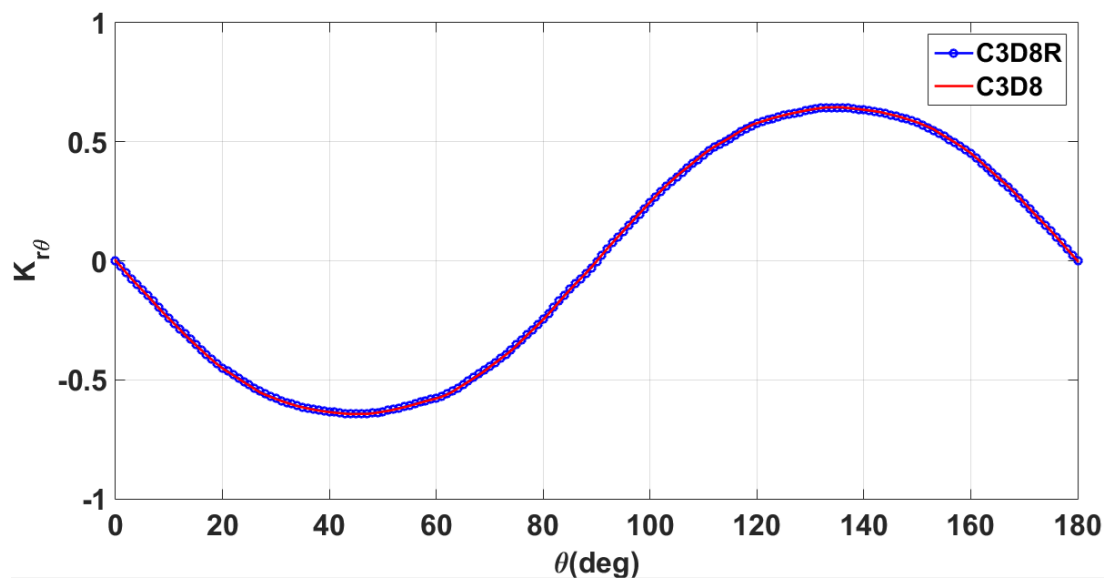


Figure 6.16. Shear stress concentration distribution for comparison with C3D8 and C3D8R type elements

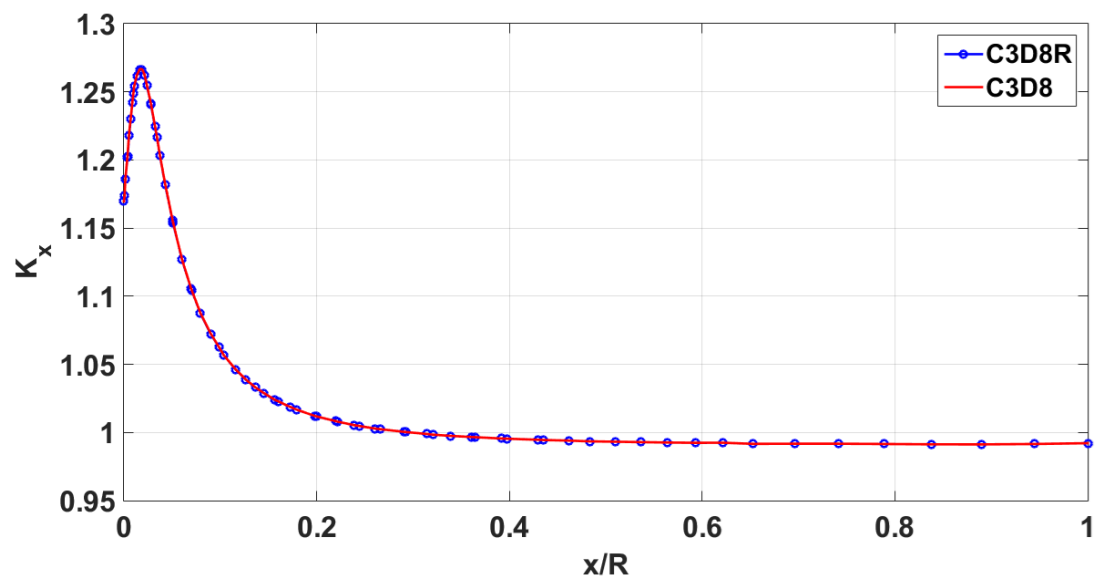


Figure 6.17. Horizontal stress concentration distribution for comparison with C3D8 and C3D8R type elements

The analyses are run for maximum transverse strain input used in the study, which is 5%. By checking the results, it is quite obvious that reduced integration element creates no difference in terms of generated stress concentrations in the vicinity of the fiber. The contour plots for both cases where the matrix is in its plastic zone are also shown below:

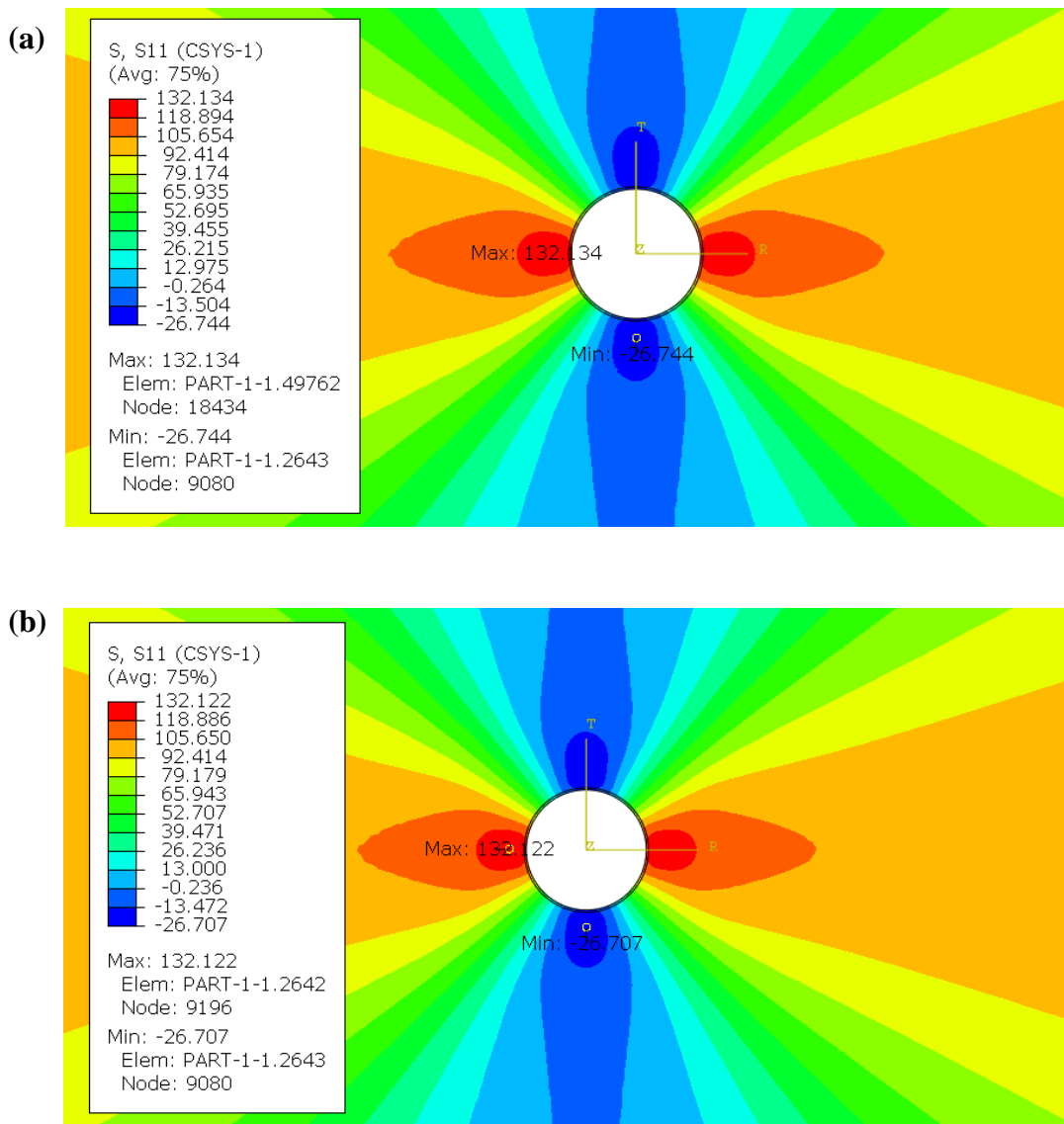


Figure 6.18. Contour plots for single RVE (a) C3D8, (b) C3D8R element type comparison with 5% transverse strain input

6.2. Hexagon RVE Results

Section 6.2 focuses on stress concentration results of hexagon RVE under prescribed boundary conditions that is mentioned in part 5.2. Studies are compiled in five main headlines: first effect of various strains for fiber volume fraction of 0.4 is observed. The same procedure is applied for fiber volume ratio of 0.6 as a second step. Thirdly, effect of volume fraction on the stress concentrations is investigated. Fourth and fifth step is again a comparison study for different volume fraction ratios that includes synthetic carbon and glass fibers. Transverse strain input to the RVE is given as 0.2 % for the comparison case study.

6.2.1. Stress Concentrations for Varying Strains (vf = 0.4)

Being different from single RVE, fiber volume fractions are introduced to hexagon RVE. According to volume fractions, dimensions of RVEs are arranged and analysis geometries are created

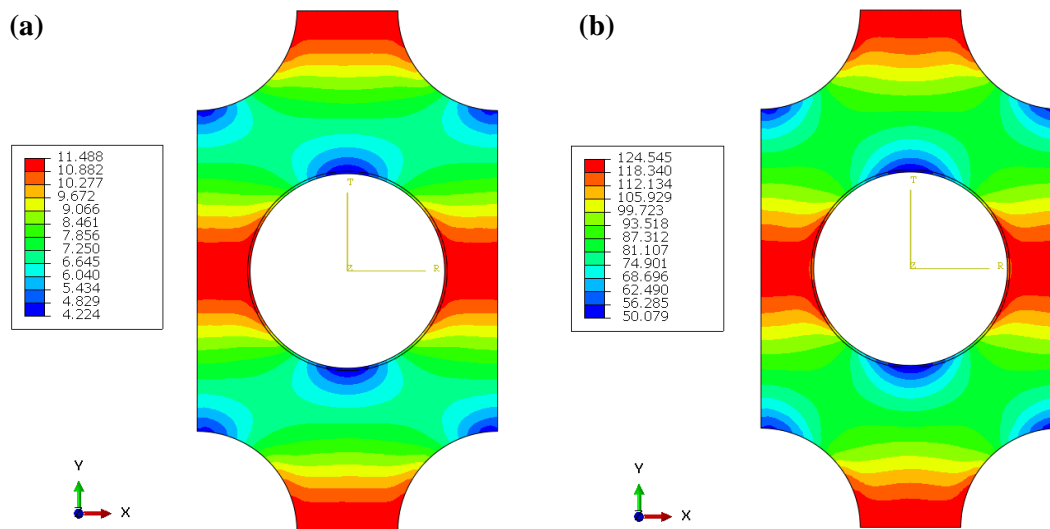


Figure 6.19. Distribution of maximum principle stresses for the input strains values of (a) 0.2 %, (b) 2.5 %

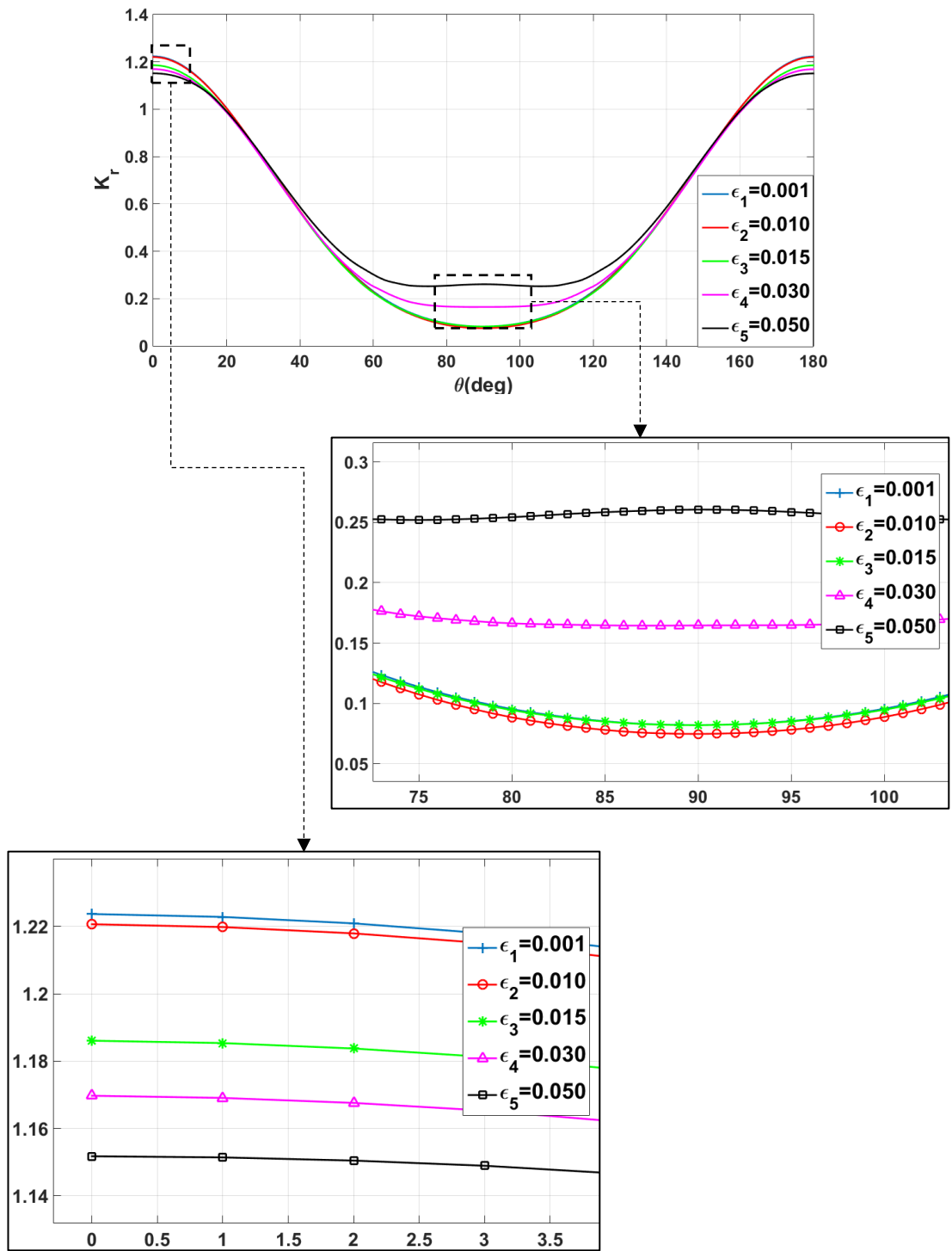


Figure 6.20. Hexagon RVE radial stress concentrations along flax-matrix interface for varying transverse strain input starting from 0.1 % to 5% with fiber volume fraction of 0.4

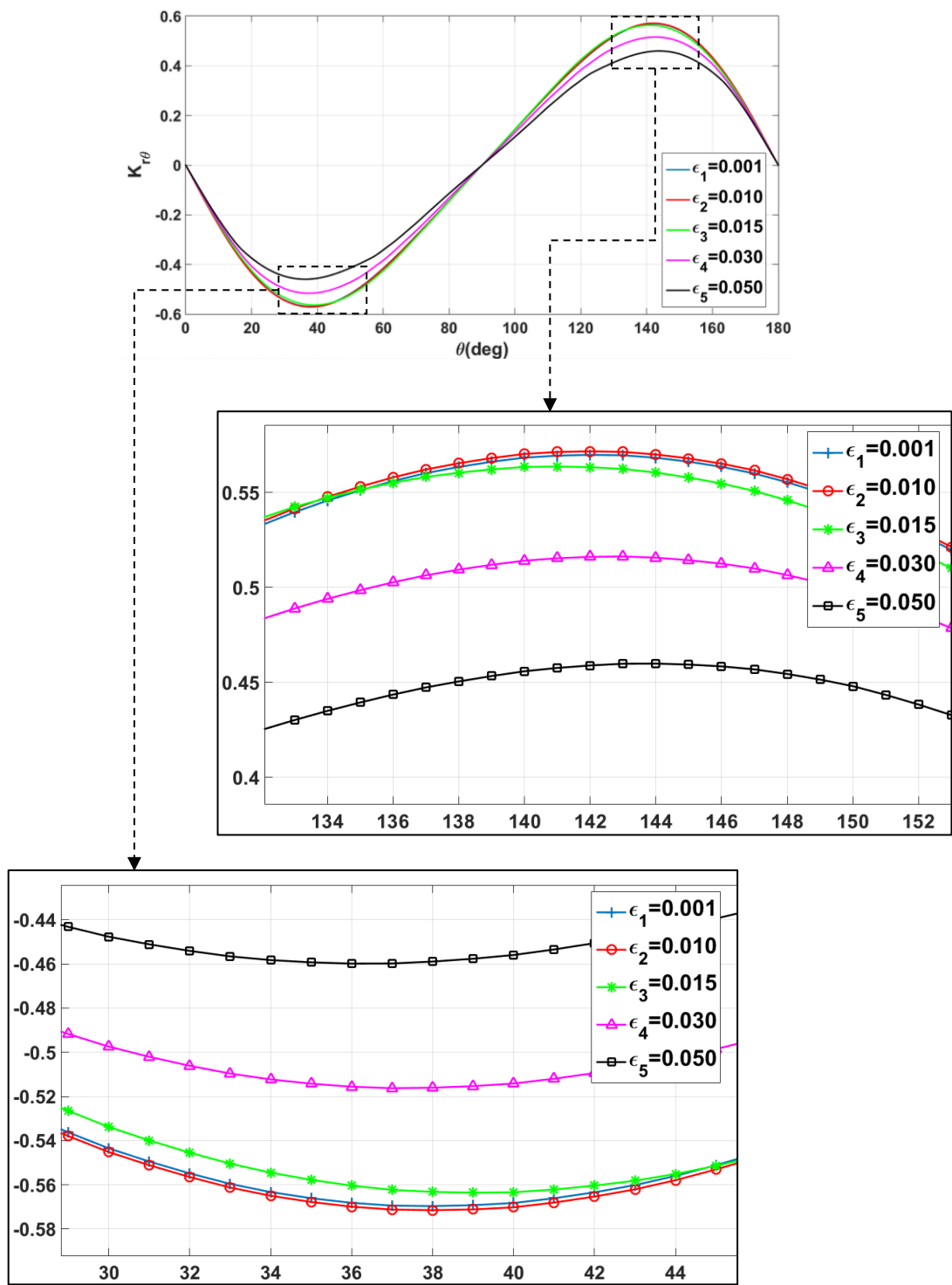


Figure 6.21. Hexagon RVE shear stress concentrations along flax-matrix interface for varying transverse strain input starting from 0.1% to 5% with fiber volume fraction of 0.4

The first case is the investigation of stress concentrations for varying strains with fiber volume fraction of 0.4. When radial and shear stress concentrations are examined (Figure 6.20 and Figure 6.21), it is seen that strains up to yield limit of polymeric matrix create concentrations similar to each other as in the case of single RVE. For this case, maximum stress concentration value is reached by lowest strain input, 0.1%. Concentrations up to the plastic limit of matrix are similar but starting from 0.015 strain, concentrations decrease gradually. From these results, it is possible to say that stress concentration is inversely proportional to strain input for hexagonal packing with volume fraction of 0.4. It can also be deduced that stress concentrations caused by high deformations are distributed in the matrix more uniformly compared to low strain response.

6.2.2. Stress Concentrations for Varying Strains (vf = 0.6)

In this part, the examination of stress concentration for different strains with fiber volume fraction of 0.6 is performed. Same procedure with 0.4 volume fraction is applied. Contour plot of two different strain input is presented in Figure 6.22.

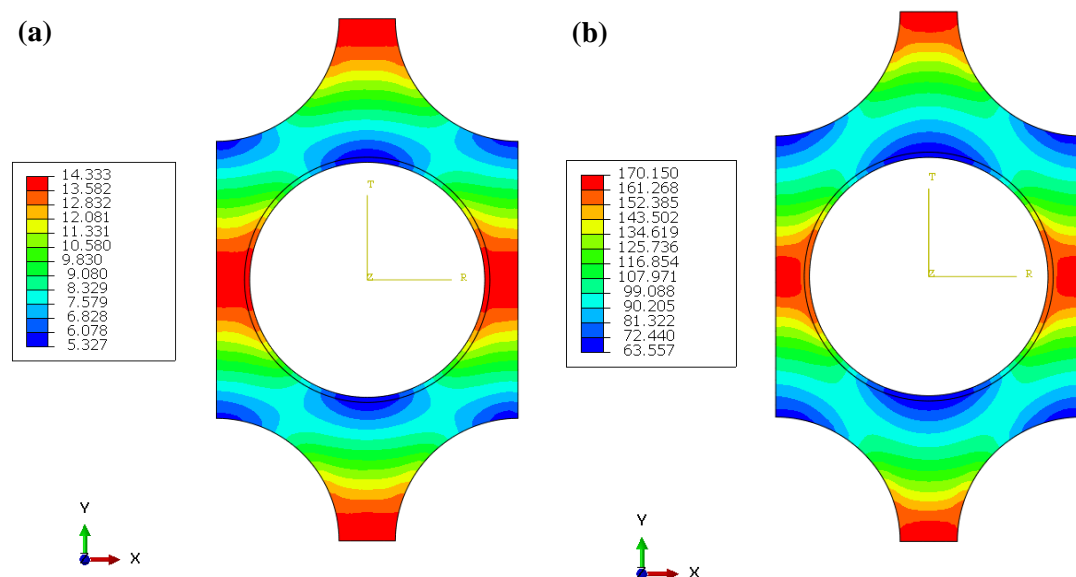


Figure 6.22. Distribution of max. principle stresses for the input strains values of (a) 0.2 %, (b) 2.5 %

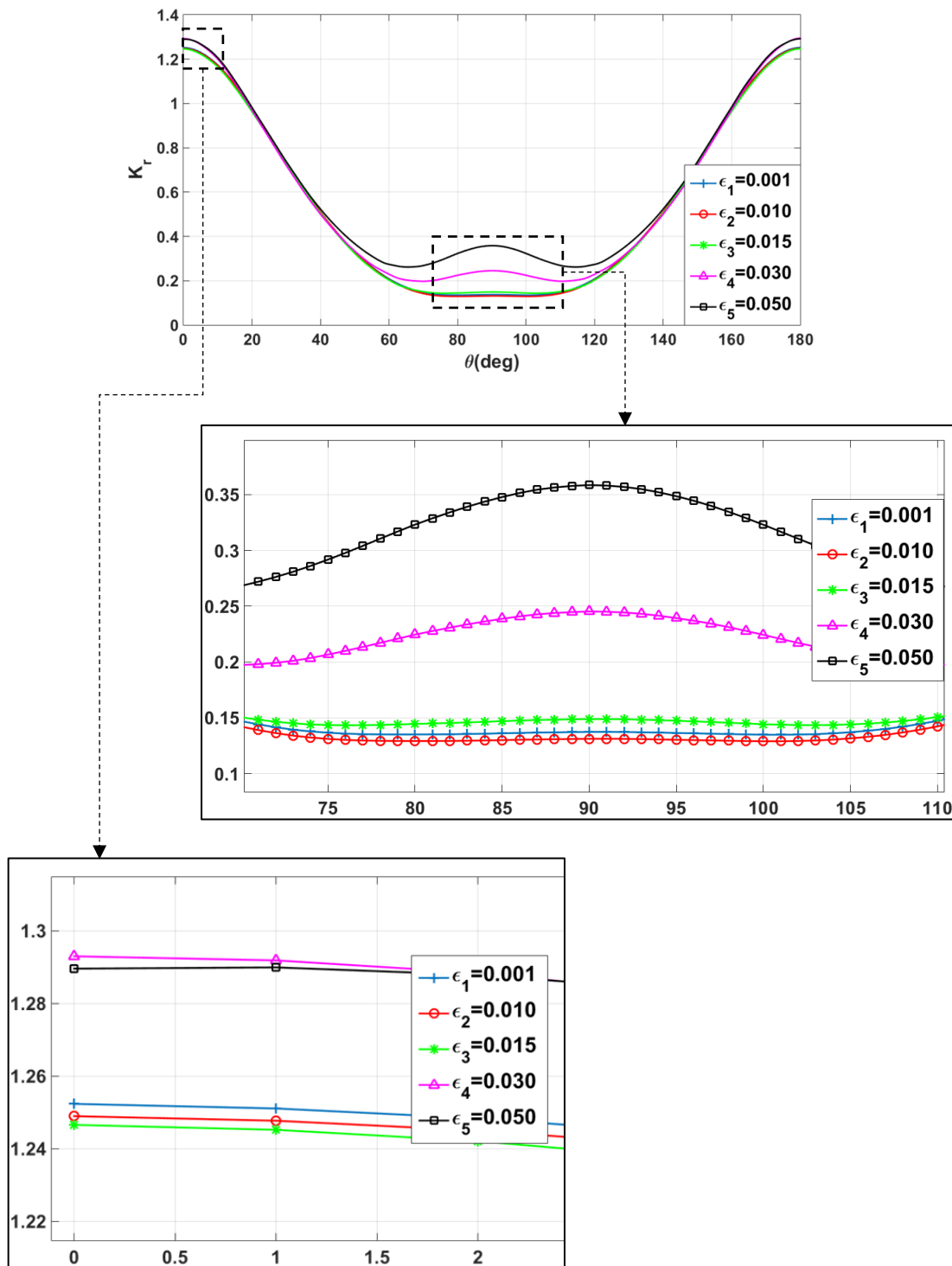


Figure 6.23. Hexagon RVE radial stress concentrations along flax-matrix interface for varying transverse strain input starting from 0.001 to 0.05 with fiber volume fraction of 0.6

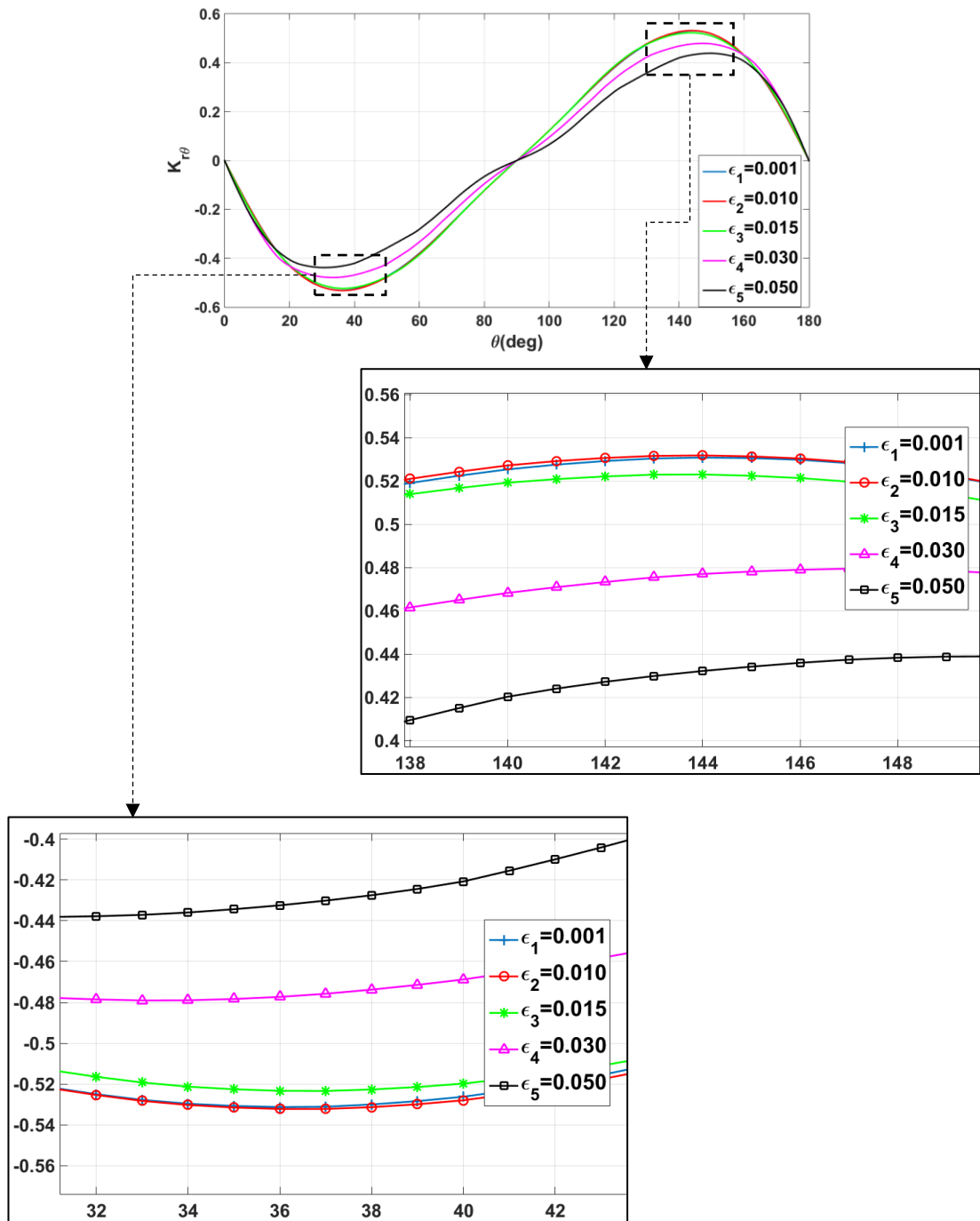


Figure 6.24. Hexagon RVE shear stress concentrations along flax-matrix interface for varying transverse strain input starting from 0.001 to 0.05 with fiber volume fraction of 0.6

The results are mostly similar to the previous case. Concentrations remaining below the yield limit nearly coincides with each other for both radial and shear stresses. Increasing strains above the plastic limit of the matrix creates lower concentrations which could be seen in Figure 6.23. For the shear stress concentrations, results resemble to the 0.4 volume fraction case which can be observed Figure 6.24, high strains cause lower concentrations. One more important result, which can be reached from 0.6 volume fraction case is that for the higher input strains, dispersion of stress concentration in the matrix is wider, i.e. transitions to the highest concentration regions are softer.

6.2.3. Stress Concentrations for Different Fiber Volume Fraction Ratios

In this analysis case a comparison study is carried out for different fiber volume fractions with the same strain input. Same 0.2 % strain input is used for both volume fractions of 0.4 and 0.6.

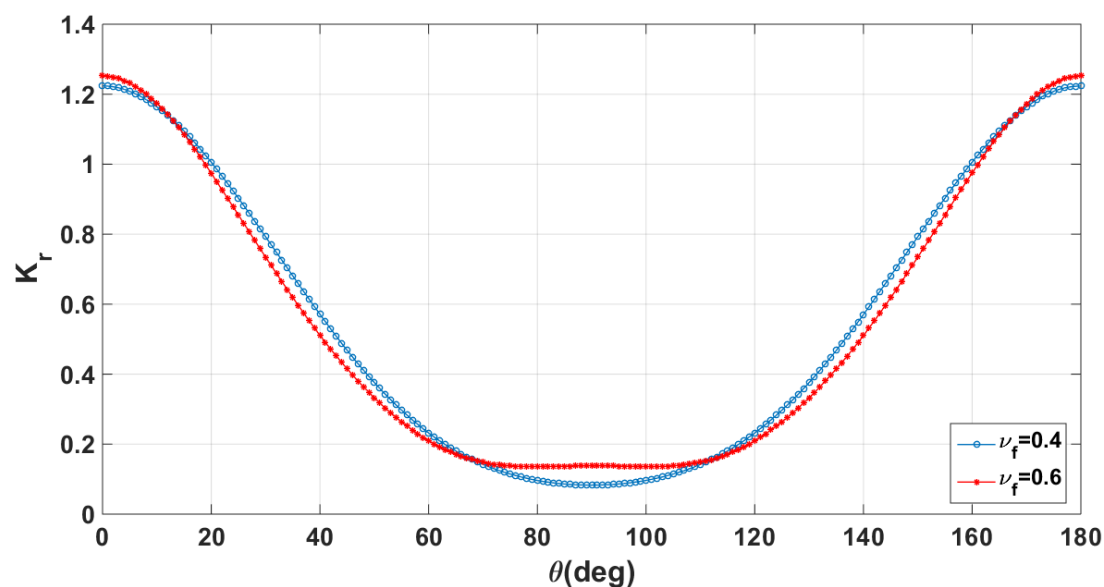


Figure 6.25. Hexagon RVE radial stress concentrations along fiber-matrix interface for fiber volume fraction of 0.4 (blue) and 0.6 (red) with 0.2 % transverse strain input

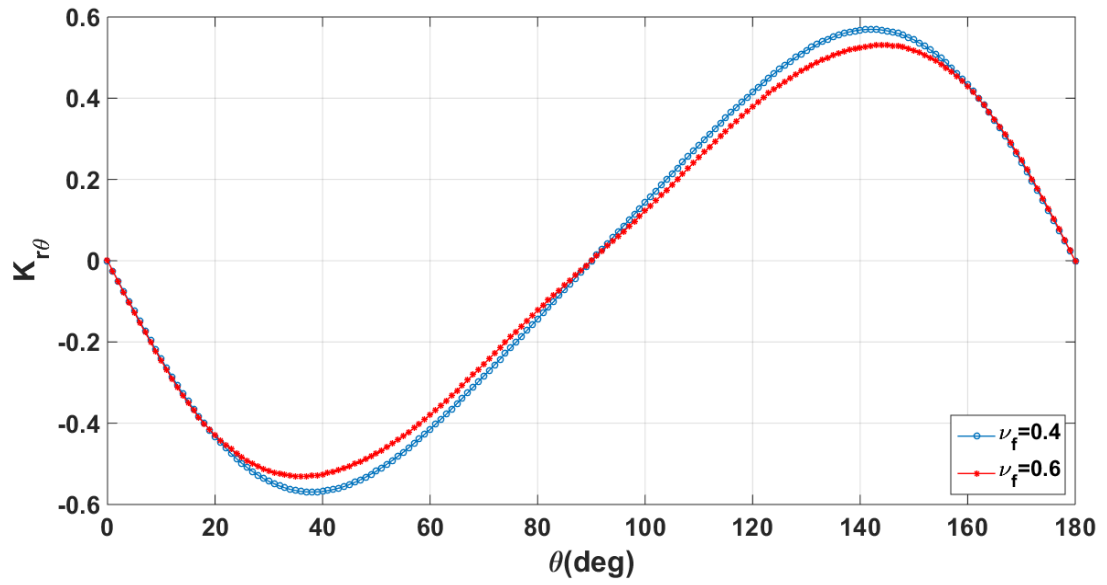


Figure 6.26. Hexagon RVE shear stress concentrations along fiber-matrix interface for fiber volume fraction of 0.4 (blue) and 0.6 (red) with 0.2% transverse strain input

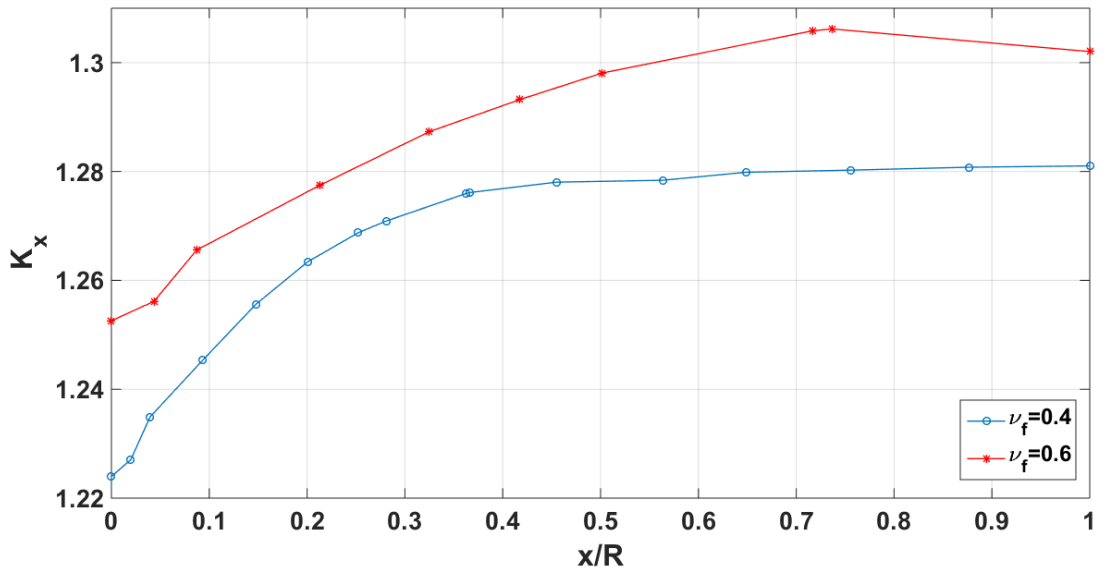


Figure 6.27. Hexagon RVE horizontal stress concentration along the path between fiber and the model edge for fiber volume fraction of 0.4 (blue) and 0.6 (red) with 0.2% transverse strain input

Obtained radial and shear stress concentrations are slightly higher for 0.6 volume fraction (Figure 6.25 and Figure 6.26). On the stress concentrations between fiber and the model edge, the model with 0.6 volume fraction apparently has higher values (Figure 6.27). Another important deduction of the study is this aspect; as the fiber volume fraction increases, local stress concentrations also increase due to stiffness contrasts in close vicinities.

6.2.4. Comparison Case Study with Glass and Carbon Fiber (vf = 0.4)

This case includes the comparison of flax, carbon and glass fibers for the same strain. The comparison is performed with constant strain input (0.2 %) for volume fraction of 0.4. Radial, shear and horizontal stress concentration results are presented below.

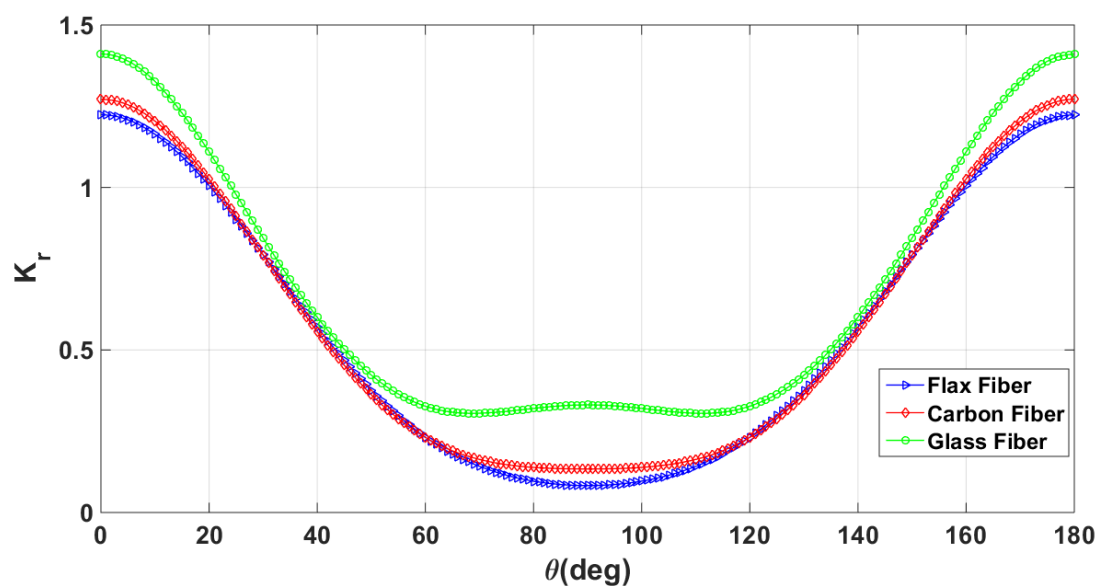


Figure 6.28. Hexagon RVE radial stress concentrations along fiber-matrix interface for flax (blue), Carbon (Red) and Glass (green) fibers with fiber volume fraction of 0.4 for 0.2% strain input

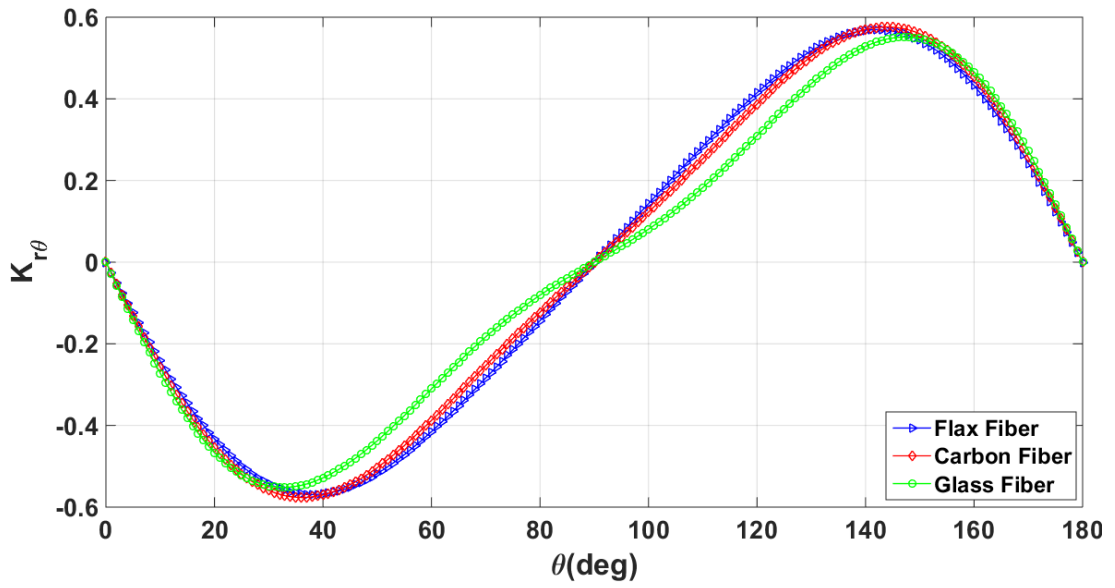


Figure 6.29. Hexagon RVE shear stress concentrations along fiber-matrix interface for flax (blue), Carbon (Red) and Glass (green) fibers with fiber volume fraction of 0.4 for 0.2% strain input

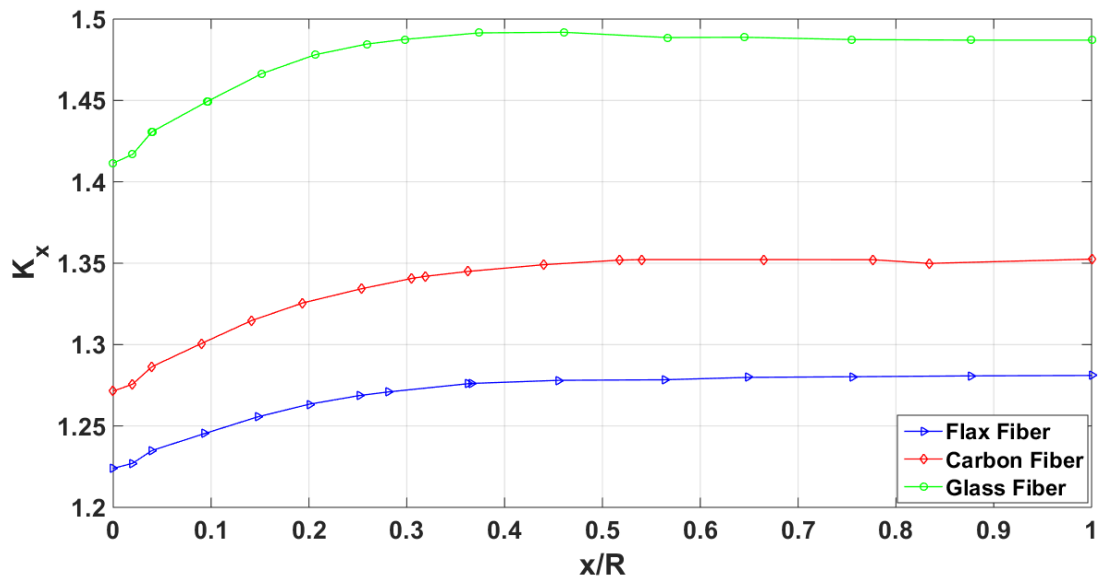


Figure 6.30. Hexagon RVE horizontal stress concentration along the path between fiber and the model edge for flax (blue), Carbon (Red) and Glass (green) fibers with fiber volume fraction of 0.4 for 0.2% strain input.

When radial stress concentrations of volume fraction of 0.4 is examined from Figure 6.28 it is seen that glass fiber has highest stress concentration. Due to the effect of quarter fibers in the directions of 60° and 120° , the trend of the curve changes compared to single fiber RVE (Figure 6.12). But due to low elastic modulus difference, carbon and flax fibers' trends resemble to the single RVE. One more factor affecting these trends is the low fiber volume ratio. Since quarter fibers are distant to the central one, their effect decreases. For the shear stress concentrations as observed in (Figure 6.29), due to same reason for the radial ones, trend of the curve for carbon and flax look like single fiber RVE. Considering the horizontal stress concentrations (Figure 6.30), glass fiber creates highest concentrations by far.

6.2.5. Comparison Case Study with Glass and Carbon Fiber ($\nu_f = 0.6$)

Comparison case study for 0.6 volume fraction is the last analysis case for hexagon RVE. Results for stress concentrations are presented in Figure 6.31, Figure 6.32 and Figure 6.33.

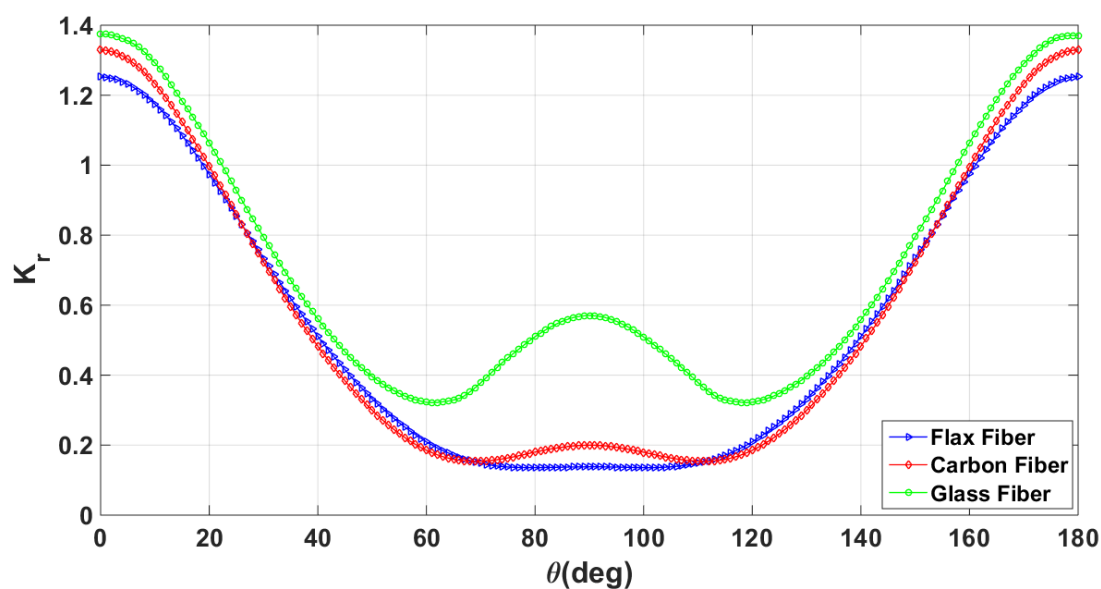


Figure 6.31. Hexagon RVE radial stress concentrations along fiber-matrix interface for flax (blue), Carbon (Red) and Glass (green) fibers with fiber volume fraction of 0.6 for 0.2% strain input

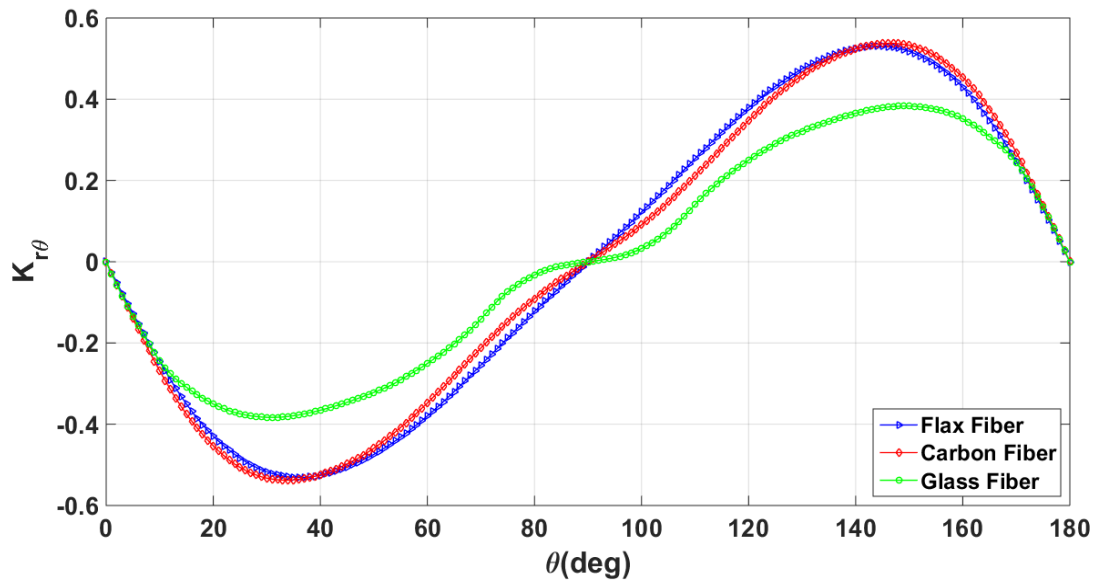


Figure 6.32. Hexagon RVE shear stress concentrations along fiber-matrix interface for flax (blue), Carbon (Red) and Glass (green) fibers with fiber volume fraction of 0.6 for 0.2% strain input

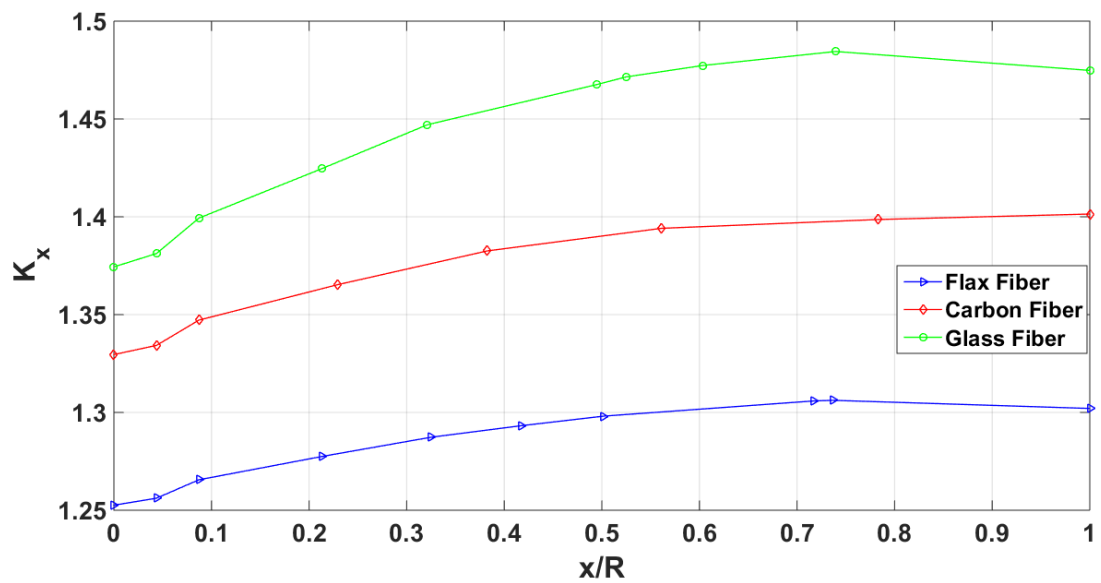


Figure 6.33. Hexagon RVE horizontal stress concentration along the path between fiber and the model edge for flax (blue), Carbon (Red) and Glass (green) fibers with fiber volume fraction of 0.6 for 0.2% strain input

Comparison analysis with 0.6 fiber volume ratio, actually, proves the effect of neighboring fibers to the central one. Maximum stress concentrations observed in 0.6 volume fraction is a bit higher compared to 0.4, which was indicated previously. However, when the trends of the stress concentration curves for both radial and shear are examined from Figure 6.31 and Figure 6.32, maximum concentrations shift towards to 60 and 120 degrees rather than 90 and that is the true effect of the other fibers to the central one. Again, due to both the high stiffness contrast and denser packing, glass fiber forms the highest concentrations. Then comes the carbon fiber of which stress concentration curve has slightly shifted to 60° and 120°. Since it has lowest transverse modulus, stiffness contrast is very low and therefore the curve trend of flax fiber is very similar to single RVE again. That is a very important deduction from the study that flax fiber is superior to glass fiber in hexagonal packing when low stress concentrations are demanded.

6.3. Random RVE Results

The last model regarding stress concentration study is the random RVE. Similar to the hexagon RVE, the model is subjected to 0.2% transverse strain input to observe the radial and shear stress concentrations in the matrix. Considering the flax fiber composites, it is the most realistic scenario and the final step of the study. In this section, stress concentrations for fiber volume fraction ratios of 0.4 and 0.6 is investigated (6.3.1, 6.3.2). The fiber, which has the highest stress concentration along its interface, is selected considering the FE results and stress concentrations along its whole interface, from 0° to 360° considering effects of the other fibers, is calculated and presented. After that, flax fiber is compared with carbon and glass for volume fractions of 0.4 and 0.6 (6.3.3, 6.3.4).

Single and hexagon RVEs have one central fiber to be evaluated but the case of random RVE is a little bit different. The fiber to be evaluated should be selected among a bundle. To do so, one of the stress distribution theories has to be employed to assess the stress state in the matrix. In this case, maximum principal stress is used to observe

stress distribution since it is a commonly used method to evaluate structural failure for brittle materials.

6.3.1. Stress Concentrations for $\nu_f = 0.4$

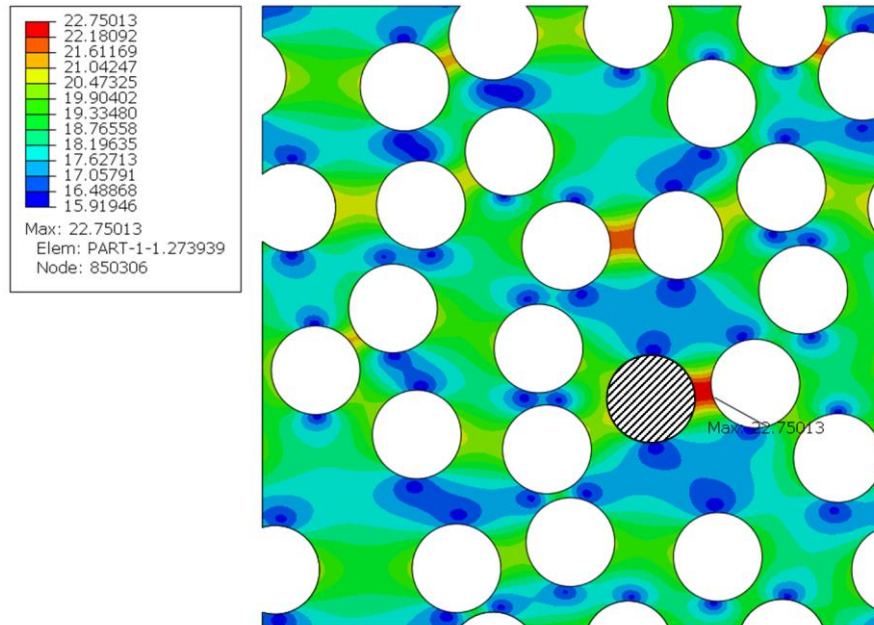


Figure 6.34. Random RVE distribution of maximum principle stresses in the matrix for flax fibers with fiber volume fraction of 0.4 for 0.2% strain input

First analysis in this section is the random RVE with fiber volume fraction of 0.4. Analysis results in terms of maximum principle stress are demonstrated on Figure 6.34. Maximum stresses were monitored between two fibers which are close to each other in loading direction. Due to its low stiffness, matrix carries most of the induced deformation in the loading direction and since there are several fibers in the vertical direction, a small volume remains to carry the load. Therefore, observed strain and the stress level at the end increase compared to the other portions in the RVE.

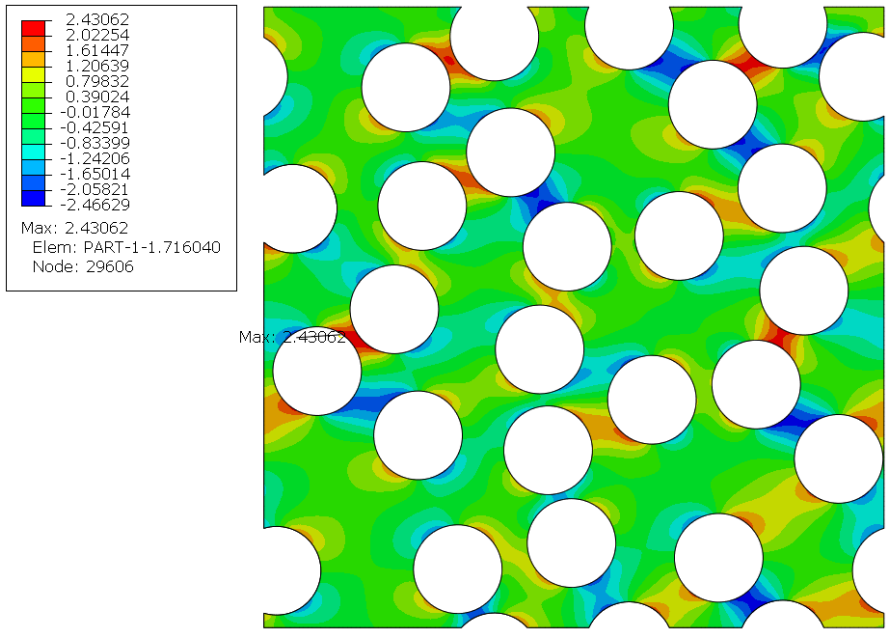


Figure 6.35. Random RVE distribution of shear stresses in the matrix for flax fibers with fiber volume fraction of 0.4 for 0.2% strain input.

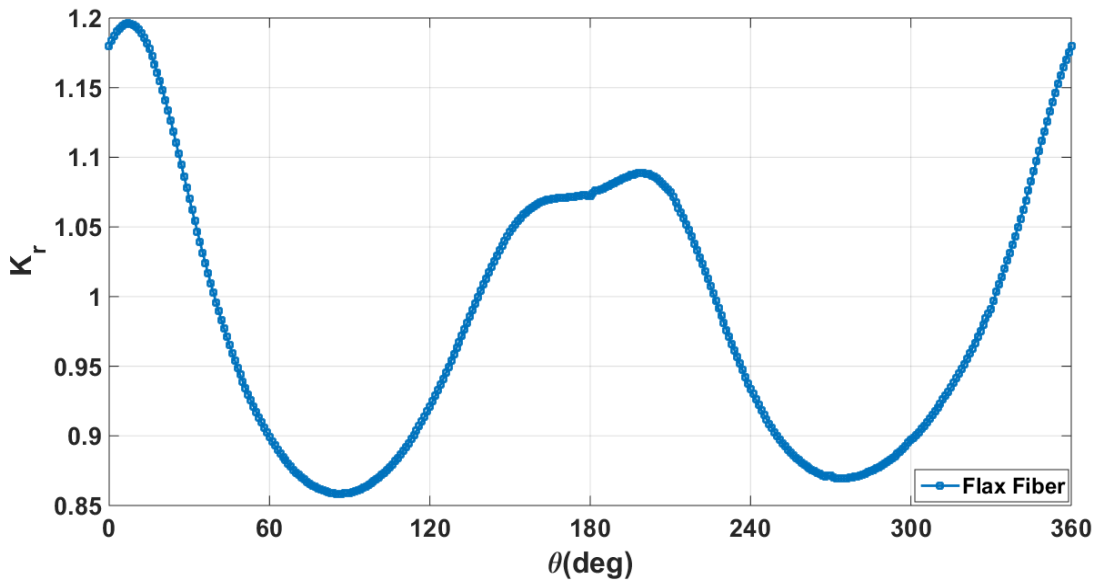


Figure 6.36. Random RVE radial stress concentrations along fiber-matrix interface for the fiber having maximum stress concentrations with fiber volume ratio of 0.4 for 0.2% strain input

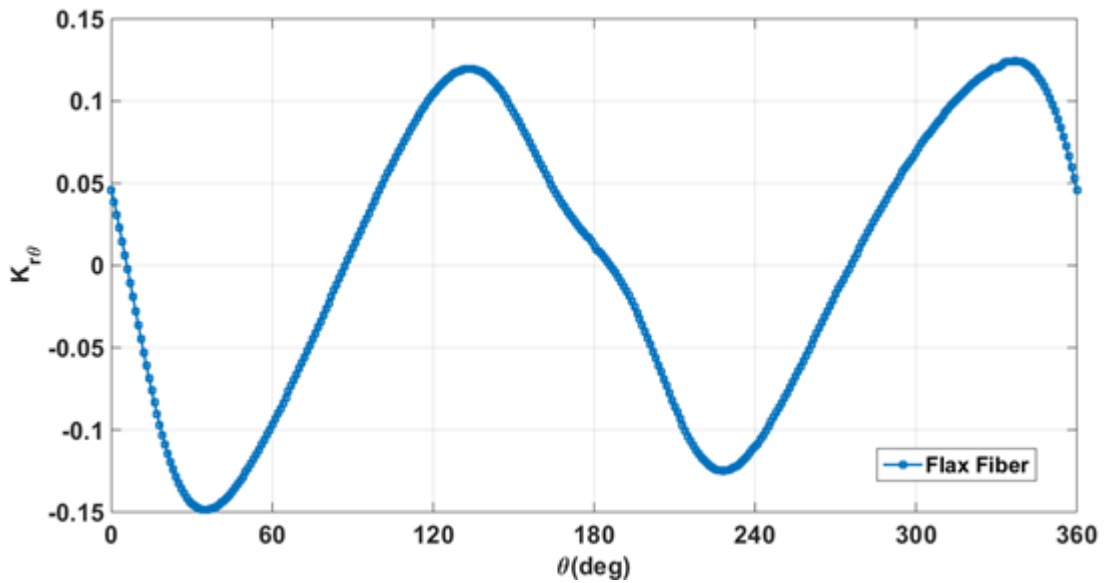


Figure 6.37. Random RVE shear stress concentrations along fiber-matrix interface for the fiber having maximum stress concentrations with fiber volume ratio of 0.4 for 0.2% strain input.

Regarding the shear stress distribution in Figure 6.35, it is observed that highest values of stresses are located in between the nearest fibers. Since the principle direction for the shear stress is in the 45° under simple tension, obtained contour plot is as expected for shear stress distribution. The fiber having highest stresses on its close vicinity is crosshatched in Figure 6.34. In the previous analysis models, stress concentration measures were given from 0° to 180° due to symmetry. Nevertheless, for random RVE case, it is not possible to show such a distribution because neighboring fibers also affect the stress state. Therefore, for the random case, radial and shear stress concentrations are given for a full fiber circumference. Radial and shear stress distribution for the indicated fiber are given in Figure 6.36 and Figure 6.37. As mentioned, a regular trend could not be observed in the plots due to the presence of other fibers located randomly in the RVE.

6.3.2. Stress Concentrations for $\nu_f = 0.6$

The next analysis case is the one with 0.6 fiber volume ratio. This time RVE is more densely packed with fibers and the remaining volume for the matrix is relatively low compared to the previous case which could be observed from Figure 6.38 and Figure 6.39.

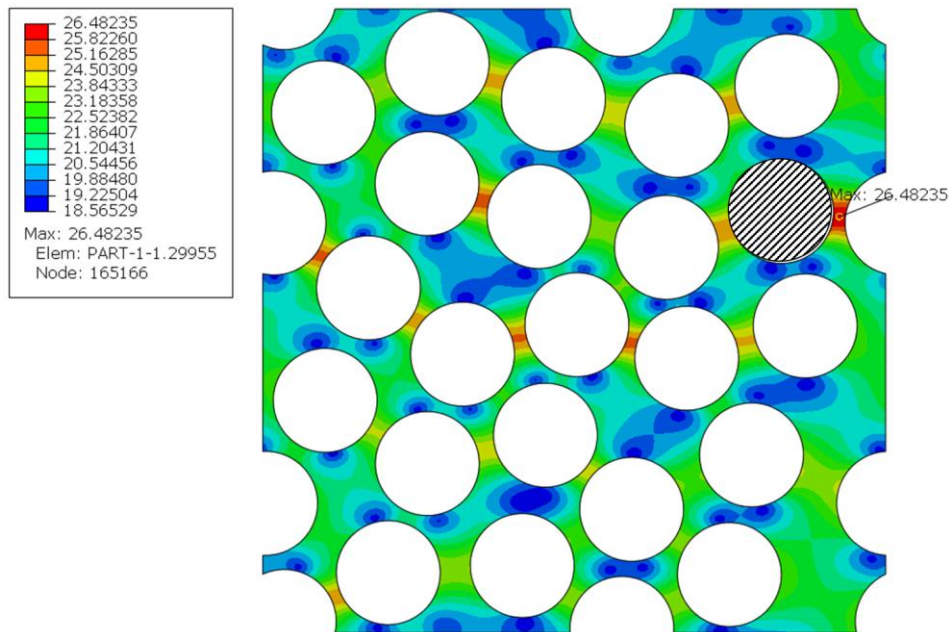


Figure 6.38. Random RVE distribution of maximum principle stresses in the matrix for flax fibers with fiber volume fraction of 0.6 for 0.2% strain input.

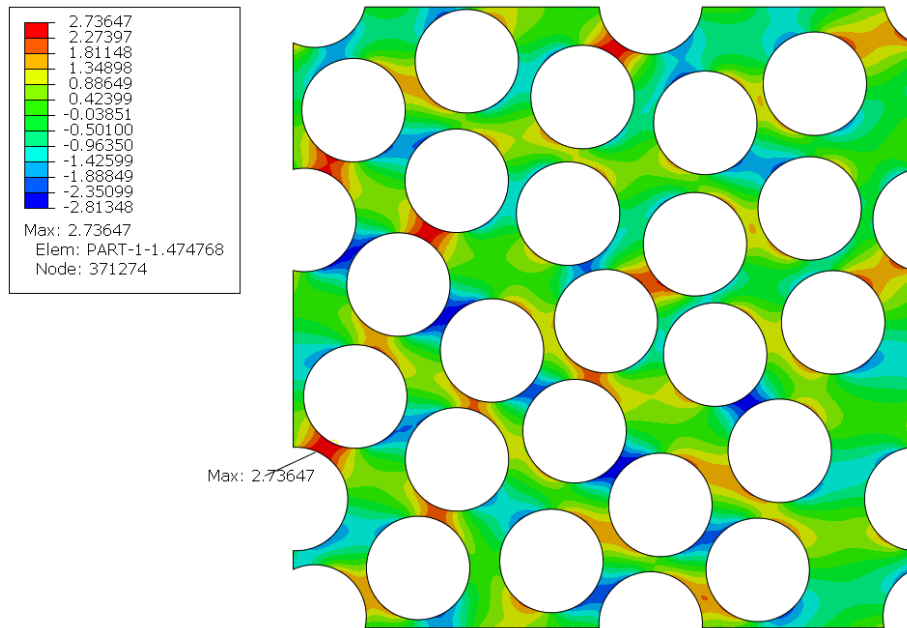


Figure 6.39. Random RVE distribution of shear stresses in the matrix for flax fibers with fiber volume fraction of 0.6 for 0.2% strain input.

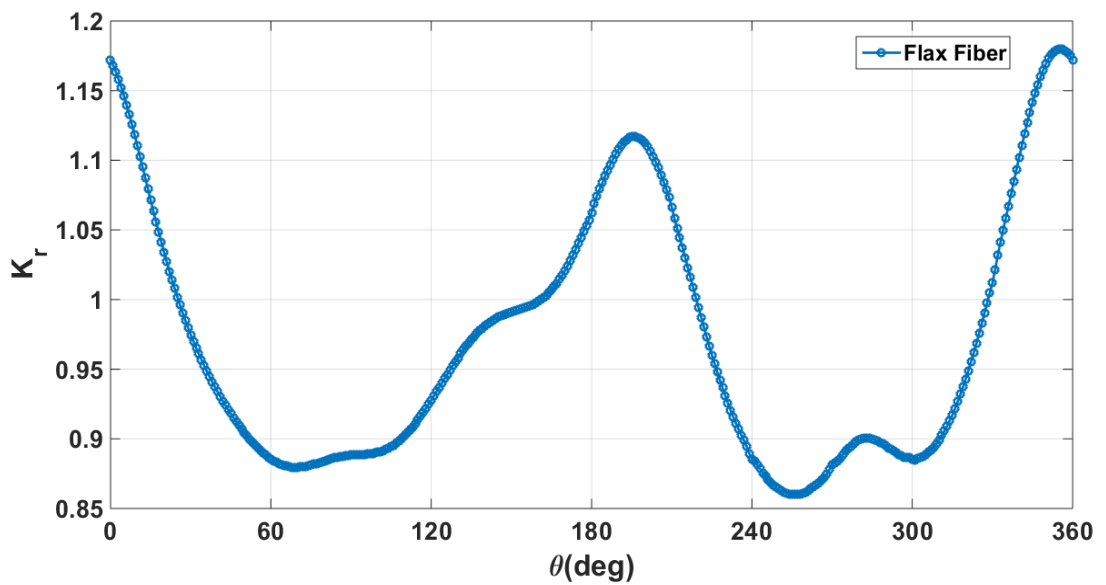


Figure 6.40. Random RVE radial stress concentrations along fiber-matrix interface for the fiber having maximum stress concentrations with fiber volume ratio of 0.6 for 0.2% strain input.

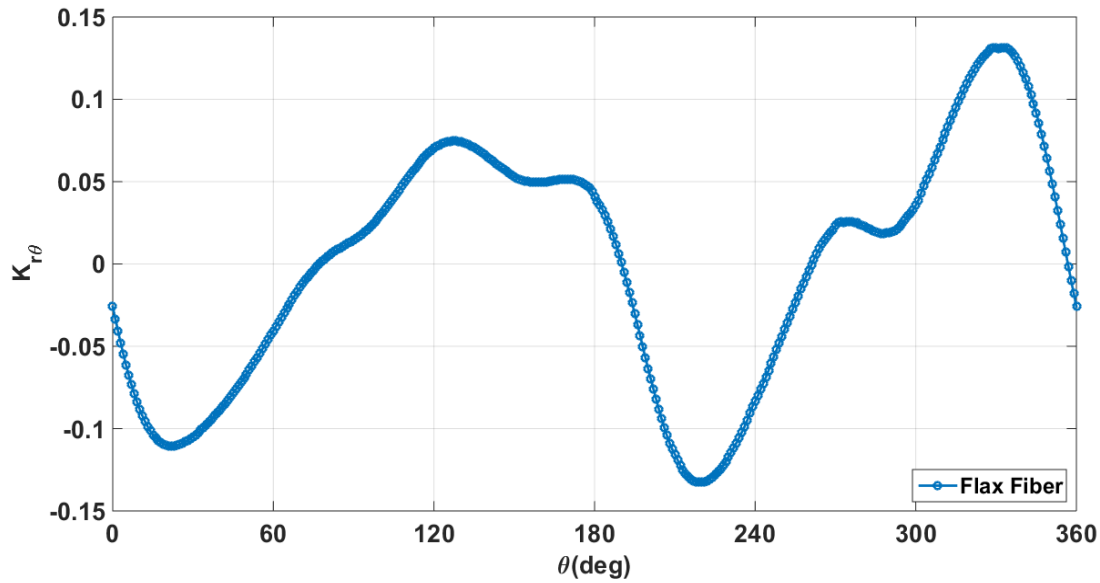


Figure 6.41. Random RVE shear stress concentrations along fiber-matrix interface for the fibers having maximum stress concentrations with fiber volume ratio of 0.6 for 0.2% strain input.

Under transverse tension, maximum principle stress is observed in the matrix where the fibers are located closest to the edges (Figure 6.38). As in the case of 0.4 volume fraction, location of maximum stress observed in the region where mostly strained area i.e. the smallest volume that matrix encloses. When the shear stress distribution is monitored (Figure 6.39), similar region with 0.4 volume fraction case is seen and it is again in the direction of 45° as expected. Radial and shear distributions of the most critical region in terms of maximum principle stress distribution are plotted in Figure 6.40 and Figure 6.41 respectively for the indicated fiber. Comparing two different volume fraction cases, it is obvious to state that increasing volume fraction has also increased the maximum stress observed in the matrix. Another important deduction from these cases is that fibers located near the edges create higher concentrations which have to be taken into account by the designers.

6.3.3. Comparison Case Study with Glass and Carbon Fiber for $v_f = 0.4$

In this analysis case, comparison of flax fiber with conventional glass and carbon fibers for fiber volume ratio of 0.4 is performed. Same procedure is applied which is the determination of highest stressed region under maximum principal stress distribution and the extraction of the stresses from the interface of the fiber that is located in the close vicinity. Radial and shear stress concentration comparison plots of these three fibers for the exact same fiber in each iteration with fiber volume ratio of 0.4 are given in Figure 6.42 and Figure 6.43 respectively.

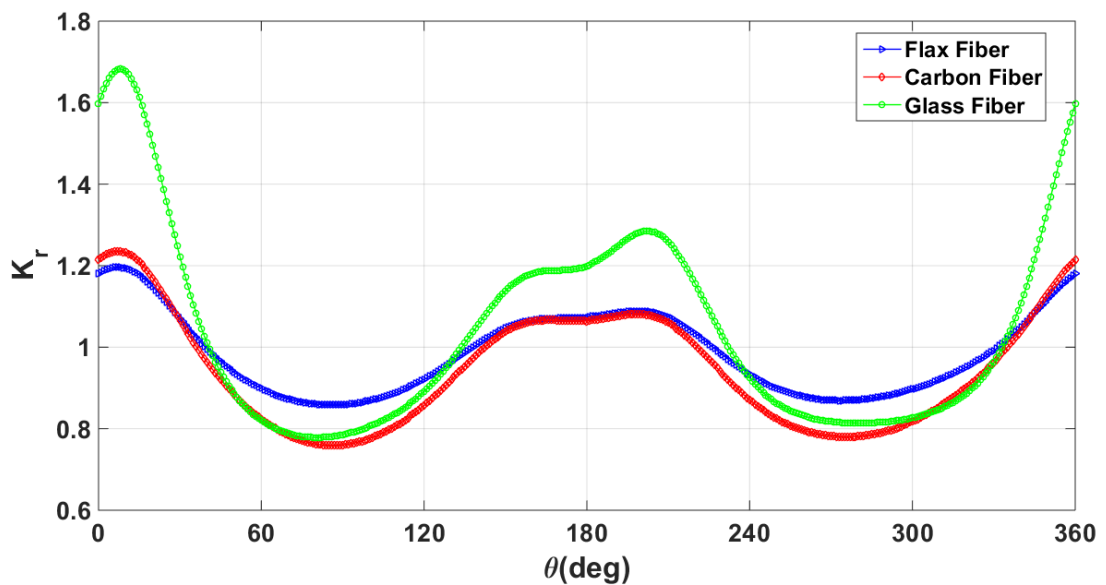


Figure 6.42. Random RVE Radial stress concentrations along the fiber-matrix interface for the fibers having maximum stress concentrations (crosshatched one in section 6.3.1) for fiber volume fraction of 0.4 for 0.2% strain input.

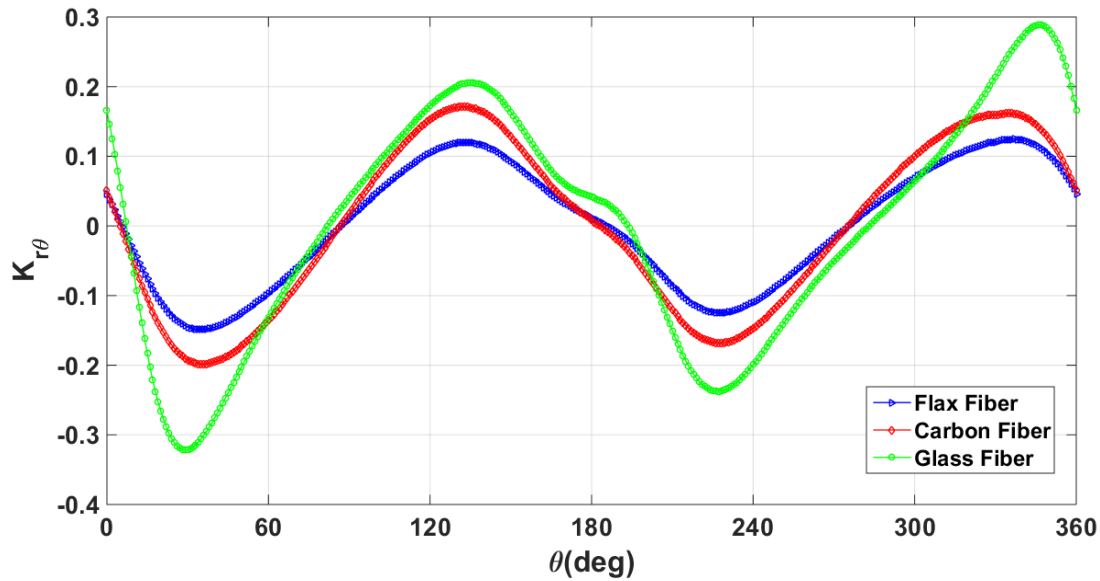


Figure 6.43. Random RVE Shear stress concentrations along the fiber-matrix interface for the fibers having maximum stress concentrations (crosshatched one in section 6.3.1) for fiber volume fraction of 0.4 for 0.2% strain input

When the radial stress concentration plot is examined, glass fiber undoubtedly becomes prominent due to its high stiffness in transverse direction. Carbon and flax fiber succeed the glass fiber respectively. The case in shear stress concentration is similar as well; glass fiber generates highest stress concentrations among the others. For this volume fraction ratio, flax fiber's behavior in terms of stress is quite stable compared to glass and carbon fibers.

6.3.4. Comparison Case Study with Glass and Carbon Fiber for $vf = 0.6$

Final analysis case is the comparison of the fibers for volume fraction of 0.6. Again, separate models with three fiber materials are run and highest loaded fiber regions in maximum principle stress invariant is selected, stresses are then extracted and plotted in terms of radial and shear concentrations. Trend of the plots are different from the previous case, since the location of the selected fiber changes for different volume

fraction. Yet, what is similar to previous case is that glass fiber again generates highest concentrations for both radial (Figure 6.44) and shear (Figure 6.45) stresses.

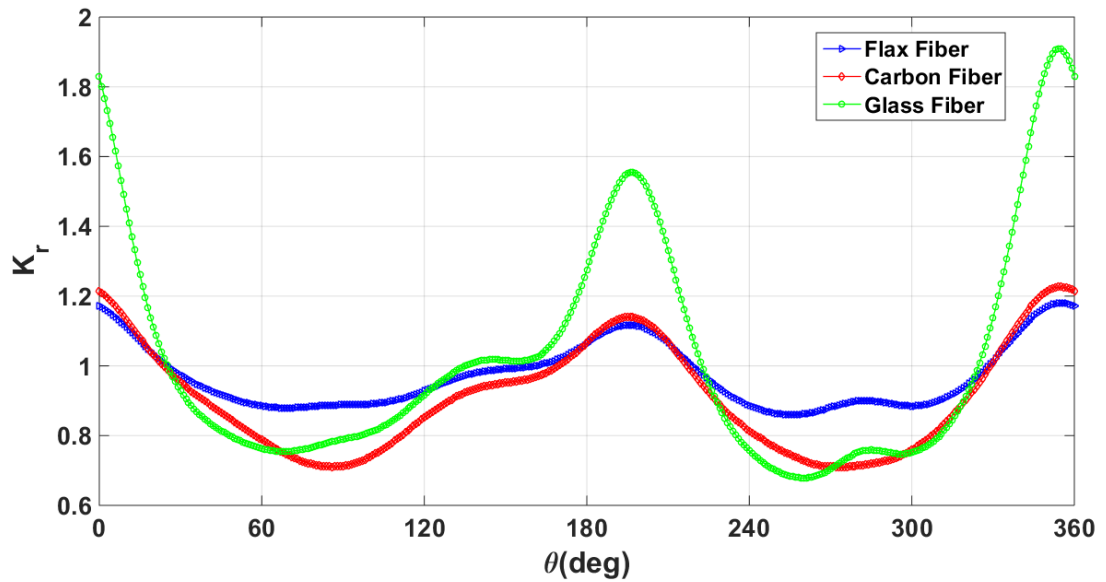


Figure 6.44. Random RVE radial stress concentrations along the fiber-matrix interface for the fibers having maximum stress concentrations (crosshatched one in section 6.3.2) for fiber volume fraction of 0.6 for 0.2% strain input.

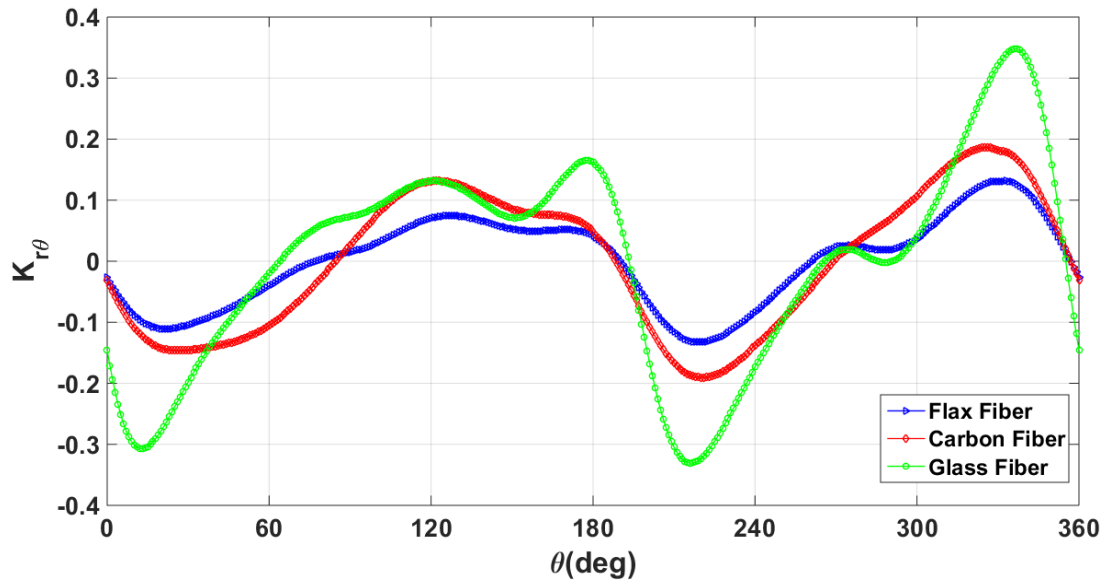


Figure 6.45. Random RVE shear stress concentrations along the fiber-matrix interface for the fibers having maximum stress concentrations (crosshatched one in section 6.3.2) for fiber volume fraction of 0.6 for 0.2% strain input

The other fibers come consecutively according to their transverse moduli i.e. second one is carbon, and then flax. These results are quite coherent with the literature [66]. When two volume fraction results are compared, it is seen that higher volume fraction also creates higher concentrations for different materials. Comparison of different fiber materials give an idea about their possible responses under transverse loading conditions. The peaks seen in the stress concentration plots are quite important for the structural integrity of the matrix since they represent the most critical regions. As mentioned previously, although glass fiber response under longitudinal loading conditions is favorable, its performance under transverse loading is not so bright. Carbon and flax fibers perform far better under such kind of loading. Comparing carbon and flax fiber, due to low transverse stiffness, flax fiber performs better. Therefore, the best performer of this comparison case study is the flax fiber. Random RVE stress concentration results of flax fiber composite are actually quite promising.

Important deductions like effect of fiber volume ratio, stiffness contrast, geometry, and fiber packing effect are obtained accordingly.

CHAPTER 7

GENERAL CONCLUSIONS

7.1. Summary

Comprehension of the mechanical behavior of natural fiber composites is an important milestone regarding the use of these material as structural elements. To be able to employ such material for load carrying applications, designers should have a fundamental understanding and perception about how this material response to mechanical effects for various conditions. In this study, a finite element model based on representative volume elements was developed to have an understanding the behavior of a natural fiber composites under transverse loading conditions. The study started with the investigation of natural fiber composites and its constituents. Mechanical properties of such materials were reviewed and a candidate fiber is selected to be worked on, namely flax fiber due to its superior properties among its counterparts. It was followed by a research about this specific fiber and its composites in Chapter 3. The mechanical properties of these type of fibers and its composites were scrutinized separately. After that, studies conducted in this field were explored thoroughly to have an idea which aspect should be investigated further. Studies conducted up to know mostly focused on longitudinal and the macro level responses of flax fiber composites. Therefore, a transverse micro modeling method was decided to be developed. In order to do so, material models were investigated in Chapter 4. Considering the available data on the literature and focal point of the study which is the transverse mechanism, material model was selected to be used in representative volume elements which is mentioned in Chapter 5. For each type of representative volume elements various number of analyses with different scenarios including different fiber volume ratios, different material models, different strain inputs and comparison of different fibers were run. Obtained results were post-processed in a

mathematical software to present them in a neat format. And finally some important deductions regarding the study is done in Chapter 6

7.2. Key Findings and Outcomes

Several outcomes and key findings are revealed by this study. They can be summarized as follows:

1. Bilinear moduli of flax fiber, presented in Figure 6.2, Figure 6.3, Figure 6.4 in Section 6.1.1, do not affect the stress concentrations extensively. Its effect is quite minimal therefore can be neglected.
2. For the strains in the elastic region of the epoxy matrix, stress concentrations show very similar trends. After the matrix passes to the plastic zone, stress concentrations mostly decrease for increasing strain inputs.
3. Transverse orthotropy assumption works well for flax fiber in the small strain setting, details are explained in Appendix A.
4. Results of stress concentration for the single RVE resemble to the classical elasticity problem “inclusion in infinite media” which is consistent with the infinite medium assumption made prior to single RVE geometry creation.
5. Results of inelastic modeling approach in single fiber RVE do not differ greatly from the orthotropic modeling approach. Yet, since hyperelastic modeling is done by using isotropic assumptions and focus point of the study is to obtain transverse response, it needs to be further improved.
6. For multiple fiber models (hexagon and random RVEs), fiber volume fraction has a direct influence on the stress concentrations. As the fiber volume fraction increases, upper limit of stress concentrations increase as well.
7. The effect of neighboring fibers to the each other is well observed for the multiple fiber RVE models.

8. Stiffness contrast i.e. difference in Young's moduli, between matrix and the fiber is the most effective factor on the stress concentrations. High contrast causes high stress concentrations. Yet in this study, it is revealed that flax fiber composites are more likely to be resistant to possible failures in transverse modes since they have much lower stress concentrations.

9. In terms of transverse loading, isotropic material reinforced composites of which fiber properties are direction independent, are inferior compared to the ones with low transverse modulus.

10. Stress concentration plots obtained in random RVE setting is quite useful to compare the integrity of an UD composite structure. As the number of peaks seen in this plot increases, the material may become more prone to possible failures.

7.3. Future Work

Considering the outcomes and findings in the study, it is possible to make suggestions for the future work. To begin with, all the finite element models are created with 3D elements instead of 2D plane stress or plane strain. The depth of the RVEs were quite minimal for this work, but considering possible future studies, the depths can further be modified and increased for nonplanar loading cases.

Furthermore, a model with failure modes can be created for static and dynamic loading. In this case properties of flax fiber should further be explored and insight of the material shall further be extended.

REFERENCES

- [1] L. Mohammed, M. N. M. Ansari, G. Pua, M. Jawaid, and M. S. Islam, "A Review on Natural Fiber Reinforced Polymer Composite and Its Applications," *International Journal of Polymer Science*, vol. 2015, p. 15, 2015, Art. no. 243947.
- [2] F. Reux, "Worldwide composites market: Main trends of the composites industry," *5th Innovative Composites Summit-JEC ASIA 2012*, pp. 26-28, 2012.
- [3] S. Schlott, "Shop window for innovations in the motor industry," *Kunststoffe-Plast Europe*, vol. 95, no. 11, pp. 96-101, 2005.
- [4] (15.12.2018). *RESOUND™ NF NATURAL FIBER REINFORCED THERMOPLASTIC COMPOSITES*. Available: <http://www.polyone.com/products/advanced-composites/fiber-reinforced-composites/resound-nf-natural-fiber-reinforced>
- [5] A. Shalwan and B. Yousif, "In state of art: mechanical and tribological behaviour of polymeric composites based on natural fibres," *Materials & Design*, vol. 48, pp. 14-24, 2013.
- [6] S. Shinoj, R. Visvanathan, S. Panigrahi, and M. Kochubabu, "Oil palm fiber (OPF) and its composites: A review," *Industrial Crops and products*, vol. 33, no. 1, pp. 7-22, 2011.
- [7] J.-C. Bénézet, A. Stanojlovic-Davidovic, A. Bergeret, L. Ferry, and A. Crespy, "Mechanical and physical properties of expanded starch, reinforced by natural fibres," *Industrial Crops and Products*, vol. 37, no. 1, pp. 435-440, 2012.
- [8] A. R. Kakroodi, S. Cheng, M. Sain, and A. Asiri, "Mechanical, thermal, and morphological properties of nanocomposites based on polyvinyl alcohol and cellulose nanofiber from Aloe vera rind," *Journal of Nanomaterials*, vol. 2014, p. 139, 2014.
- [9] U. Riedel and J. Nickel, "Applications of natural fiber composites for constructive parts in aerospace, automobiles, and other areas," *Biopolymers Online: Biology• Chemistry• Biotechnology• Applications*, vol. 10, 2005.
- [10] O. Faruk, A. K. Bledzki, H.-P. Fink, and M. Sain, "Biocomposites reinforced with natural fibers: 2000–2010," *Progress in Polymer Science*, vol. 37, no. 11, pp. 1552-1596, 2012/11/01/ 2012.

- [11] D. U. Shah, "Developing plant fibre composites for structural applications by optimising composite parameters: a critical review," *Journal of Materials Science*, vol. 48, no. 18, pp. 6083-6107, 2013.
- [12] S.-Y. Fu, B. Lauke, E. Mäder, C.-Y. Yue, and X. Hu, "Tensile properties of short-glass-fiber-and short-carbon-fiber-reinforced polypropylene composites," *Composites Part A: Applied Science and Manufacturing*, vol. 31, no. 10, pp. 1117-1125, 2000.
- [13] M. Kamath, G. Bhat, D. Parikh, and D. Mueller, "Cotton fiber nonwovens for automotive composites," *International Nonwovens Journal*, vol. 14, no. 1, pp. 34-40, 2005.
- [14] Y. Li, Y.-W. Mai, and L. Ye, "Sisal fibre and its composites: a review of recent developments," *Composites science and technology*, vol. 60, no. 11, pp. 2037-2055, 2000.
- [15] S. Mishra, A. K. Mohanty, L. T. Drzal, M. Misra, and G. Hinrichsen, "A review on pineapple leaf fibers, sisal fibers and their biocomposites," *Macromolecular Materials and Engineering*, vol. 289, no. 11, pp. 955-974, 2004.
- [16] A. Shahzad, "Hemp fiber and its composites—a review," *Journal of Composite Materials*, vol. 46, no. 8, pp. 973-986, 2012.
- [17] J. Summerscales, N. Dissanayake, A. Virk, and W. Hall, "A review of bast fibres and their composites. Part 2—Composites," *Composites Part A: Applied Science and Manufacturing*, vol. 41, no. 10, pp. 1336-1344, 2010.
- [18] N. Venkateshwaran and A. Elayaperumal, "Banana fiber reinforced polymer composites-a review," *Journal of Reinforced Plastics and Composites*, vol. 29, no. 15, pp. 2387-2396, 2010.
- [19] E. Zini and M. Scandola, "Green composites: an overview," *Polymer composites*, vol. 32, no. 12, pp. 1905-1915, 2011.
- [20] F. Bensadoun, "In-service behaviour of flax fibre reinforced composites for high performance applications," 2016.
- [21] G. Romhany, J. Karger-Kocsis, and T. Czigany, "Tensile fracture and failure behavior of technical flax fibers," *Journal of Applied Polymer Science*, vol. 90, no. 13, pp. 3638-3645, 2003.
- [22] R. Umer, S. Bickerton, and A. Fernyhough, "The effect of yarn length and diameter on permeability and compaction response of flax fibre mats," *Composites Part A: Applied Science and Manufacturing*, vol. 42, no. 7, pp. 723-732, 2011.
- [23] E. Sparnins, "Mechanical properties of flax fibers and their composites," Luleå tekniska universitet, 2009.

- [24] S. Shibata, Y. Cao, and I. Fukumoto, "Press forming of short natural fiber-reinforced biodegradable resin: Effects of fiber volume and length on flexural properties," *Polymer testing*, vol. 24, no. 8, pp. 1005-1011, 2005.
- [25] H. L. Bos, *The potential of flax fibres as reinforcement for composite materials*. Technische Universiteit Eindhoven Eindhoven, 2004.
- [26] A. Hassan, A. A. Salema, F. N. Ani, and A. A. Bakar, "A review on oil palm empty fruit bunch fiber-reinforced polymer composite materials," *Polymer Composites*, vol. 31, no. 12, pp. 2079-2101, 2010.
- [27] D. Parikh, D. Thibodeaux, and B. Condon, "X-ray crystallinity of bleached and crosslinked cottons," *Textile Research Journal*, vol. 77, no. 8, pp. 612-616, 2007.
- [28] V. Placet, F. Trivaudey, O. Cisse, V. Gucheret-Retel, and M. L. Boubakar, "Diameter dependence of the apparent tensile modulus of hemp fibres: A morphological, structural or ultrastructural effect?," *Composites Part A: Applied Science and Manufacturing*, vol. 43, no. 2, pp. 275-287, 2012.
- [29] A. Thygesen, J. Oddershede, H. Lilholt, A. B. Thomsen, and K. Ståhl, "On the determination of crystallinity and cellulose content in plant fibres," *Cellulose*, vol. 12, no. 6, p. 563, 2005.
- [30] H. Ku, H. Wang, N. Pattarachaiyakoop, and M. Trada, "A review on the tensile properties of natural fiber reinforced polymer composites," *Composites Part B: Engineering*, vol. 42, no. 4, pp. 856-873, 2011.
- [31] R. Malkapuram, V. Kumar, and Y. S. Negi, "Recent development in natural fiber reinforced polypropylene composites," *Journal of Reinforced Plastics and Composites*, vol. 28, no. 10, pp. 1169-1189, 2009.
- [32] K. Pickering, *Properties and performance of natural-fibre composites*. Elsevier, 2008.
- [33] A. O'donnell, M. Dweib, and R. Wool, "Natural fiber composites with plant oil-based resin," *Composites science and technology*, vol. 64, no. 9, pp. 1135-1145, 2004.
- [34] K. Oksman, M. Skrifvars, and J.-F. Selin, "Natural fibres as reinforcement in polylactic acid (PLA) composites," *Composites science and technology*, vol. 63, no. 9, pp. 1317-1324, 2003.
- [35] J. Girones, J. Lopez, P. Mutje, A. J. F. d. Carvalho, A. A. d. S. Curvelo, and F. Vilaseca, "Natural fiber-reinforced thermoplastic starch composites obtained by melt processing," *Composites Science and Technology*, vol. 72, no. 7, pp. 858-863, 2012.

- [36] M. Z. Rong, M. Q. Zhang, Y. Liu, G. C. Yang, and H. M. Zeng, "The effect of fiber treatment on the mechanical properties of unidirectional sisal-reinforced epoxy composites," *Composites Science and technology*, vol. 61, no. 10, pp. 1437-1447, 2001.
- [37] W. Liu, L. T. Drzal, A. K. Mohanty, and M. Misra, "Influence of processing methods and fiber length on physical properties of kenaf fiber reinforced soy based biocomposites," *Composites Part B: Engineering*, vol. 38, no. 3, pp. 352-359, 2007.
- [38] M. Miao and N. Finn, "Conversion of natural fibres into structural composites," *Journal of textile engineering*, vol. 54, no. 6, pp. 165-177, 2008.
- [39] T. Yu, J. Ren, S. Li, H. Yuan, and Y. Li, "Effect of fiber surface-treatments on the properties of poly (lactic acid)/ramie composites," *Composites Part A: Applied Science and Manufacturing*, vol. 41, no. 4, pp. 499-505, 2010.
- [40] A. Valadez-Gonzalez, J. Cervantes-Uc, R. Olayo, and P. Herrera-Franco, "Chemical modification of henequen fibers with an organosilane coupling agent," *Composites Part B: Engineering*, vol. 30, no. 3, pp. 321-331, 1999.
- [41] M. M. Haque, M. Hasan, M. S. Islam, and M. E. Ali, "Physico-mechanical properties of chemically treated palm and coir fiber reinforced polypropylene composites," *Bioresource technology*, vol. 100, no. 20, pp. 4903-4906, 2009.
- [42] G. Cantero, A. Arbelaiz, R. Llano-Ponte, and I. Mondragon, "Effects of fibre treatment on wettability and mechanical behaviour of flax/polypropylene composites," *Composites science and technology*, vol. 63, no. 9, pp. 1247-1254, 2003.
- [43] P. Saha, S. Manna, S. R. Chowdhury, R. Sen, D. Roy, and B. Adhikari, "Enhancement of tensile strength of lignocellulosic jute fibers by alkali-steam treatment," *Bioresource technology*, vol. 101, no. 9, pp. 3182-3187, 2010.
- [44] S. B. Brahim and R. B. Cheikh, "Influence of fibre orientation and volume fraction on the tensile properties of unidirectional Alfa-polyester composite," *Composites Science and Technology*, vol. 67, no. 1, pp. 140-147, 2007.
- [45] M. Jacob, S. Thomas, and K. T. Varughese, "Mechanical properties of sisal/oil palm hybrid fiber reinforced natural rubber composites," *Composites science and Technology*, vol. 64, no. 7-8, pp. 955-965, 2004.
- [46] L. Wen, W.-g. LEI, and R. Chao, "Effect of volume fraction of ramie cloth on physical and mechanical properties of ramie cloth/UP resin composite," *Transactions of Nonferrous Metals Society of China*, vol. 16, pp. s474-s477, 2006.

- [47] N. Venkateshwaran, A. Elayaperumal, and G. Sathiya, "Prediction of tensile properties of hybrid-natural fiber composites," *Composites Part B: Engineering*, vol. 43, no. 2, pp. 793-796, 2012.
- [48] H. Hargitai, I. Rácz, and R. D. Anandjiwala, "Development of hemp fiber reinforced polypropylene composites," *Journal of Thermoplastic Composite Materials*, vol. 21, no. 2, pp. 165-174, 2008.
- [49] B.-H. Lee, H.-J. Kim, and W.-R. Yu, "Fabrication of long and discontinuous natural fiber reinforced polypropylene biocomposites and their mechanical properties," *Fibers and Polymers*, vol. 10, no. 1, pp. 83-90, 2009.
- [50] R. Hu and J.-K. Lim, "Fabrication and mechanical properties of completely biodegradable hemp fiber reinforced polylactic acid composites," *Journal of Composite Materials*, vol. 41, no. 13, pp. 1655-1669, 2007.
- [51] L. Liu, J. Yu, L. Cheng, and W. Qu, "Mechanical properties of poly (butylene succinate)(PBS) biocomposites reinforced with surface modified jute fibre," *Composites Part A: Applied Science and Manufacturing*, vol. 40, no. 5, pp. 669-674, 2009.
- [52] M. Balter, "Clothes make the (Hu) man," ed: American Association for the Advancement of Science, 2009.
- [53] (2016, 15.11.2018). *Fantastic Flax, the Original Eco-Fiber*. Available: <https://www.coyuchi.com/the-naturalista/flax>
- [54] C. Baley, Y. Perrot, F. Busnel, H. Guezenoc, and P. Davies, "Transverse tensile behaviour of unidirectional plies reinforced with flax fibres," *Materials letters*, vol. 60, no. 24, pp. 2984-2987, 2006.
- [55] C. Baley, "Analysis of the flax fibres tensile behaviour and analysis of the tensile stiffness increase," *Composites Part A: Applied Science and Manufacturing*, vol. 33, no. 7, pp. 939-948, 2002.
- [56] L. Yan, N. Chouw, and K. Jayaraman, "Flax fibre and its composites—a review," *Composites Part B: Engineering*, vol. 56, pp. 296-317, 2014.
- [57] J. W. S. Hearle, "The fine structure of fibers and crystalline polymers. III. Interpretation of the mechanical properties of fibers," *Journal of Applied Polymer Science*, vol. 7, no. 4, pp. 1207-1223, 1963.
- [58] S. Kalia, B. Kaith, and I. Kaur, "Pretreatments of natural fibers and their application as reinforcing material in polymer composites—a review," *Polymer Engineering & Science*, vol. 49, no. 7, pp. 1253-1272, 2009.
- [59] K. Charlet, J.-P. Jernot, M. Gomina, L. Bizet, and J. Bréard, "Mechanical properties of flax fibers and of the derived unidirectional composites," *Journal of Composite Materials*, vol. 44, no. 24, pp. 2887-2896, 2010.

- [60] F. Bensadoun *et al.*, "Impregnated fibre bundle test for natural fibres used in composites," *Journal of Reinforced Plastics and Composites*, vol. 36, no. 13, pp. 942-957, 2017.
- [61] K. Charlet, S. Eve, J. Jernot, M. Gomina, and J. Breard, "Tensile deformation of a flax fiber," *Procedia Engineering*, vol. 1, no. 1, pp. 233-236, 2009.
- [62] G. Coroller *et al.*, "Effect of flax fibres individualisation on tensile failure of flax/epoxy unidirectional composite," *Composites Part A: Applied Science and Manufacturing*, vol. 51, pp. 62-70, 2013.
- [63] A. Arbelaiz, B. Fernandez, J. Ramos, A. Retegi, R. Llano-Ponte, and I. Mondragon, "Mechanical properties of short flax fibre bundle/polypropylene composites: Influence of matrix/fibre modification, fibre content, water uptake and recycling," *Composites science and technology*, vol. 65, no. 10, pp. 1582-1592, 2005.
- [64] S. Garkhail, R. Heijenrath, and T. Peijs, "Mechanical properties of natural-fibre-mat-reinforced thermoplastics based on flax fibres and polypropylene," *Applied Composite Materials*, vol. 7, no. 5-6, pp. 351-372, 2000.
- [65] D. U. Shah, P. J. Schubel, M. J. Clifford, and P. Licence, "The tensile behavior of off-axis loaded plant fiber composites: An insight on the nonlinear stress-strain response," *Polymer Composites*, vol. 33, no. 9, pp. 1494-1504, 2012.
- [66] M. Kersani, S. V. Lomov, A. W. Van Vuure, A. Bouabdallah, and I. Verpoest, "Damage in flax/epoxy quasi-unidirectional woven laminates under quasi-static tension," *Journal of composite materials*, vol. 49, no. 4, pp. 403-413, 2015.
- [67] M. Baiardo, E. Zini, and M. Scandola, "Flax fibre-polyester composites," *Composites Part A: Applied Science and Manufacturing*, vol. 35, no. 6, pp. 703-710, 2004.
- [68] H. Cox, "The elasticity and strength of paper and other fibrous materials," *British journal of applied physics*, vol. 3, no. 3, p. 72, 1952.
- [69] B. Lamy and C. Baley, "Stiffness prediction of flax fibers-epoxy composite materials," *Journal of Materials Science Letters*, journal article vol. 19, no. 11, pp. 979-980, June 01 2000.
- [70] B. Madsen and H. Lilholt, "Physical and mechanical properties of unidirectional plant fibre composites—an evaluation of the influence of porosity," *Composites Science and Technology*, vol. 63, no. 9, pp. 1265-1272, 2003.
- [71] I. Straumit, D. Vandepitte, M. Wevers, and S. V. Lomov, "Identification of the flax fibre modulus based on an impregnated quasi-unidirectional fibre bundle

- test and X-ray computed tomography," *Composites Science and Technology*, vol. 151, pp. 124-130, 2017.
- [72] J. Modniks and J. Andersons, "Modeling the non-linear deformation of a short-flax-fiber-reinforced polymer composite by orientation averaging," *Composites Part B: Engineering*, vol. 54, pp. 188-193, 2013.
- [73] A. Beakou and K. Charlet, "Mechanical properties of interfaces within a flax bundle—Part II: Numerical analysis," *International Journal of Adhesion and Adhesives*, vol. 43, pp. 54-59, 2013.
- [74] J. Sliseris, L. Yan, and B. Kasal, "Numerical modelling of flax short fibre reinforced and flax fibre fabric reinforced polymer composites," *Composites part B: engineering*, vol. 89, pp. 143-154, 2016.
- [75] A. Thuault, J. Bazin, S. Eve, J. Breard, and M. Gomina, "Numerical study of the influence of structural and mechanical parameters on the tensile mechanical behaviour of flax fibres," *Journal of Industrial Textiles*, vol. 44, no. 1, pp. 22-39, 2014.
- [76] J. Andersons, J. Modniks, and E. Spārniņš, "Modeling the nonlinear deformation of flax-fiber-reinforced polymer matrix laminates in active loading," *Journal of Reinforced Plastics and Composites*, vol. 34, no. 3, pp. 248-256, 2015.
- [77] A. Lagzdīņš, G. Teters, and A. Zilauca, "Nonlinear deformation of composites with consideration of the effect of couple-stresses," *Mechanics of composite materials*, vol. 34, no. 5, pp. 403-418, 1998.
- [78] C. Poilâne, Z. Cherif, F. Richard, A. Vivet, B. B. Doudou, and J. Chen, "Polymer reinforced by flax fibres as a viscoelastoplastic material," *Composite Structures*, vol. 112, pp. 100-112, 2014.
- [79] A. Rubio-López, T. Hoang, and C. Santiuste, "Constitutive model to predict the viscoplastic behaviour of natural fibres based composites," *Composite Structures*, vol. 155, pp. 8-18, 2016.
- [80] B. Sabuncuoglu, S. Orlova, L. Gorbatikh, S. V. Lomov, and I. Verpoest, "Micro-scale finite element analysis of stress concentrations in steel fiber composites under transverse loading," *Journal of Composite Materials*, vol. 49, no. 9, pp. 1057-1069, 2015.
- [81] M. H. Sadd, *Elasticity: theory, applications, and numerics*. Academic Press, 2009.
- [82] A. U. Manual, "Abaqus Theory Guide," *Version*, vol. 6, p. 14, 2014.
- [83] S. Liang, P. Gning, and L. Guillaumat, "Fatigue behavior of flax/epoxy composite," in *18th International Conference on Composite Materials*, 2011.

- [84] K. Charlet and A. Béakou, "Mechanical properties of interfaces within a flax bundle – Part I: Experimental analysis," *International Journal of Adhesion and Adhesives*, vol. 31, no. 8, pp. 875-881, 2011/12/01/ 2011.
- [85] C. Baley, A. Kervoëlen, A. Le Duigou, C. Goudenhoofft, and A. Bourmaud, "Is the low shear modulus of flax fibres an advantage for polymer reinforcement?," *Materials Letters*, vol. 185, pp. 534-536, 2016.
- [86] P. BARANOWSKI, R. GIELETA, J. MAŁACHOWSKI, and Ł. MAZURKIEWICZ, "Rubber structure under dynamic loading–computational studies," *Engineering Transactions*, vol. 61, no. 1, pp. 33–46, 2013.
- [87] T. Okabe, K. Ishii, M. Nishikawa, and N. Takeda, "Prediction of tensile strength of unidirectional CFRP composites," *Advanced Composite Materials*, vol. 19, no. 3, pp. 229-241, 2010.
- [88] I. M. Gitman, H. Askes, L. J. Sluys, and O. Lloberas, "The concept of representative volume for elastic, hardening and softening materials," in *Proceedings of XXXII International Summer School-Conference "Advanced problems in Mechanics"*, 2004, pp. 180-184.
- [89] M. Rask, B. Madsen, B. F. Sørensen, J. L. Fife, K. Martyniuk, and E. M. Lauridsen, "In situ observations of microscale damage evolution in unidirectional natural fibre composites," *Composites Part A: Applied Science and Manufacturing*, vol. 43, no. 10, pp. 1639-1649, 2012.
- [90] M. Aghdam and A. Dezhsetan, "Micromechanics based analysis of randomly distributed fiber reinforced composites using simplified unit cell model," *Composite Structures*, vol. 71, no. 3-4, pp. 327-332, 2005.
- [91] A. Melro, P. Camanho, and S. Pinho, "Generation of random distribution of fibres in long-fibre reinforced composites," *Composites Science and Technology*, vol. 68, no. 9, pp. 2092-2102, 2008.
- [92] Y. Zhong, L. Q. N. Tran, U. Kureemun, and H. P. Lee, "Prediction of the mechanical behavior of flax polypropylene composites based on multi-scale finite element analysis," *Journal of Materials Science*, journal article vol. 52, no. 9, pp. 4957-4967, May 01 2017.
- [93] S. Kurukuri, "Homogenization of Damaged Concrete Mesostructures using Representative Volume Elements-Implementation and Application to SLang," 2005.

APPENDIX A

In the investigations that are conducted in epoxy matrix, the fiber itself is excluded. The focal point in this study, flax fiber, is selected orthotropic elastic instead of hyperelastic as it is mentioned Section 4.3 and the elastic properties of selected flax fiber is given in Table 4.1. This assumption is valid in the case that fiber strains are within the elastic limits. In this part, stress and strain distribution of fiber is studied to check if the flax fibers remain in linear elastic zone. In single RVE configuration, model is exposed to maximum transverse strain of 0.05, which is the highest strain used in this study, from the right end left hand sides of RVE as given in section 5.1. The maximum principle stress and strain distributions are presented in Figure 8.1:

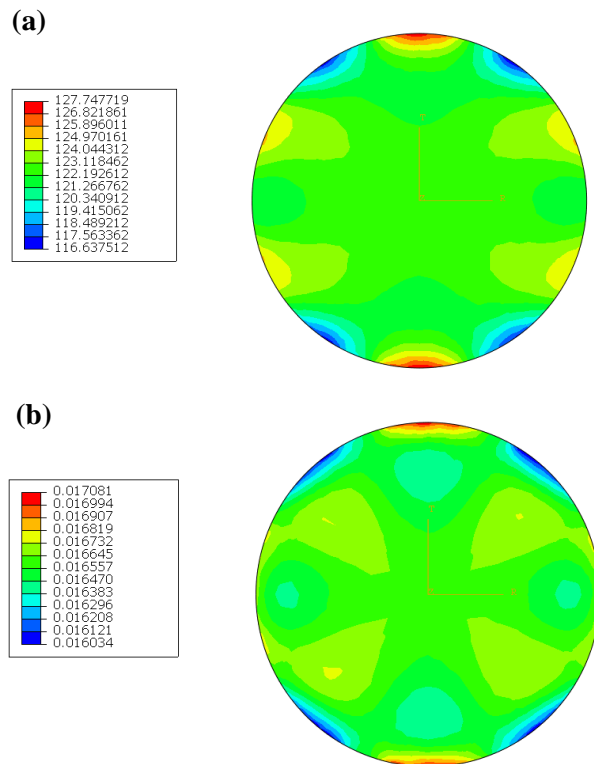


Figure 8.1. Maximum (a) Principal stress and (b) strain distributions of flax fiber under transverse loading

Maximum strain that fiber is exposed from Figure 8.1 is calculated as 0.017. The available data on the literature indicates that bilinear stress-strain behavior of the flax fiber is seen in between 0 and 0.3 % of strain and 1.5% to the final rupture [61]. Based on this information and the analysis results which is the investigation of dual modulus presented in Section 6.1.1 (Figure 6.2, Figure 6.3, and Figure 6.4), the orthotropic elastic material model assumption is considered to be acceptable for the stress concentration analyses. Stress strain plot of highest strained element is also given in Figure 8.2.

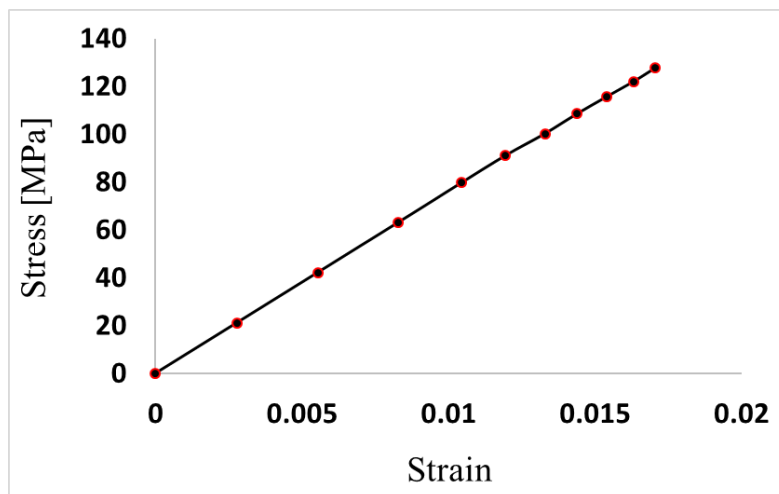


Figure 8.2. Stress Strain curve of maximum strained element

